Εθνικο Μετσοβιο Πολυτεχνειο
Σχολη Εφαρμοσμενων Μαθηματικων και Φυσικων Επιστημων
Τομεας Φυσικης Υψηλων Ενεργειων

Μέτρηση της μάζας του top quark σε συγκρούσεις πρωτονίων στα $\sqrt{s} = 13TeV$ στο πείραμα CMS

Διπλωματικη Εργασια

Καμιναρης Δημητριος

Επιβλέπων: Κωνσταντίνος Κουσουρής
Αναπληρωτής Καθηγητής ΣΕΜΦΕ

Αθήνα, Σεπτέμβριος 2021

Εθνικο Μετσοβιο Πολυτεχνειο
Σχολη Εφαρμοσμενων Μαθηματικων και Φυσικων Επιστημων
Τομεας Φυσικης Υψηλων Ενεργειων

Καμινάρης Δημήτριος
Διπλωματούχος Σχολής Εφαρμοσμένων Μαθηματικών και Φυσικών Επιστημών
Ε.Μ.Π.

National Technical University of Athens

School of Mathematical and Physical Sciences
Division of High Energy Physics

Measurement of the top quark mass with single top events at $\sqrt{s} = 13$TeV

Diploma Thesis

Kaminaris Dimitrios

Supervisor: Kousouris Konstantinos
Associate Professor, National Technical University of Athens

Athens, September 2021

Περίληψη

Ο σκοπός της παρούσας διπλωματικής εργασίας είναι η μέτρηση της μάζας του top quark σε γεγονότα που περιέχουν αποκλειστικά και μόνο top quark και πιο συγκεκριμένα στο t-κανάλι λειτουργίας. Αυτό το κανάλι έχει τη μεγαλύτερη ενεργό διατομή και μπορεί να διακρίνει αποτελεσματικά τα γεγονότα σήματος από τις διεργασίες υποβάθρου.

Ο στόχος είναι να εξαχθεί μια εκτίμηση για τη θεωρητική τιμή της μάζας, εκτελώντας μια προσαρμογή μέγιστης πιθανοφάνειας στα πραγματικά δεδομένα. Τα δεδομένα, που χρησιμοποιούνται σε αυτήν την εργασία, προέρχονται από συγκρούσεις πρωτονίων στον LHC και συλλέχθηκαν κατά το έτος 2016 με ενσωματωμένη φωτεινότητα $L = 35.9 fb^{-1}$.

Πριν από την προσαρμογή στα δεδομένα, πραγματοποιείται μια παραμετροποίηση του σήματος και των διάφορων διαδικασιών υποβάθρου. Στη συνέχεια, μέσω της μελέτης Toy Monte Carlo, ο εκτιμητής και το σφάλμα του ελέγχονται ως προς την αμεροληψία τους. Τέλος, το σφάλμα και η πραγματική τιμή της μάζας εκτιμούνται μέσω βαθμονόμησης των Monte Carlo προσαρμογών και έπειτα, μέσω διάδοσης σφάλματος.

Επίσης, εξετάζεται το αμετάβλητο της CPT συμμετρίας, μετρώντας ξεχωριστά τη μάζα του top quark και του anti-top quark και υπολογίζοντας την τιμή του πηλίκου τους, καθώς και την διαφορά τους. Τα τελικά αποτελέσματα παρατηρούνται σε συμφωνία με τις θεωρητικές προβλέψεις του Καθιερωμένου Προτύπου, καθώς και με αποτελέσματα προηγούμενων μετρήσεων.

Abstract

The goal of this thesis is the measurement of the mass of top quark in events that contain only top quarks, specifically in the t-channel mode. This channel has the largest single top cross section and can discriminate efficiently the signal events from the background processes.

The objective is to extract an estimation for the theoretical value by performing a maximum likelihood fit on data. The data used in this thesis come from proton-proton collisions at LHC collected during the year 2016 with an integrated luminosity of $L = 35.9fb^{-1}$.

Before the fit on data, a parametrisation of the probability density function that describes both the signal and the various background processes is performed. Then, through Toy Monte Carlo study the estimator and its error are checked for any biases that they may contain. Finally, the true error and the true value of the mass are estimated through calibration on Monte Carlo samples and afterwards, through error propagation.

Another key point of this thesis, is the validation of the CPT invariance by measuring separately the mass of the top quark and the anti-top quark and calculating their ratio and their difference. The final results are in agreement with the theoretical predictions of the Standard Model and with those of previous measurements.

Ευχαριστίες

Θα ήθελα να ευχαριστήσω τον επιβλέποντα καθηγητή μου, κ. Κωνσταντίνο Κουσουρή, για όλη τη βοήθεια, την στήριξη και τις γνώσεις που μου προσέφερε καθόλη τη διάρκεια της ενασχόλησης μου στην Διπλωματική Εργασία. Επίσης, ευχαριστώ πολύ τον κ. Γεώργιο Τσιπολίτη, για την συνεπίβλεψη και τις συμβουλές που μου παρείχε καθώς και όλη την ομάδα του CMS στο Εθνικό Μετσόβιο Πολυτεχνείο.

Ευχαριστώ επιπλεόν την οικογένεια μου και τους φίλους μου, για την στήριξή τους όλα αυτά τα χρόνια.

Καμινάρης Δημήτριος
Αθήνα, Σεπτέμβριος 2021

Contents

Κατάλογος Σχημάτων

Εκτεταμένη Περίληψη

Εισαγωγή

Μετά από πολυάριθμες θεωρίες, πειράματα και ανακαλύψεις έχουμε αποκτήσει εικόνα για τη θεμελιώδη δομή της ύλης: τα πάντα στο σύμπαν είναι φτιαγμένα από μικροσκοπικά δομικά στοιχεία που ονομάζουμε θεμελιώδη σωματίδια, τα οποία διέπονται από τέσσερις θεμελιώδεις δυνάμεις. Όλα όσα γνωρίζουμε μέχρι τώρα, για τη φύση και τις αλληλεπιδράσεις αυτών των σωματιδίων και δυνάμεων περιγράφονται στο Καθιερωμένο Πρότυπο. Το Καθιερωμένο Πρότυπο, αναπτύχθηκε στις αρχές του 1970 και πρόκειται για μία άκρως πειραματικά επιβεβαιωμένη θεωρία.

Οι τέσσερις θεμελιώδεις δυνάμεις είναι: η βαρυτική δύναμη, η ηλεκτρομαγνητική δύναμη, η ασθενής και η ισχυρή δύναμη. Έχουν διαφορές ως προς το σθένος και το εύρος μέχρι το οποίο δρουν. Η βαρύτητα είναι η πιο ασθενής, αλλά έχει άπειρη εμβέλεια. Η ηλεκτρομαγνητική δύναμη έχει επίσης άπειρη εμβέλεια, αλλά είναι πολύ ισχυρότερη από τη βαρύτητα. Η ασθενής και η ισχυρή δύναμη κυριαρχούν σε υποατομικό επίπεδο.

Υπάρχουν δύο κύριες κατηγορίες θεμελιωδών σωματιδίων, τα φερμιόνια και τα μποζόνια, η κύρια διαφορά βρίσκεται στο spin. Τα μποζόνια έχουν ακέραιο spin και τα φερμιόνια έχουν ημιακέραιο spin.

Τα φερμιόνια χωρίζονται σε δύο κατηγορίες. Στην πρώτη ανήκουν τα λεπτόνια (ηλεκτρόνιο,μιόνιο,ταυ), το καθένα εκ των οποίων έχει και ένα αντίστοιχο νετρίνο. Τα λεπτόνια έχουν ίδιο φορτίο και διαφέρουν μόνο στις επιμέρους μάζες τους. Τα νετρίνα είναι αφόρτιστα και έχουν πολύ μικρή μάζα[1]. Η δεύτερη κατηγορία φερμιονίων είναι τα quarks, τα οποία είναι έξι στο σύνολο. Τα έξι quarks χωρίζονται σε τρεις γενιές - το "up quark" και το "down quark" αποτελούν την πρώτη γενιά, ακολουθούμενα από το "charm quark" και το "strange quark" και, στη συνέχεια από τα "top quark" και "bottom ή beauty quark". Τα quarks έρχονται επίσης σε τρία διαφορετικά "χρώματα" και αναμειγνύονται μόνο με τέτοιο τρόπο ώστε να σχηματίζουν "άχρωμα" αντικείμενα. Όλη η σταθερή ύλη στο σύμπαν αποτελείται από σωματίδια που ανήκουν στην πρώτη γενιά.

[1]Μέχρι πριν κάποια χρόνια η μάζα τους θεωρούταν αμελητέα

Τα μποζόνια επίσης χωρίζονται σε δύο κατηγορίες. Στην πρώτη ανήκουν τα μποζόνια βαθμίδας (gauge bosons), τα οποία είναι τα φωτόνια,τα γκλουόνια και τα $W^{\pm}$,Z^0. Καθένα από αυτά είναι φορέας μίας εκ των τεσσάρων δυνάμεων στη φύση. Το φωτόνιο είναι φορέας της ηλεκτρομαγνητικής, τα γκλουόνια της ισχυρής και τα $W^{\pm}$,Z^0 της ασθενούς αλληλεπίδρασης. Φορείς της βαρυτικής δύναμης καλούνται βαρυτόνια, αλλά δεν έχουν παρατηρηθεί πειραματικά ακόμα. Η δεύτερη κατηγορία περιέχει το μποζόνιο Higgs, το οποίο κατά το αυθόρμητο σπάσιμο της συμμετρίας της ηλεκτρασθενούς αλληλεπίδρασης προσδίδει μάζα στα $W^{\pm}$,Z^0. Το συγκεκριμένο μποζόνιο έχει spin 0. Όλα τα στοιχειώδη σωματίδια μαζί με τις ιδιότητες τους παρατίθενται στο ακόλουθο Σχήμα 1:

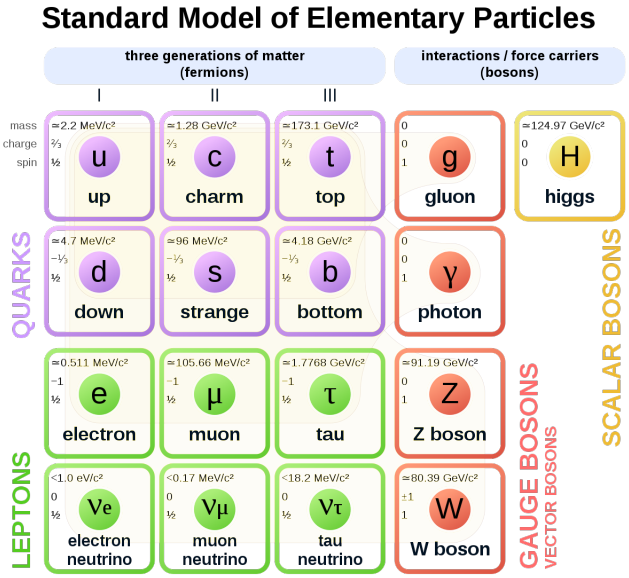

Σχήμα 1: *Καθιερωμένο Πρότυπο Σωματιδιακής Φυσικής*

Το top quark και η παραγωγή του

Όπως αναφέραμε προηγουμένως, το top κουάρκ είναι ένα από τα έξι quarks. Η ύπαρξή του ήταν αναμενόμενη από το 1977, λόγω του ότι τα quarks έρχονται σε διπλέτες spin, όταν το bottom quark ανακαλύφθηκε στο Fermilab. Μέχρι το 1995 και μετά από πολλά πειράματα, το top κουάρκ ανακαλύφθηκε από τα πειράματα CDF και *DØ* στον επιταχυντή Tevatron. Σε αυτά τα πειράματα, βρέθηκε μεγάλη παραγωγή ζευγαριών $t\bar{t}$.

Το top κουάρκ είναι άξιο μελέτης διότι είναι το βαρύτερο και έτσι διασπάται πριν από την αδρονοποίηση (hadronisation). Η μάζα του είναι μια από τις πιο σημαντικές ιδιότητες για το Καθιερωμένο Πρότυπο, τόσο για θεωρητικούς όσο και για πειραματικούς λόγους. Αποτελεί σημαντική συμβολή στις παγκόσμιες ηλεκτρασθενείς προσαρμογές, που χρησιμοποιούνται για την επαλήθευση της αυτοσυνέπειας του Καθιερωμένου Προτύπου. Η τιμή της σχετίζεται επίσης άμεσα με τη σταθερότητα του ηλεκτρασθενούς

κενού, επειδή μεταξύ όλων των σωματιδίων του ΚΠ είναι ο μεγαλύτερος συνεισφέρων, όσον αφορά στις διορθώσεις ακτινοβολίας στη μάζα και στην ιδιοσύξευξη του μποζονίου Higgs. Από πειραματική άποψη, προσφέρει ένα ιδανικό σημείο αναφοράς για την απόδοση του ανιχνευτή, ως προς τους αλγόριθμους ανακατασκευής.

Η τωρινή πιο ακριβής μέτρηση της μάζας του top quark είναι:

$$m_{top} = 172.04 \pm 0.19(stat + JSF) \pm 0.75(syst)GeV. \quad (1)$$

Το top quark διασπάται με ηλεκτρασθενή τρόπο σε ένα W μποζόνιο και σε ένα εκ των d, s, d quarks. Το πλάτος της αλληλεπίδρασης είναι:

$$\Gamma(t \longrightarrow W^+q) = \frac{|V_{tq}|^2 m_t^3}{16\pi u^2}\left(1 - \frac{M_W^2}{m_t^2}\right)^2\left(1 + 2\frac{M_W^2}{m_t^2}\right)\left[1 - \frac{2a_s}{3\pi}\left(\frac{2\pi^2}{3} - \frac{5}{2}\right)\right] \quad (2)$$

Δεδομένου ότι $|V_{tb}| \approx 0.99$ και άρα $BR(t \longrightarrow W^+q) = \frac{|V_{tb}|^2}{\sum_q |V_{tq}|^2} \approx 1$ καταλήγουμε στο ότι το top quark διασπάται τις περισσότερες φορές σε bottom quark.

Το top quark παρασκευάζεται στον LHC μέσω ισχυρών και ηλεκτρασθενών αλληλεπιδράσεων. Η παραγωγή μέσω ισχυρών οδηγεί σε δημιουργία ζεύγους $t\bar{t}$. Οι τρόποι παραγωγής $t\bar{t}$ είναι:

- **Σύντηξη Γκλουονίων**:

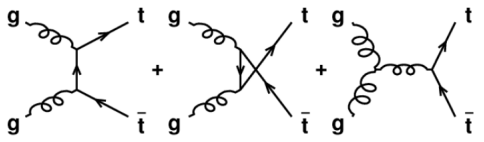

Σχήμα 2: *Παραγωγή $t\bar{t}$ μέσω σύντηξης γκλουονίων*

- **Αλληλεπιδράσεις $q\bar{q}$**:

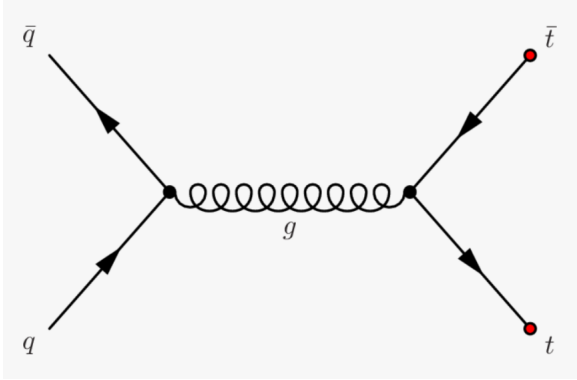

Σχήμα 3: *Παραγωγή $t\bar{t}$ μέσω $q\bar{q}$ αλληλεπιδράσεων*

Η ενεργός διατομή για την παραγωγή $t\bar{t}$ μετρημένη στα $\sqrt{s} = 13TeV$ είναι:

$$\sigma_{t\bar{t}} = 832.8^{+19.8+35.1}_{-29.2-35.1}pb \tag{3}$$

Η παραγωγή μέσω ηλεκτρασθενών αλληλεπιδράσεων οδηγεί σε ένα top quark στην τελική κατάσταση ("single top" παραγωγή). Όπως θα δούμε παρακάτω, υπάρχουν τρεις βασικές εκδοχές της "single top" παραγωγής, με την κυρίαρχη να έχει ενεργό διατομή ίση με:

$$\sigma_{t,t-ch} = 130 \pm 1(stat.) \pm 19(syst). \tag{4}$$

Η single top παραγωγή παρέχει ένα ανεξάρτητο στατιστικό δείγμα για τη μέτρηση της μάζας του top quark. Αυτή η διαδικασία συμβαίνει σε χαμηλότερη ενεργειακή κλίμακα σε σύγκριση με την παραγωγή $t\bar{t}$. Το t-channel της single top παραγωγής υπαγορεύει τη "χρωματική" σύνδεση μόνο μεταξύ του top quark και του πρωτονίου, από το οποίο έρχεται το αρχικό bottom quark, και όχι σε ολόκληρο το γεγονός όπως παρατηρείται στο $t\bar{t}$. Επομένως, τέτοιες μετρήσεις παρέχουν έναν χρήσιμο έλεγχο για μεγάλες άγνωστες συστηματικές επιδράσεις, που προκύπτουν λόγω της μοντελοποίησης των μη διαταρακτικών διαδικασιών της QCD σε προσομοιώσεις Monte Carlo.

Ο Ανιχνευτής CMS

Ο Large Hardron Collider(LHC) είναι ο μεγαλύτερος (27χλμ) και ο πιο ισχυρός επιταχυντής σωματιδίων, που έχει κατασκευαστεί ποτέ. Επιταχύνει πρωτόνια κοντά στην ταχύτητα του φωτός, δεξιόστροφα και αριστερόστροφα και τα συγκρούει σε τέσσερα συγκεκριμένα σημεία στην περίμετρό του. Σε αυτά τα τέσσερα σημεία, η ενέργεια από τις συγκρούσεις μετατρέπεται σε μάζα, εκτοξεύοντας σωματίδια προς όλες τις κατευθύνσεις.

Ο ανιχνευτής Compact Muon Solenoid (CMS), βρίσκεται σε ένα από αυτά τα τέσσερα σημεία. Λειτουργεί ως μια γιγαντιαία κάμερα, παίρνοντας "στιγμιότυπα" από τις συγκρούσεις σωματιδίων, ακόμη και 40 εκατομμύρια ανά δευτερόλεπτο. Παρόλο που τα περισσότερα σωματίδια που δημιουργούνται είναι ασταθή, διασπώνται σε πιο σταθερά που ανιχνεύονται από τον CMS. Ανιχνεύοντας όλα τα σταθερά σωματίδια, μετρώντας την ορμή και την ενέργειά τους, ο ανιχνευτής μπορεί να ανασυνθέσει την "εικόνα" της σύγκρουσης για περαιτέρω μελέτη.

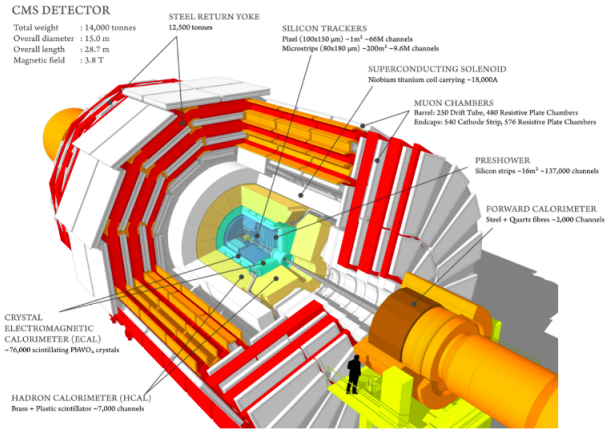

Σχήμα 4: *Ανιχνευτής CMS*

Το όνομα του ανιχνευτή προέρχεται από το γεγονός ότι αν και ο ανιχνευτής είναι μικρός (15μ ύψος και 20μ μήκος - **Compact**), πετυχαίνει τον στόχο του. Επίσης, έχει σχεδιαστεί για να ανιχνεύει μιόνια (**Muon**) με μεγάλη ακρίβεια και αποτελείται από τον μεγαλύτερο υπεραγώγιμο μαγνήτη(**Solenoid**).

Η λειτουργία του βασίζεται στα εξής:

- **Κάμψη και Χαρτογράφηση σωματιδίων**: Χρειάζεται ένας ισχυρός μαγνήτης για να "κάμψει" τα φορτισμένα σωματίδια, καθώς βγαίνουν από το σημείο των συγκρούσεων. Αυτή η "κάμψη" έχει δύο στόχους:
  - Τον προσδιορισμό του φορτίου του σωματιδίου, καθώς τα θετικά και αρνητικά σωματίδια κάμπτονται σε διαφορετικές κατευθύνσεις όταν εφαρμόζεται το ίδιο μαγνητικό πεδίο.
  - Τη μέτρηση της ορμής του σωματιδίου, λόγω του ότι τα σωματίδια υψηλής ορμής κάμπτονται λιγότερο από εκείνα χαμηλότερης ορμής.

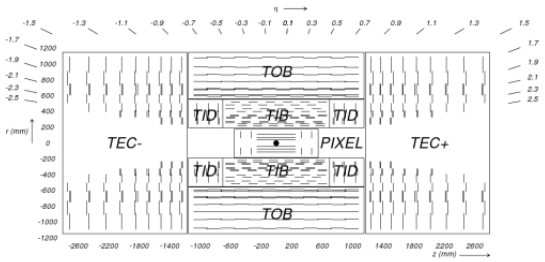

Σχήμα 5: *Ανιχνευτής Τροχιάς του CMS*

- **Μέτρηση Ενέργειας**: Οι πληροφορίες σχετικά με τις ενέργειες των σωματιδίων, που παράγονται κατά τη διάρκεια των συγκρούσεων, είναι πολύ σημαντικές για να καταλάβουμε τι πραγματικά συμβαίνει κατά τη διάρκεια αυτών των συγκρούσεων.

Οι πληροφορίες αυτές συλλέγονται από δύο θερμιδόμετρα. Το Ηλεκτρομαγνητικό Θερμιδομέτρο(ECAL) είναι το εσωτερικό στρώμα και μετρά την ενέργεια των φωτονίων και των ηλεκτρονίων σταματώντας τα εντελώς. Τα αδρόνια, τα οποία αποτελούνται από κουάρκ και γλουόνια, περνούν από το ECAl και σταματούν στο εξωτερικό στρώμα, το Αδρονικό Θερμιδόμετρο(HCAL). Τα θερμιδόμετρα αποικονίζονται στα ακόλουθα σχήματα:

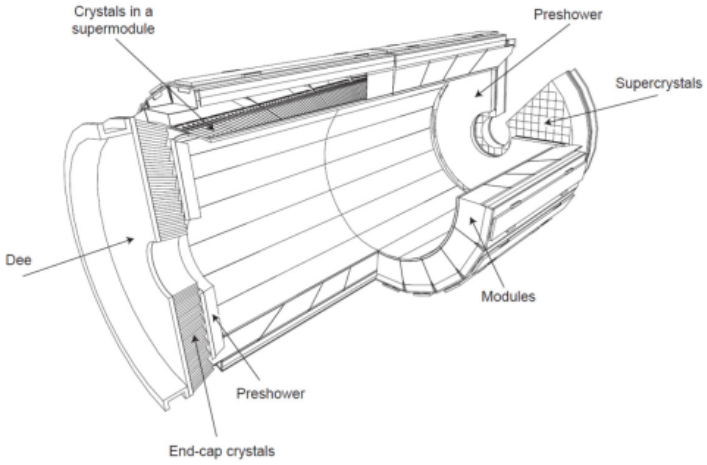

Σχήμα 6: *Θερμιδόμετρο ECAL*

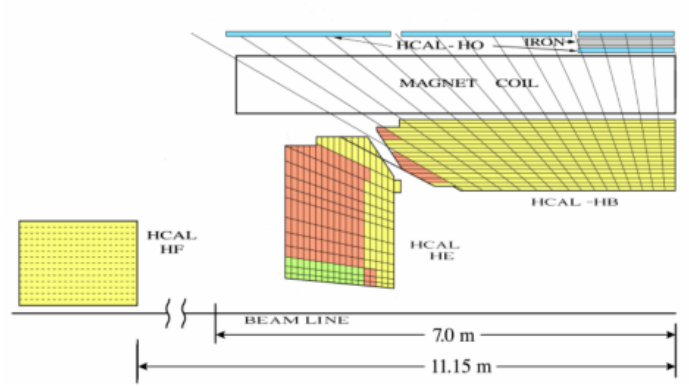

Σχήμα 7: *Θερμιδόμετρο HCAL*

- **Ανίχνευση Μιονίων**: Το σωματίδιο που ανιχνεύεται από τον CMS είναι το μιόνιο, το οποίο είναι 200 φορές βαρύτερο από το ηλεκτρόνιο. Τα μιόνια δεν σταματούν στα θερμιδόμετρα, οπότε έπρεπε να δημιουργηθεί ένα ειδικό σύστημα ανίχνευσης μιόνων. Το σύστημα ανίχνευσης μιονίων (Σχήμα 8) έχει συνολική κάλυψη $|\eta| < 2.4$ και αποτελείται από ένα συνδυασμό ανιχνευτών τριών διαφορετικών τύπων[2]:

[2]Περισσότερες πληροφορίες για τους επιμέρους τύπους θα δοθούν στο αγγλικό μέρος της εργασίας

– **Drift Tube (DT) Chambers**
– **Cathode Strip Chamber (CSC)**
– **Resistive Plate Chambers (CSC)**

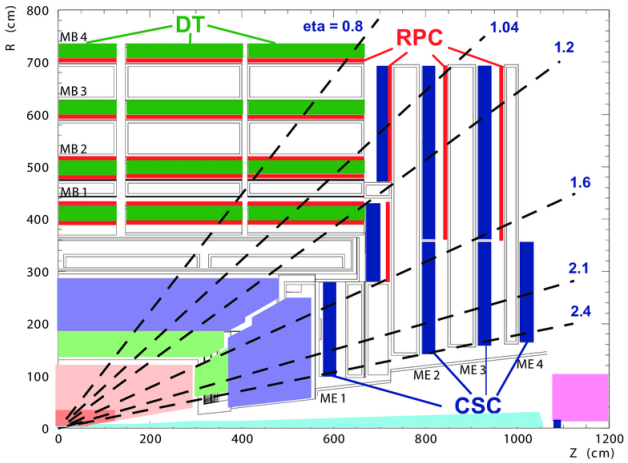

Σχήμα 8: *Διαμήκης όψη του συστήματος ανίχνευσης μιονίων*

Γεγονότα Σήματος και Υποβάθρου

Η single top παραγωγή επιτυγχάνεται δια της αλληλεπίδρασης φορτίου-ρεύματος μέσω ανταλλαγής μποζονίου W και χωρίζεται σε τρεις κατηγορίες: το t-κανάλι[3], το tW-κανάλι και το s-κανάλι. Από αυτά, το t-channel είναι το κυρίαρχο. Αντιμετωπίζουμε το t-channel ως σήμα. Σε αυτόν το φασικό χώρο, η τελική κατάσταση αποτελείται από ένα νετρίνο, ένα λεπτόνιο και έναν πίδακα (jet) αποτελούμενος από b quarks[4]. Το διάγραμμα Feynman είναι:

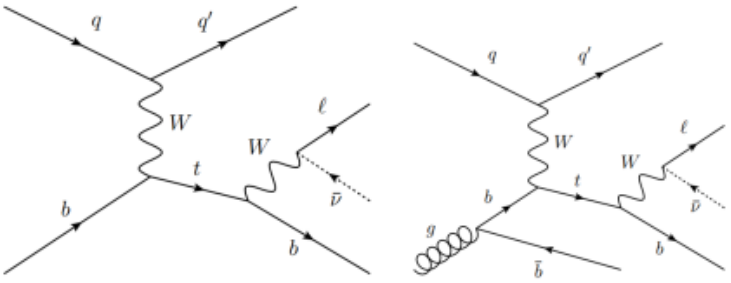

Σχήμα 9: *Διαγράμματα Feynman single top παραγωγής*

[3]Στο εξής θα αναφέρεται ως t-channel
[4]Θα καλείται b-tagged jet στη συνέχεια

Στην παρούσα ανάλυση θα ασχοληθούμε με το αριστερό διάγραμμα Feynman.

Στην παραγωγή $t\bar{t}$, η περίπτωση ενδιαφέροντος είναι αυτή όπου το μποζόνιο W που προέρχεται από το top κουάρκ διασπάται λεπτονικά, ενώ το άλλο διασπάται αδρονικά. Το διάγραμμα Feynman είναι:

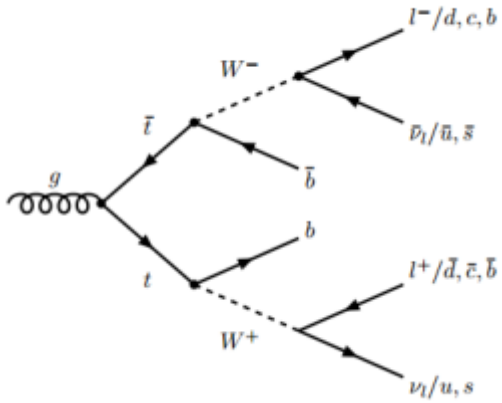

Σχήμα 10: *Διάγραμμα Feynman $t\bar{t}$ παραγωγής*

Στην ανάλυση μας, έχουμε και δύο επιπλέον διεργασίες υποβάθρου τις $W+jets$[5] και QCD Multijet, οι οποίες χαρακτηρίζονται ως δευτερεύοντα υπόβαθρα. Τα αντίστοιχα διαγράμματα Feynman είναι:

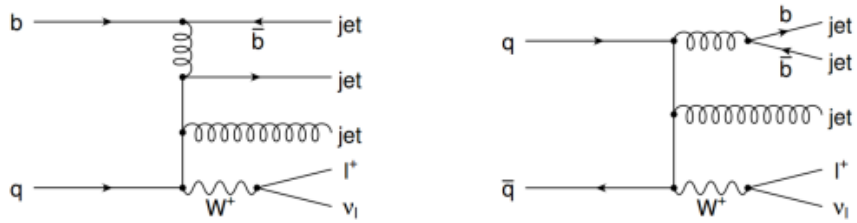

Σχήμα 11: *Διαγράμματα Feynman $W+jets$ διεργασίας*

[5]Θεωρείται ως το ηλεκτρασθενές υπόβαθρο

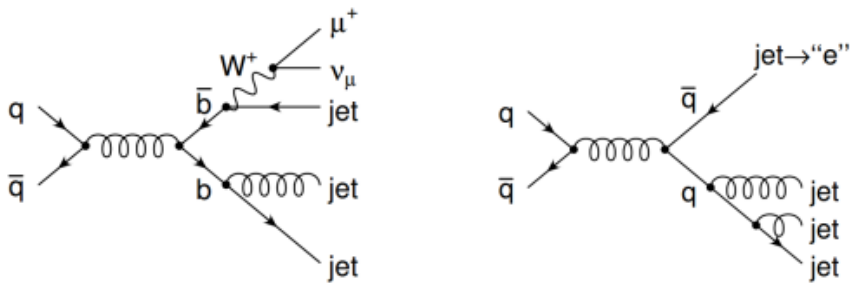

Σχήμα 12: *Διάγραμμα Feynman QCD Multijet διεργασίας*

Ανάλυση Δεδομένων

Όλη η ανάλυση ξεκίνησε από τη μοντελοποίηση των διαθέσιμων Monte Carlo δειγμάτων. Κάθε δείγμα περιέχει ορισμένες στατιστικές διακυμάνσεις, που συσχετίζονται με τον αριθμό των συμβάντων που δημιουργούνται. Όσα περισσότερα γεγονότα δημιουργούνται, τόσο λιγότερες είναι οι διακυμάνσεις. Αντιμετωπίζουμε κάθε δείγμα ως ξεχωριστό σύνολο δεδομένων. Όπως έχουμε αναφέρει, η τελική κατάσταση σήματος αποτελείται από ένα απομονωμένο λεπτόνιο, ένα νετρίνο και δύο jets, ένα εκ των οποίων πρέπει να είναι b-tagged. Για το λεπτόνιο, εξετάζουμε την περίπτωση του μιονίου (αντι-μιονίου). Όλα αυτά είναι, στην ουσία, κανόνες επιλογής που εφαρμόζονται στα δείγματα και καλούνται cuts (περιορισμοί). Πιο συγκεκριμένα, όλοι οι περιορισμοί που εφαρμόζονται για την απόκτηση της επιθυμητής τελικής κατάστασης είναι:

- Ακριβώς δύο jets, εκ των οποίων το ένα να είναι b-tagged
- Ακριβώς ένα λεπτόνιο, είτε μιόνιο είτε αντι-μιόνιο
- Καθόλου isolated και veto λεπτόνια
- Για την εγκάρσια ορμή του λεπτονίου $\longrightarrow p_{T,lepton} > 30$ GeV με $|\eta| < 2.4$
- Για την εγκάρσια ορμή των jets $\longrightarrow p_{T,jets} > 30$ GeV με $|\eta| < 2.4$ για το b-tagged και $|\eta| < 4.7$ για το non b-tagged (ή αλλιώς light jet).

Επίσης, τα λεπτόνια πρέπει να ενεργοποιούν τους HL triggers της "ισχυρής απομόνωσης", οι οποίοι για τα μυόνια είναι οι:

- HLT_IsoMu27_v
- HLT_IsoTkMu24_v

Αλγόριθμος ανακατασκευής του top κουάρκ

Όπως γνωρίζουμε, σε κάθε κορυφή ενός διαγράμματος Feynman, η τετραορμή διατηρείται. Για την tWb κορυφή έχουμε:

$$p_{top} = p_W + p_b \tag{5}$$

και για την Wlv αντίστοιχα:

$$p_W = p_l + p_v \tag{6}$$

Το νετρίνο δεν ανιχνέυεται, άρα πρέπει με κάποιον τρόπο να εκτιμήσουμε την ορμή του. Για το εγκάρσιο επίπεδο ορίζουμε την "Ελλείπουσα Εγκάρσια Ορμή" ως:

$$\not{\vec{p}}_T = -\sum_i \vec{p}_{T,i} \tag{7}$$

και υποθέτουμε ότι ισούται με την εγκάρσια ορμή του νετρίνο. Όμως, ακόμα και με αυτή την υπόθεση, η συντεταγμένη της ορμής στο άξονα z παραμένει άγνωστη. Για να την εκτιμήσουμε, θεωρούμε ότι το μποζόνιο W έχει σταθερή μάζα ίση με $M_W = 80.4\text{GeV}$. Έτσι καταλήγουμε στην εξής σχέση:

$$p_{z,v} = \frac{\Lambda p_{z,l}}{p_{T,l}^2} \pm \frac{1}{p_{T,l}^2}\sqrt{\Lambda^2 p_{z,l}^2 - p_{T,l}^2\,(E_l^2 \not{p}_T^2 - \Lambda^2)}, \qquad \Lambda = \frac{M_W^2}{2} + \vec{p}_{T,l} \cdot \not{\vec{p}}_T \tag{8}$$

Στην περίπτωση της θετικής διακρίνουσας προκύπτουν δύο λύσεις και διαλέγουμε την μικρότερη κατά απόλυτη τιμή. Για την αρνητική διακρίνουσα, προκύπτουν μη πραγματικές λύσεις, κάτι το οποίο είναι μη φυσικά αποδεκτό. Η λύση σε αυτό το πρόβλημα έρχεται από της εξής διαδικασία:

- Απαιτούμε την διακρίνουσα να είναι μηδέν
- Αυτή η νέα συνθήκη δίνει δύο καμπύλες στο εγκάρσιο επίπεδο. Κάθε μία είναι υποψήφια για την $\vec{p}_{T,v}$.
- Επιλέγεται η λύση που αντιστοιχεί στην ελάχιστη απόσταση μεταξύ $\vec{p}_{T,v}$ και $\not{\vec{p}}_T$.

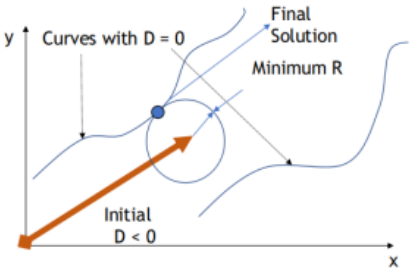

Σχήμα 13: *Σχηματική αναπαράσταση του αλγόριθμου για την περίπτωση αρνητικής διακρίνουσας*

Διαχωρισμός Σήματος και Υποβάθρου

Σε αυτό το σημείο να αναφέρουμε ότι, η κανονικοποιήση των δεδομένων, έχει γίνει σε αναλογία με την ενεργό διατομή της κάθε διεργασίας, σύμφωνα με τον τύπο:

$$N_{exp} = \sum_i \sigma_i L_{int} \frac{Ni, pass}{N_{i,gen}} \tag{9}$$

Αναφέραμε προηγουμένως, ότι ο στόχος μας είναι ένας καλός διαχωρισμός μεταξύ του σήματος και των διάφορων υποβάθρων. Επίσης, από τον αλγόριθμο ανακατασκευής, έχουμε έναν εκτιμητή για τη μάζα του top quark. Τώρα, εάν ορίσουμε κάποιες μεταβλητές, οι οποίες έχουν ισχυρή συσχέτιση με τον εκτιμητή και μπορούν να διακρίνουν το σήμα από το υπόβαθρο, η διαχωρησιμότητα θα επιτευχθεί.

Οι μεταβλητές που χρησιμοποιούμε είναι οι εξής:

- Ψευδο-ωκύτητα του light jet($\eta_{lightjet}$): Από το διάγραμμα Feynman της single top παραγωγής παρατηρούμε ότι το q quark είναι forward.

- $cos(\theta^*)$: Πρόκειται για την γωνία μεταξύ του λεπτονίου και του non b-tagged jet στο σύστημα κέντρου μάζας του top quark. Την επιλέγουμε λόγω του ότι το top quark είναι αρκετά πολωμένο.

- Γωνιακή απόσταση μεταξύ του λεπτονίου και του light jet($DR_{lep/lightjet}$): Η συγκεκριμένη μεταβλητή επιλέγεται για να διαχωρίσει τα ηλεκτρασθενή υπόβαθρα.

Κοιτώντας τα ιστογράμματα των άνω μεταβλητών, μπορούμε να αποφανθούμε, για μία αρχική εκτίμηση, σε ποια τιμή αρχίζει να διαφαίνεται ο διαχωρισμός μεταξύ σήματος και υποβάθρων.

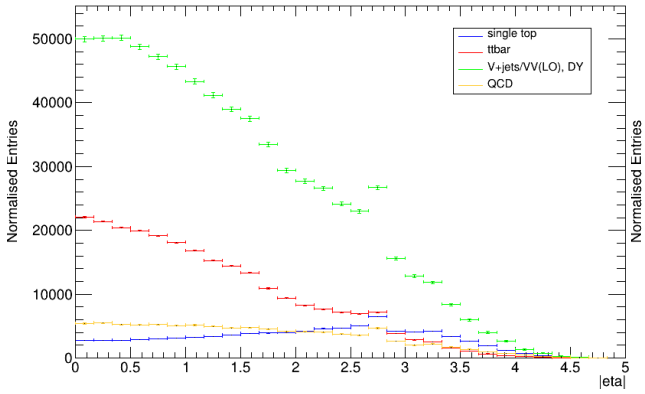

(a) $\eta_{lighjet}$

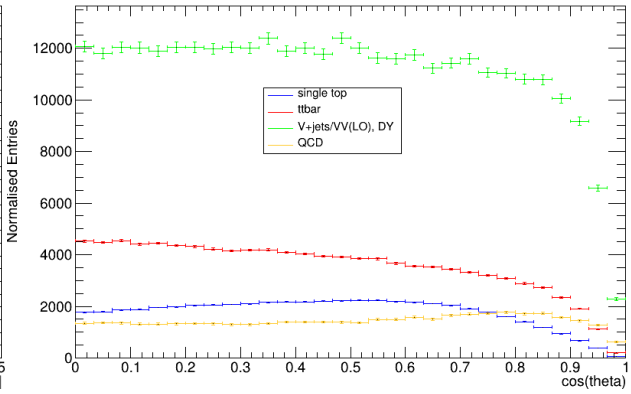

(b) $cos\theta^*$

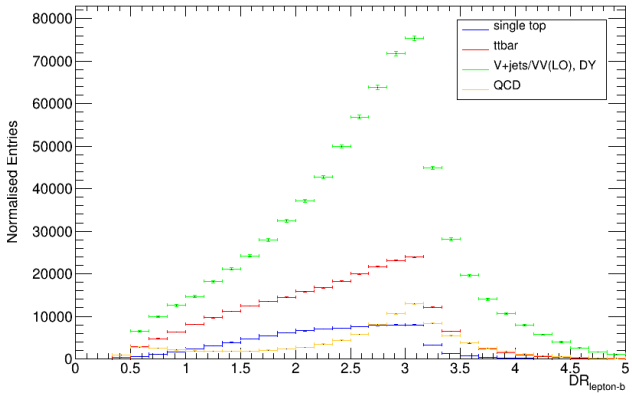

(c) $DR_{lep/lightjet}$

Σχήμα 14: *Υποψήφιες μεταβλητές*

Στη συνέχεια, ξεκινώντας από μία εκ των τριών μεταβλητών και παίρνοντας σαν αρχική τιμή (pivot value) την αρχική εκτίμηση, ορίζουμε ένα βήμα μεταβολής. Έπειτα, εξετάζουμε κάθε φορά την τιμή του πηλίκου των γεγονότων σήματος προς τα γεγονότα υποβάθρου. Όταν βρούμε ένα μέγιστο, σταματάμε, εφαρμόζουμε την παρούσα τιμή ως cut (περιορισμό) για την μεταβλητή και συνεχίζουμε στην επόμενη μεταβλητή.

Για να ελαχιστοποιήσουμε το υπόβαθρο της QCD ορίζουμε μία τέταρτη μεταβλητή, την εγκάρσια μάζα του μποζονίου W. Ο λόγος που επιλέξαμε τη συγκεκρίμενη μεταβλητή, στηρίζεται στο γεγονός ότι στην QCD δεν έχουμε W μποζόνια. Οι τιμές των περιορισμών (cuts) για κάθε μεταβλητή είναι:

- $|\eta_{lightjet}| > 2.5$
- $cos\theta^* > 0.2$
- $DR_{lep/lightjet} < 2.2$
- $m_{T,W} > 50\text{GeV}$

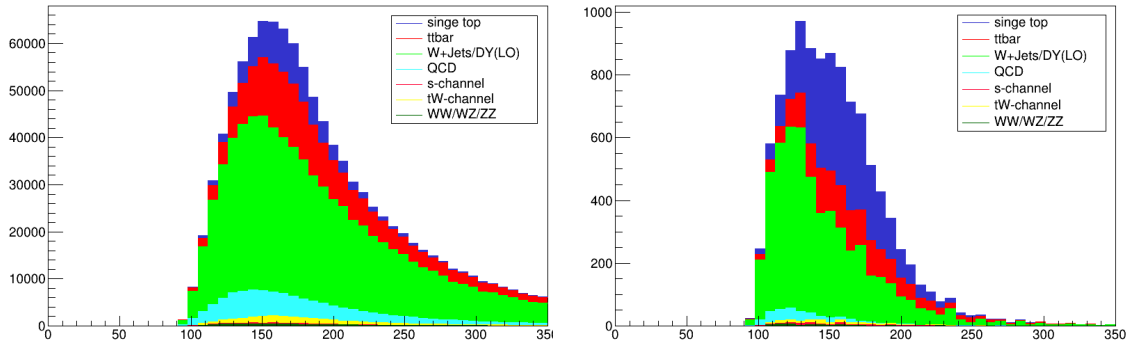

(a) *Πριν την εφαρμογή των cuts* **(b)** *Μετά την εφαρμογή των cuts*

Σχήμα 15: *Εκτιμητής* m_{lvb}

Μοντελοποίηση Σήματος και Υποβάθρων

Σε αυτό το σημείο, πρέπει να βρούμε μια συνάρτηση ή έναν συνδυασμό συναρτήσεων, που να περιγράφουν τις συναρτήσεις πυκνότητας πιθανότητας του σήματος και των υποβάθρων.

Για το σήμα χρησιμοποιούμε την εξής συνάρτηση πυκνότητα πιθανότητας:

$$F_{t-ch} = f_{sig} Lognormal(\mu_{log}, \sigma_{log}) + (1 - f_{sig}) CrystallBall(\mu_{log}, \sigma_{CB}, a_{CB}, n_{CB}) \quad (10)$$

με τον συντελεστή f_{sig} να δείχνει τη σχετική συνεισφορά μεταξύ της Lognormal και της Crystal Ball κατανομής για την περιγραφή. Εργαζόμενοι για το δείγμα 172.5GeV προκύπτει το ακόλουθο σχήμα:

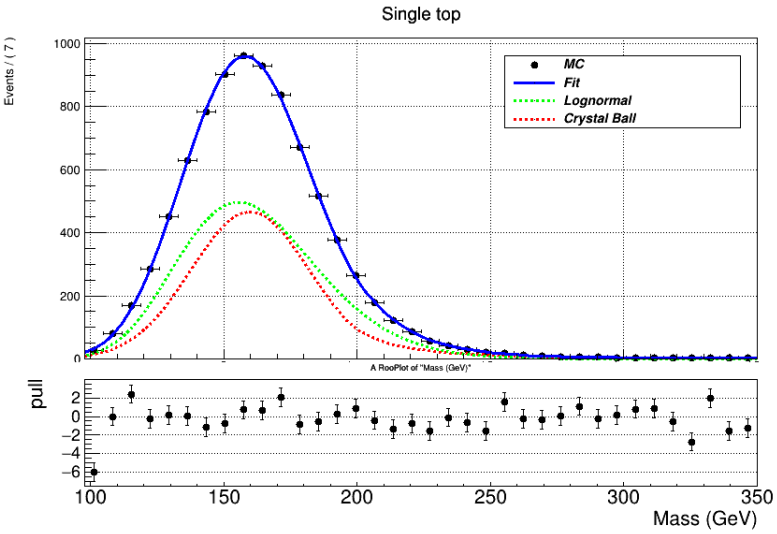

Σχήμα 16: *Προσαρμογή συνάρτησης πυκνότητας πιθανότητας στα δεδομένα σήματος*

Για το κύριο υπόβαθρο, προερχόμενο από $t\bar{t}$ παραγωγή, χρησιμοποιούμε την εξής συνάρτηση:

$$F_{t\bar{t}} = f_{t\bar{t}} Gauss(\mu_g, \sigma_g) + (1 - f_{t\bar{t}}) Novosibirsk(\mu_g, \sigma_{novo}, \tau) \tag{11}$$

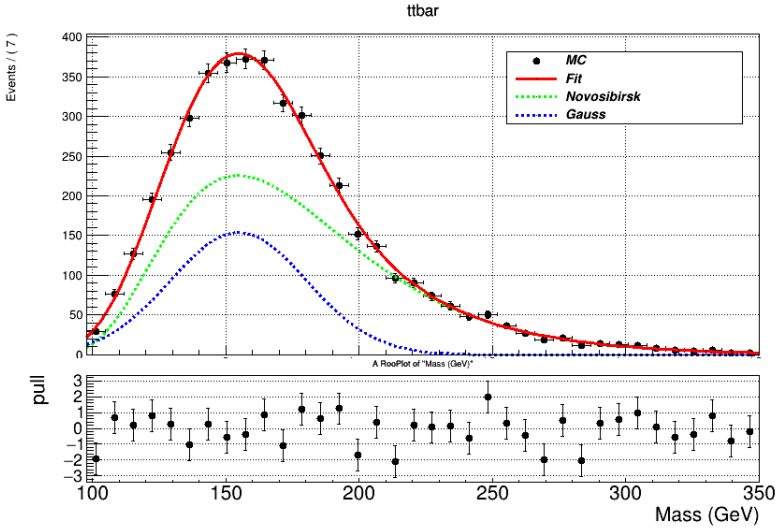

Σχήμα 17: *Προσαργμογή συνάρτησης πυκνότητας πιθανότητας στα δεδομένα $t\bar{t}$ παραγωγής*

Για το ηλεκτρασθενές υπόβαθρο εργαζόμαστε με την εξής κατανομή:

$$F_{EWK} = Novosibirsk(\mu_{EWK}, \sigma_{EWK}, \tau) \tag{12}$$

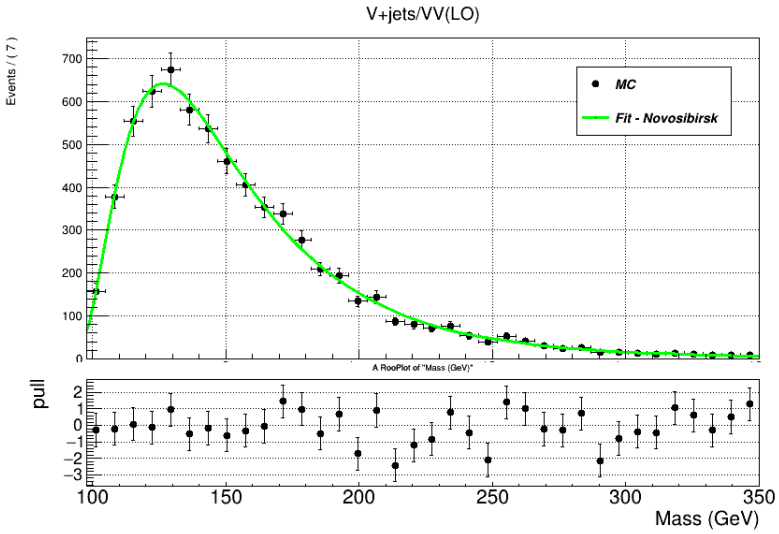

Σχήμα 18: *Προσαρμογή συνάρτησης πυκνότητας πιθανότητας στα δεδομένα ηλεκτρασθενούς υποβάθρου*

Όσον αφορά στην περιγραφή της QCD, πρέπει να αναφέρουμε ότι η μοντελοποίηση της συνάρτησης πυκνότητας πιθανότητας δεν έγινε από τα Monte Carlo δείγματα. Ο βασικός λόγος στηρίζεται στο γεγονός ότι μετά την εφαρμογή όλων των cuts, των βασικών για την τελική κατάσταση και των επιπλέον για τη μεγιστοποίηση της διαχωρισιμότητας του σήματος, ο αριθμός των τελικών γεγονότων από τα δείγματα της QCD ήταν αρκετά μικρός, με αποτέλεσμα να μην υπάρχει ικανοποιητική στατιστική περιγραφή. Η μοντελοποίηση λοιπόν έγινε μέσω των δεδομένων. Η διαδικασία που ακολουθήθηκε είναι η εξής:

- Στην single top περιοχή, απαιτήσαμε να μην έχουμε απομονωμένα λεπτόνια και οι triggers που θα ενεργοποιηθούν, να αντιστοιχούν στα μη απομονωμένα λεπτόνια.

- Στη συνέχεια, μεταβαίνουμε στον φασικό χώρο των απομονωμένων λεπτονίων και απαιτούμε μόνο απομονωμένα λεπτόνια μαζί με την ενεργοποίηση των αντίστοιχων triggers.

- Τέλος, για να μπορούμε να χρησιμοποιήσουμε αυτή τη θεώρηση στην ανάλυση των Monte Carlo δειγμάτων, πρέπει να κανονικοποιηθούν τα τελικά events (γεγονότα) με τον παράγοντα που παίρνουμε από την υπόθεση: $N_{QCD} = N_{data} - N_{MC}$.

Η συνάρτηση πυκνότητας πιθανότητας, που περιγράφει την QCD διεργασία, είναι:

$$F_{QCD} = Novosibirsk(\mu_{QCD}, \sigma_{QCD}, \tau) \tag{13}$$

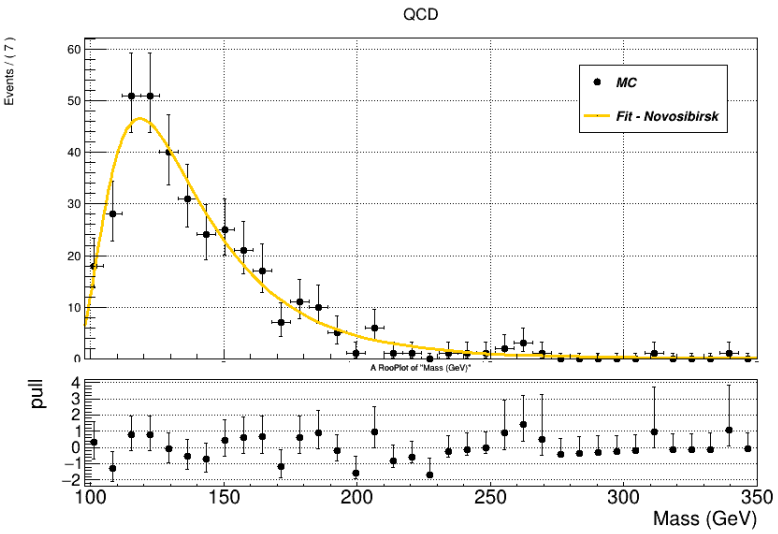

Σχήμα 19: *Προσαρμογή συνάρτησης πυκνότητας πιθανότητας στα δεδομένα της QCD διεργασίας*

Ολική Προσαρμογή στα δείγματα Monte Carlo

Βρίσκοντας την κατάλληλη κατανομή για κάθε διεργασία, είμαστε σε θέση να εξάγουμε την κατανομή για την ολική περιγραφή των διεργασιών. Η ολική συνάρτηση πυκνότητας πιθανότητας γράφεται ως:

$$F_{total} = r_{sig}F_{t-ch} + r_{t\bar{t}}F_{t\bar{t}} + r_{EWK}F_{EWK} + r_{QCD}F_{QCD} \tag{14}$$

όπου οι συντελεστές r_i δείχνουν τη συνεισφορά κάθε διεργασίας.

Το διάγραμμα της ολικής προσαρμογής στα δείγματα Monte Carlo είναι:

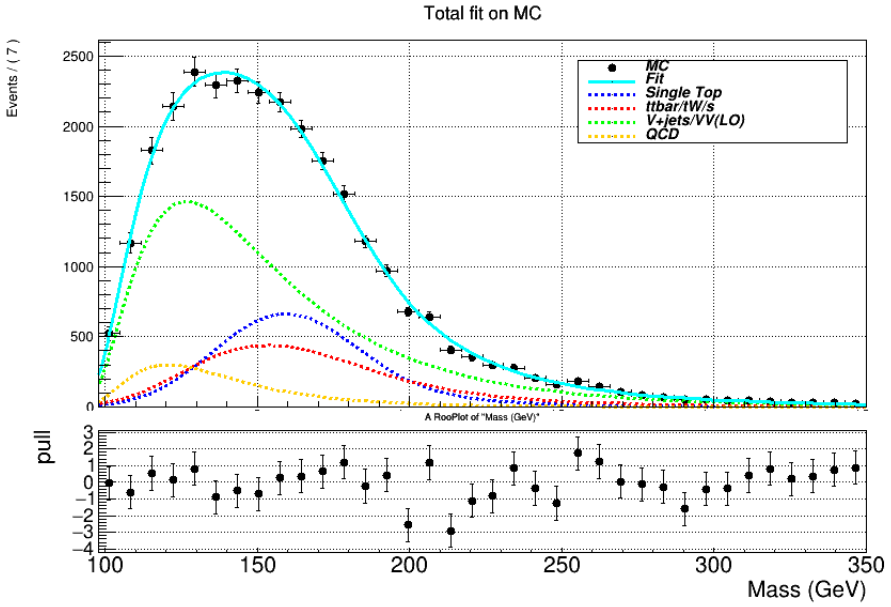

Σχήμα 20: *Ολική Προσαρμογή στα MC*

Ένας τρόπος να ελέχξουμε αν η περιγραφή εκτελείται σωστά είναι να δούμε αν οι συναρτήσεις μέγιστης πιθανοφάνειας της εκτιμώμενης ποσότητας m_{top}^{MC} και των συντελεστών r_i διέπονται από συνεχή παραβολική περιγραφή.

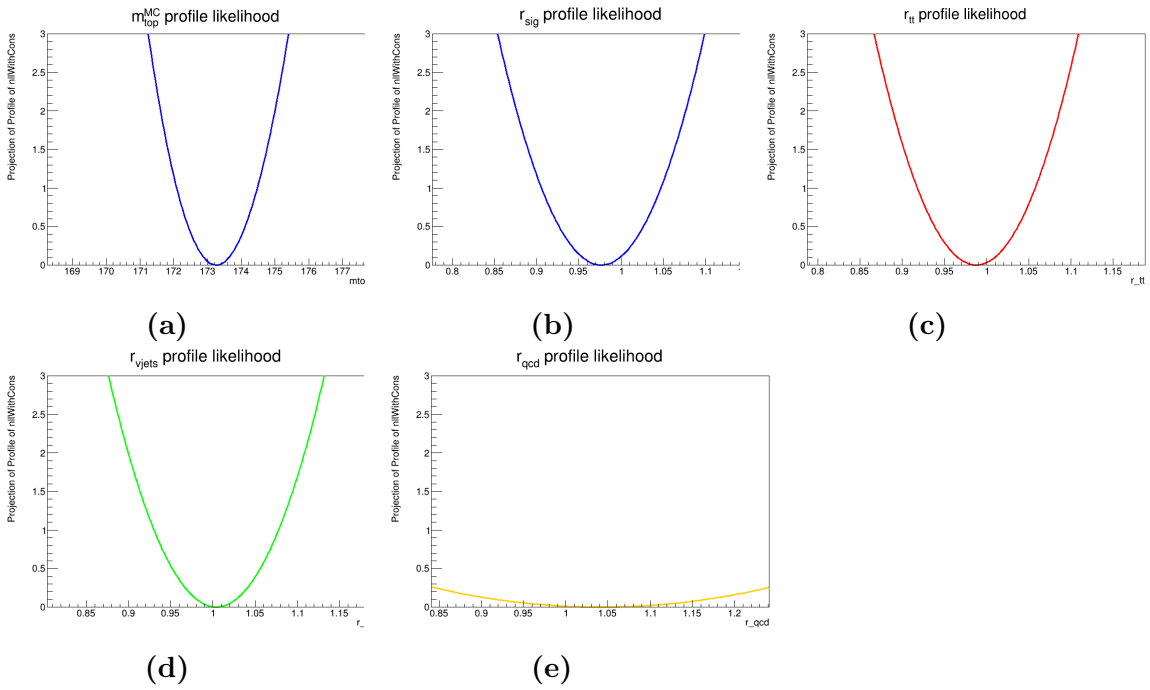

Σχήμα 21: *Συναρτήσεις Μέγιστης Πιθανοφάνειας*

Στη συνέχεια, πρέπει να ελέγξουμε την αμεροληψία του εκτιμητή. Τον έλεγχο τον πραγματοποιούμε μέσω των toys Monte Carlo. Τα βήματα που ακολουθούμε είναι:

- Χρησιμοποιούμε το μοντέλο που έχουμε φτιάξει, ως γεννήτρια ψευδο-δεδομένων.
- Παράγουμε ένα αρκετά μεγάλο αριθμό ψευδο-δεδομένων και πραγματοποιούμε την ολική προσαρμογή σε αυτά.
- Επαναλαμβάνουμε πολλες φορές ($N_{toys} = 1000$).

Αναμένουμε όλα τα toys να ακολουθούν γκαουσιανή κατανομή, με μέση τιμή 0 και τυπική απόκλιση 1. Δεδομένων στατιστικών διακυμάνσεων, θέλουμε τις τιμές αυτές όσο το δυνατόν πιο κοντά στις θεωρητικά αναμενόμενες.

Εκτελώντας όλη τη διαδικασία προκύπτουν τα ακόλουθα:

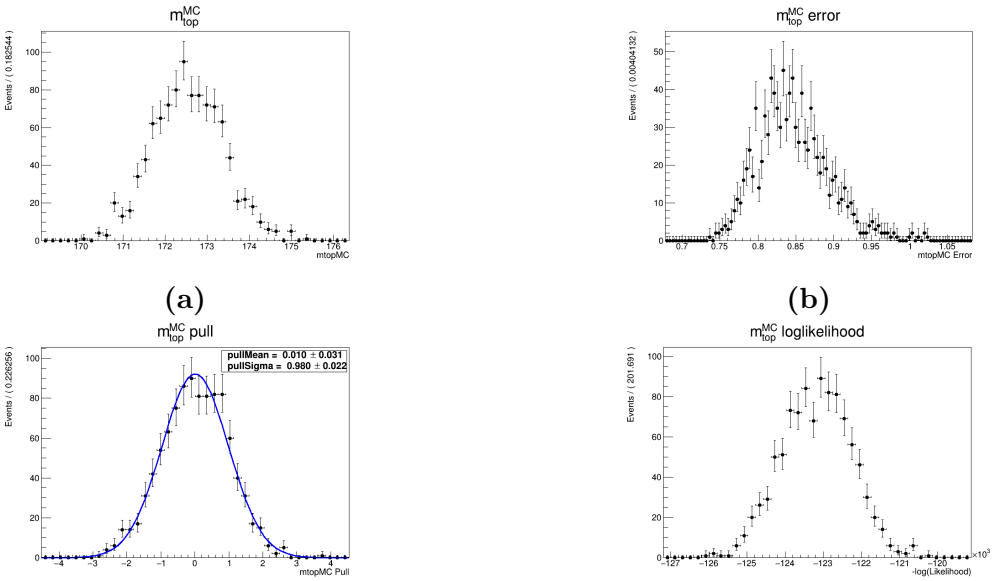

Σχήμα 22: *Monte Carlo toys*

Ολική Προσαρμογή στα δεδομένα

Έχοντας ελέχξει την υγιή συμπεριφορά της ολικής περιγραφής και επιβεβαιώσει την αμεροληψία του εκτιμητή, μπορούμε τώρα να εφαρμόσουμε το μοντέλο αυτό στα πραγματικά δεδομένα. Ως αποτέλεσμα προκύπτει το ακόλουθο σχήμα:

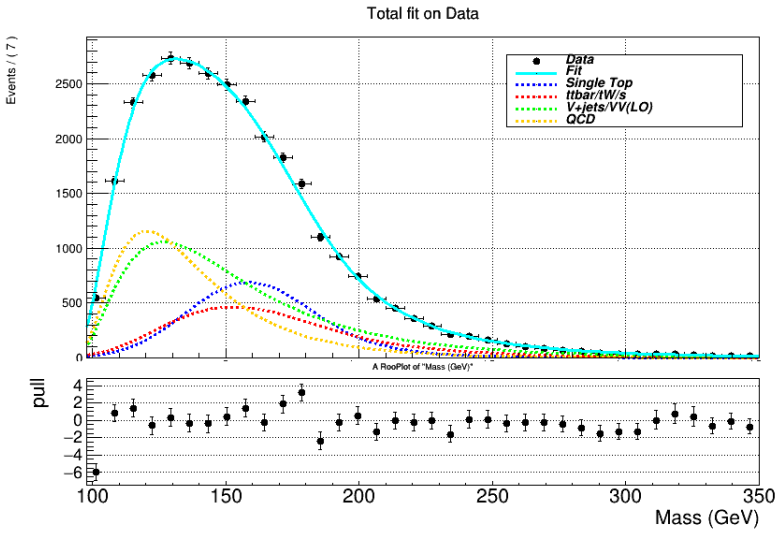

Σχήμα 23: *Ολική προσαρμογή στα δεδομένα*

Από την ολική προσαρμογή στα δεδομένα, προκύπτει μια εκτίμηση για την μάζα του top κουάρκ, την m_{fit}, καθώς και για το αντίστοιχο σφάλμα της, οι οποίες όμως

δεν είναι οι πραγματικές τιμές. Για να προκύψουν οι πραγματικές τιμές, θεωρούμε τον εξής γραμμικό μετασχηματισμό:

$$m_{fit} = a * m_{true} + b \Leftrightarrow m_{true} = \frac{m_{fit} - b}{a} \tag{15}$$

Οι συντελεστές a, b, καθώς και τα αντίστοιχα σφάλματά τους, θα προέλθουν από την βαθμόνηση των Monte Carlo δειγμάτων, όπου απαιτούμε γραμμική εξάρτηση του εκτιμητή. Η βαθμονόμηση δίνει:

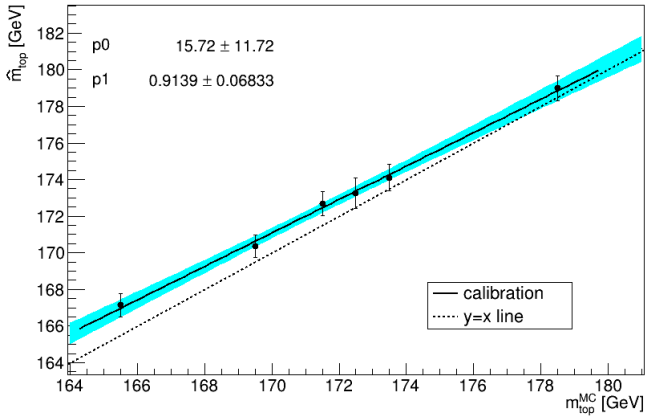

Σχήμα 24: *Μέθοδος Βαθμονόμησης*

Όσον αφορά στο σφάλμα της μέτρησης, το σφάλμα της m_{true}, θα προέλθει μέσω διάδοσης του σφάλματος σύμφωνα με τον τύπο:

$$(\sigma_y)^2 = \sum_{i=1}^{N}\sum_{j=1}^{N} \frac{\partial y}{\partial P_i}\frac{\partial y}{\partial P_j}\rho_{ij\sigma_{P_i}\sigma_{P_j}} \tag{16}$$

Οι συντελεστές συσχέτισης ρ_{ij} θα υπολογισθούν μέσω του πίνακα συνδιακύμανσης.

Αποτελέσματα

Έχοντας εφαρμόσει όλα όσα αναφέραμε, εξάγουμε την ακόλουθη τιμή για την μάζα του top quark:

$$m_t = 171.31 \pm 0.85(stat.) \tag{17}$$

Η συγκεκριμένη μάζα προκύπτει από θεώρηση ότι στην τελική κατάσταση απαιτούμε μιόνιο ανέξαρτητα φορτίου. Αν απαιτήσουμε μόνο θετικά μιόνια και μόνο αρνητικά μιόνια, έχουμε αντίστοιχα:

$$\begin{aligned} m_t &= 171.66 \pm 1.08(stat.)GeV \\ m_{\bar{t}} &= 170.77 \pm 1.29(stat.)GeV \end{aligned} \tag{18}$$

Το πηλίκο της μάζας του anti-top quark προς το top quark είναι:

$$R_{m_t} = \frac{m_t}{m_{\bar{t}}} = 0.995 \pm 0.009(stat.) \tag{19}$$

και η διαφορά μάζας εκτιμάται ίση με:

$$\Delta_{m_t} = m_t - m_{\bar{t}} = 0.89 \pm 1.56(stat.)GeV \tag{20}$$

Παρατηρούμε ότι οι τιμές στις μάζες είναι αρκετά κοντά, η διαφορά τους κοντά στο 0 και ο λόγος τους περίπου ίσος με 1. Οι μετρήσεις αυτές, λειτουργούν ως ένα μέσο επαλήθευσης της αναλλοιώτητας της CPT συμμετρίας. Τα αποτελέσματα είναι συμβατά με την πρόβλεψη του Καθιερωμένου Προτύπου.

Chapter 1

Introduction

1.1 Standard Model

1.1.1 A Brief Introduction

After numerous theories, experiments and discoveries we have gained insight into the fundamental structure of matter: everything in the universe is made from tiny building blocks that we call fundamental particles, which are governed by four fundamental forces. Everything we know so far, about the nature and the interactions of these particles and forces is encapsulated in the **Standard Model** of particle physics. The Standard Model, developed in the early 1970s, is a well-tested modern physics theory.

The four fundamental forces are: the gravitational force, the electromagnetic force, the weak and the strong force. They have differences in the strength and the range that they work. Gravity is the weakest but has infinite range. The electromagnetic force has also infinite range but is much stronger than the gravity. The weak and the strong force dominate at subatomic level.

There are two main categories of fundamental particles, fermions and bosons. The main difference is the spin, bosons have integer spin and fermions have half-integer spin.

The fermions are divided in two categories:

- **Leptons**: This category consists of three elementary particles(electron,muon,tau) and each one of them has a corresponding neutrino(electron neutrino,muon neutrino, tau neutrino). The three leptons differ only in their masses and they have the same charge. The neutrinos are charge-less and their mass is significally low.

- **Quarks**: This category consists of six elementary particles. The six quarks are paired in three generations – the "up quark" and the "down quark" form

the first generation, followed by the "charm quark" and "strange quark", then the "top quark" and "bottom (or beauty) quark". Quarks also come in three different "colours" and only mix in such ways as to form colourless objects. The lightest and most stable particles make up the first generation, whereas the heavier and less-stable particles belong to the second and third generations. All stable matter in the universe is made from particles that belong to the first generation, the heavier particles quickly decay to more stable ones.

The bosons are also divided in two categories:

- **Gaugse Bosons**: This category consists of four particles(photon,gluon,Z^0 and $W^{\pm}$ boson). These particles are called "force carries" because in a sense they "carry" the fundamental forces. What happens in reality is that a fundamental force results with the exchange of one of these particles whenever a particle interaction occurs. The photon carries the electromagnetic, the gluon carries the strong force and the Z^0 and $W^{\pm}$ bosons carry the weak force. For gravity, the hypothesized force carrier is the graviton which is yet to be discovered.

- **Scalar Bosons**: The only one scalar boson which has been found until today is the Higgs boson. Through Higgs mechanism, the Higgs boson in a sence "gives" mass to the Z^0, $W^{\pm}$ and to fermions. The Higgs boson is mass-less and has 0 spin.

All the fundamental particles along with their characteristics are summarised in the next figure:

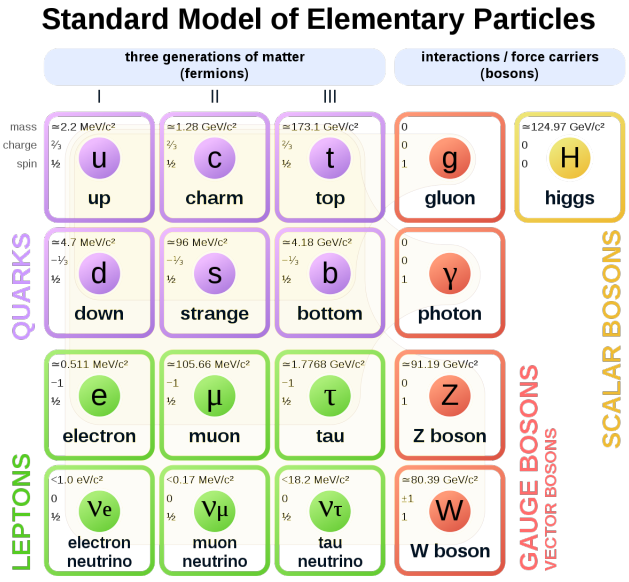

Figure 1.1: *Standard Model of Particle Physics*

1.1.2 Lagrangian of Standard Model

The symmetry group that describes the Standard Model is $SU(3) \times U(1) \times SU(2)$. In the next sections we will make a short analysis of each part in order to understand the nature that Standard Model describes.

1.1.3 U(1) gauge transformation - QED Lagrangian

We begin by defining two kinds of gauge transformations, the global and the local:

$$\begin{aligned} Global: \quad & \Psi \longrightarrow e^{ia}\Psi, \quad a \in \mathbb{R} \\ Local: \quad & \Psi \longrightarrow e^{iQ\theta(x)}\Psi \end{aligned} \tag{21}$$

We know that fermions of spin$\frac{1}{2}$ satisfy the Lagrangian:

$$\mathcal{L} = \overline{\Psi}(i\not{\partial} - m)\Psi \tag{22}$$

This Lagrangian expression is invariant under the global U(1) transformation, which from Noether's theorem, means that we have a conservation of a quantity. In our case, that quantity is the total charge. But, if we demand conservation of local charge, meaning applying the local transformation, the invariance breaks [1]. So we have to modify the Lagrangian expression. We do that by defining a covariant derivative as follows:

$$D_\mu = \partial_\mu + iQA_\mu \tag{23}$$

The covariant derivative must satisfy the following local U(1) transformations:

$$\begin{aligned} D_\mu &\longrightarrow D'_\mu = \partial_\mu + iQA'_\mu \\ D_\mu\Psi &\longrightarrow D'_\mu\Psi' = e^{iQ\theta(x)}\Psi D_\mu\Psi \end{aligned} \tag{24}$$

So, the Lagrangian expression becomes:

$$\mathcal{L} = \overline{\Psi}(i\not{D} - m)\Psi \tag{25}$$

We see that from equations (23),(24), the field A_μ transforms as:

$$A_\mu \longrightarrow A'_\mu = A_\mu - \partial_\mu\theta(x) \tag{26}$$

The Lagrangian is now:

$$\mathcal{L} = \overline{\Psi}(i\not{\partial} - m)\Psi - QA^\mu j_\mu \tag{27}$$

j_μ is the Dirac current $j_\mu = \overline{\Psi}\gamma_\mu\Psi$ with $\partial^\mu j_\mu = 0$.

[1] The kinematic term transforms as $\overline{\Psi}i\not{\partial}\Psi \longrightarrow \overline{\Psi'}i\not{\partial}\Psi' = \overline{\Psi}i\not{\partial}\Psi - Q\overline{\Psi}\gamma^\mu(\partial_\mu\theta)\Psi$

We see that, the Dirac current interacts with the field A_μ exactly like in Electromagnetic theory with coupling constant the charge Q. The field A_μ must be mass-less because if we introduce mass terms like $\frac{1}{2}m^2A^\mu A_\mu$ the local invariance breaks.

Now, in order to consider the A_μ as the gauge field of the photon, we have to introduce a new term in the Lagrangian expression. This new term must be invariant under Lorentz and local U(1) transformations and it has to be the kinetic term of the A_μ field.

We define the tensor of the electromagnetic field $F_{\mu\nu}$ as:

$$F_{\mu\nu} = \partial_\mu A_\nu - \partial_\nu A_\mu \tag{28}$$

If we input a term $F_{\mu\nu}F^{\mu\nu}$ for the Lorentz invariance, we obtain the Lagrangian expression for the QED:

$$\mathcal{L}_{QED} = \overline{\Psi}(i\not{\partial} - m)\Psi - QA^\mu j_\mu - \frac{1}{4}F_{\mu\nu}F^{\mu\nu} \tag{29}$$

1.1.4 SU(3) Gauge transformations - QCD Lagrangian

The symmetry that governs the strong interactions is the local gauge transformations of SU(3) group. The SU(3) group has 8 generators A^α_μ and is described by three color fields $\varphi_1, \varphi_2, \varphi_3$. The generators commute as:

$$[T_a, T_b] = if_{abc}T_c \tag{30}$$

We define the covariant derivative as:

$$D_\mu = \partial_\mu + igT_\alpha A^\alpha_\mu \tag{31}$$

So, we obtain the Lagrangian expression for QCD:

$$\mathcal{L}_{QCD} = \overline{\Phi}(i\not{\partial} - m)\Phi - g\sum_{\alpha=1}^{8}(\overline{\Phi}\gamma^\mu T_\alpha \Phi)A^\alpha_\mu - \sum_{\alpha=1}^{8}\frac{1}{4}G^\alpha_{\mu\nu}G^{\mu\nu}_\alpha \tag{32}$$

With the $G^\alpha_{\mu\nu}$ being the field tensor of QCD and is defines as:

$$G^\alpha_{\mu\nu} = \partial_\mu A_\nu - \partial_\nu A_\mu \tag{33}$$

The Lagrangian expression of QCD describes interactions of 3 color fields $\Phi = (\varphi 1 \varphi 2 \varphi 3)^T$ and 8 gluons with coupling constant g.

Analogically with U(1) that demands mass-less photons, the SU(3) invariance demands mass-less gluons.

1.1.5 Higgs Mechanism

From the previous sections, we saw that the invariance under local transformations demands the force carriers to be mass-less. Although, from various experiments we know that the force carriers of the weak interactions($Z^0, W^{\pm}$) have a large mass. To solve that problem, the Higgs Mechanism was introduced.

The mechanism works as:

- We consider a Lagrangian expression symmetric to local transformations
- We consider a potential and with some pertrubations around the region of minimum energy, the symmetry breaks spontaneously giving mass to bosons
- The procedure must satisfy a renormalisation

We consider the following Lagrangian expression:

$$\mathcal{L} = \frac{1}{2}(\partial_\mu \varphi_i)^2 - V(\varphi_i) \tag{34}$$

With $V(\varphi_i)$ being:

$$V(\varphi_i) = \frac{1}{2}\mu^2\varphi_i^2\frac{1}{4} + \lambda\varphi_i^4 \tag{35}$$

For $\lambda > 0$ we have two cases:

- $\mu^2 > 0$ meaning that potential would only have a minimum at 0 and therefore the bosons could not obtain mass with pertrubations
- $\mu^2 < 0$ which is the case we consider

By setting to zero the first derivative of the potential we find the minimum to be a hypersphere of N dimensions and radius $\sqrt{\frac{-\mu^2}{\lambda}}$.

We consider the field $\varphi_{i,0}$:

$$u \equiv \varphi_{i,0} = \frac{-\mu^2}{\lambda} \tag{36}$$

For N=2 we have:

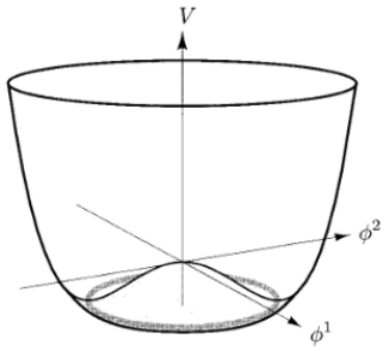

Figure 1.2: *Potential for N=2,* $\lambda > 0$ *and* $\mu^2 < 0$

We consider now the pertrubations and we obtain:

$$\varphi_i(x) = (\xi^\kappa, u + \sigma(x))\,, \quad \kappa = 1, ..., N-1 \quad ||\xi^\kappa||, ||\sigma(x)|| << 1 \tag{37}$$

The Lagrangian becomes:

$$\mathcal{L} = \frac{1}{2}(\partial_\mu \xi^\kappa)^2 + \frac{1}{2}(\partial_\mu \sigma)^2 - \frac{1}{2}(-2\mu^2)\sigma^2 + Interaction\, terms \tag{38}$$

We know also that the Lagrangian expression:

$$\mathcal{L} = \frac{1}{2}(\partial_\mu \varphi)^2 - \frac{1}{2}m^2\varphi^2 \tag{39}$$

describes the scalar potential of particle with mass m and spin 0, because if we take the Euler-Lagrnange equations we obtain the Klein-Gordon equation:

$$(\partial_\mu \partial^\mu + m^2)\varphi = 0 \tag{40}$$

So, the Lagrangian (18) describes N-1 scalar fealds, ξ^κ , $\kappa = 1, ..., N-1$ with zero mass and one scalar field σ with mass $\sqrt{-2\mu^2}$ that they interact with one another.

We came to this conclusion because the field σ describes a pertrubation in radial direction in which the potential has non zero component [2]. The scalar fields ξ^κ describe pertrubations in tangential direction in which the potential has zero component.

The spontaneous symmetry breaking that leads to mass-less particles is called Goldstone Theorem, which indicated that in every spontaneous symmetry breaking we must have at least one mass-less particle that is called Goldstone Boson.

1.1.6 The Weinberg-Salam Model

The Weinberg Salam model describes the symmetry breaking of the Electroweak interaction, in which the bosons $(Z^0, W^\pm)$ gain mass. The initial symmetry is invariant under the transformations SU(2) isospin and U(1) hypercharge.

We know that:

$$Q = I_3 + \frac{Y}{2} \tag{41}$$

We consider the left-handed lepton in doublets of given hypercharge and the right-handed in singlets.

So we have:

$$L_e = \begin{bmatrix} v_e \\ e^- \end{bmatrix}_L, \quad L_\mu = \begin{bmatrix} v_\mu \\ \mu^- \end{bmatrix}_L, \quad L_\tau = \begin{bmatrix} v_\tau \\ \tau^- \end{bmatrix}_L \tag{42}$$

[2] That explains the non zero mass of σ field

The right-handed are: e_R, μ_R, τ_R and the neutrions are always left-handed as mass-less particles.

	ν_{eL}	e_L	e_R	u_L	d_L	u_R	d_R
	$\nu_{\mu L}$	μ_L	μ_R	c_L	s_L	c_R	s_R
	$\nu_{\tau L}$	τ_L	τ_R	t_L	b_L	t_R	b_R
I_3	$+\frac{1}{2}$	$-\frac{1}{2}$	0	$+\frac{1}{2}$	$-\frac{1}{2}$	0	0
Y	-1	-1	-2	$+\frac{1}{3}$	$+\frac{1}{3}$	$+\frac{4}{3}$	$-\frac{2}{3}$
Q	0	-1	-1	$+\frac{2}{3}$	$-\frac{1}{3}$	$+\frac{2}{3}$	$-\frac{1}{3}$

Figure 1.3: *Quantum numbers Q, I_3, Y for leptons*

The transformation $SU(2)_L \times U(1)_Y$ for left-handed and right-handed is respectively:

$$\begin{aligned} L \longrightarrow L' = e^{i\frac{t_\alpha}{2}\theta^\alpha(x) - iY_L\theta(x)} L \\ R \longrightarrow R' = e^{-iY_R\theta(x)} R \end{aligned} \tag{43}$$

In order for the bosons($Z^0, W^\pm$) to gain mass we have to introduce four scalar fields $\varphi_i,\ \ i = 1, 2, 3, 4$. From previous, three mass-less Goldstone bosons will occur and one with mass, the Higgs field.

We have:

$$\begin{aligned} \Phi = \begin{bmatrix} \varphi^+ \\ \varphi^0 \end{bmatrix} \\ \varphi^+ \equiv \frac{\varphi_1 + i\varphi_2}{\sqrt{2}},\ \ \varphi^0 \equiv= \frac{\varphi_3 + i\varphi_4}{\sqrt{2}} \end{aligned} \tag{44}$$

For the potential $V(\Phi^\dagger\Phi) = \lambda(\Phi'^\dagger\Phi)^2 + \mu^2(\Phi^\dagger\Phi)$ with $\lambda > 0$ and $\mu^2 < 0$ we perform a pertrubation around its minimum:

$$(\Phi^\dagger\Phi)_{min} \equiv \frac{u^2}{2} = -\mu^2/\lambda \tag{45}$$

For symmetry breaking, we choose the point $\Phi_0 = \frac{1}{\sqrt{2}}\begin{bmatrix} 0 \\ u \end{bmatrix}$.

We write the Langrangian expression as:

$$\mathcal{L} = \mathcal{L}_{kin} + \mathcal{L}_f + \mathcal{L}_{Yuk} + \mathcal{L}_H \tag{46}$$

We start with the kinematic term of the gauge fields $\mathcal{L}_{kin}$.

$$\mathcal{L}_{kin} = -\frac{1}{4}\sum_{\alpha=1}^{3} G^\alpha_{\mu\nu} G^{\mu\nu}_\alpha - \frac{1}{4} B_{\mu\nu} B^{\mu\nu} \tag{47}$$

where $G^{\alpha}_{\mu\nu} = \partial_\mu A^{\alpha}_{\nu} - \partial_\nu A_\mu - g\varepsilon^{\alpha jk} A^{j}_{\mu} A^{k}_{\nu}$ and $B_{\mu\nu} = \partial_\mu A_\nu - \partial_\nu A_\mu$.

The kinematic term of fermions is defined as:

$$\mathcal{L}_f = \sum_{e,\mu,\tau} \left[\overline{L}_m i\gamma^\mu \left(\partial_\mu + i\frac{g'}{2} Y_{L,lep} B_\mu + i\frac{g}{2} t_\alpha A^{\alpha}_{\mu} \right) L_m + \overline{m}_R i\gamma^\mu \left(\partial_\mu + \frac{g'}{2} Y_{R,lep} B_\mu \right) m_R \right]$$
$$+ \sum_{x=u,c,t} \left[\overline{L}_x i\gamma^\mu \left(\partial_\mu + i\frac{g'}{2} Y_{L,x} B_\mu + i\frac{g}{2} t_\alpha A^{\alpha}_{\mu} \right) L_x \right] + \sum_{u,d,c,s,t,b} \left[\overline{k}_R i\gamma^\mu \left(\partial_\mu + \frac{g'}{2} Y_{R,k} B_k \right) k_R \right] \tag{48}$$

The term $\mathcal{L}_{Yuk}$ is called the Yukawa term and is responsible to give mass to quarks and leptons, but not to their neutrinos, after the symmetry breaking:

$$\mathcal{L}_{Yuk} = - \sum_{m=e,\mu,\tau} G_m \left(\overline{L}_m m_R \Phi + \Phi^\dagger \overline{m}_R L_m \right) + L_{Yuk,q} \tag{49}$$

Finally, the term $\mathcal{L}_H$ is the kinematic and dynamic term for the fiels Φ, from which the mass for the Higgs field will occur, as well as for the masses of bosons $(Z^0, W^\pm)$:

$$\mathcal{L}_H = \left| \left(\partial_\mu + i\frac{g'}{2} Y_\Phi B_\mu + i\frac{g}{2} t_\alpha A^{\alpha}_{\mu} \right) \Phi \right|^2 - \lambda(\Phi^\dagger\Phi)^2 - \mu^2(\Phi^\dagger\Phi) \tag{50}$$

After the pertrubation around the Φ_0 the potential becomes:

$$\Phi = \frac{1}{\sqrt{2}} \begin{bmatrix} \xi_1 + i\xi_2 \\ (\eta + \upsilon) + i\xi_3 \end{bmatrix}, \quad ||\eta||, ||\xi_i|| << 1 \tag{51}$$

So, the Lagrangian expressin becomes:

$$\mathcal{L}_H = \frac{1}{2}(\partial_\mu \xi_1)^2 + \frac{1}{2}(\partial_\mu \xi_2)^2 + \frac{1}{2}(\partial_\mu \xi_3)^2 + \frac{1}{2}(\partial_\mu \eta)^2 - \frac{1}{2}(-2\mu^2)\eta^2 + ... \tag{52}$$

From which we get that the ξ_i are the Goldstone bosons and the η is the Higgs field with mass $m_\eta = \sqrt{-2\mu^2}$.

After gauge fixing[3] we obtain that:

$$A^{\alpha}_{\mu} \longrightarrow A'^{\alpha}_{\mu} = A^{\alpha}_{\mu} - \frac{1}{g}\partial_\mu \theta^\alpha - \varepsilon^{\alpha jk} \theta_j A_{\mu k}, \;\; \theta_1 \equiv \frac{2\xi_2}{\upsilon}, \;\; \theta_2 \equiv \frac{2\xi_1}{\upsilon}, \;\; \theta_3 = \theta = \frac{2\xi_3}{\upsilon} \tag{53}$$

The new field Φ' is:

$$\Phi' = \frac{1}{\sqrt{2}} \begin{bmatrix} 0 \\ \upsilon + \eta \end{bmatrix} \tag{54}$$

The Goldstone bosons are encapsulated in the new fields $B'^{\alpha}_{\mu}, A'^{\alpha}_{\mu}$. The masses of $Z^0, W^\pm$ we will see that they are a linear combination of the gauge fields.

[3] A procedure that encapsulates the Goldstone bosons to their fields

We have:

$$(D_\mu\Phi)^\dagger(D^\mu\Phi) = \left\{ \begin{bmatrix} 0 & \frac{\partial_\mu\eta}{\sqrt{2}} \end{bmatrix} - i\frac{g'}{2}B_\mu \begin{bmatrix} 0 & \frac{\upsilon+\eta}{\sqrt{2}} \end{bmatrix} - i\frac{g}{2} \begin{bmatrix} 0 & \frac{\upsilon+\eta}{\sqrt{2}} \end{bmatrix} \begin{bmatrix} A^3_\mu & A^1_\mu - iA^2_\mu & A^1_\mu + iA^2_\mu & -A^3_\mu \end{bmatrix} \right\}$$
$$\left\{ \begin{bmatrix} 0 \\ \frac{\partial^\mu\eta}{\sqrt{2}} \end{bmatrix} + i\frac{g'}{2}B^\mu \begin{bmatrix} 0 \\ \frac{\upsilon+\eta}{\sqrt{2}} \end{bmatrix} + i\frac{g}{2} \begin{bmatrix} A^{\mu 3} & A^{\mu 1} - iA^{\mu 2} \\ A^{\mu 1} + iA^{\mu 2} & -A^{\mu 3} \end{bmatrix} \begin{bmatrix} 0 \\ \frac{\upsilon+\eta}{2} \end{bmatrix} \right\} =$$
$$\left\{ \begin{bmatrix} 0 & \frac{\partial_\mu\eta}{\sqrt{2}} \end{bmatrix} + i\left(\frac{g}{2}A^3_\mu - \frac{g'}{2}B_\mu\right)\frac{\upsilon+\eta}{\sqrt{2}} \begin{bmatrix} 0 & 1 \end{bmatrix} - i\frac{g}{2}\left(A^1_\mu + A^2_\mu\right)\frac{\upsilon+\eta}{\sqrt{2}} \begin{bmatrix} 1 \\ 0 \end{bmatrix} \right\}$$
$$\left\{ \begin{bmatrix} 0 \\ \frac{\partial^\mu\eta}{\sqrt{2}} \end{bmatrix} - i\left(\frac{g}{2}A^{\mu 3} - \frac{g'}{2}B^\mu\right)\frac{\upsilon+\eta}{\sqrt{2}} \begin{bmatrix} 0 \\ 1 \end{bmatrix} + i\frac{g}{2}\left(A^{\mu 1} - iA^{\mu 2}\right)\frac{\upsilon+\eta}{\sqrt{2}} \begin{bmatrix} 1 \\ 0 \end{bmatrix} \right\} \tag{55}$$

So, we obtain:

$$(D_\mu\Phi)^\dagger(D^\mu\Phi) = \frac{1}{2}\left(\partial_\mu\eta\right)^2 + \frac{g^2(\upsilon+\eta)^2}{8}\left(A^1_\mu + iA^2_\mu\right)\left(A^{\mu 1} - iA^{\mu 2}\right) + \frac{(\upsilon+\eta)^2}{8}\left(gA^3_\mu - g'B_\mu\right)^2 \tag{56}$$

We define the following physical states with respect that we want the photon(A_μ) to be mass-less:

$$\begin{aligned} W^\pm_\mu &\equiv (A^1_\mu \mp iA^2_\mu) \\ Z^\mu &\equiv \frac{gA^3_\mu - g'B_\mu}{\sqrt{g^2+g'^2}} \\ A_\mu &\equiv \frac{g'A^3_\mu + gB_\mu}{\sqrt{g^2+g'^2}} \end{aligned} \tag{57}$$

We also define an angle θ_W as $cos\theta_W = \frac{g}{\sqrt{g^2+g'^2}}$ in order to express the states Z_μ, A_μ as a linear combination of B_μ and A^3_μ. The linear combination is:

$$\begin{bmatrix} A_\mu \\ Z_\mu \end{bmatrix} = \begin{bmatrix} cos\theta_W & sin\theta_W \\ -sin\theta_W & cos\theta_W \end{bmatrix} \begin{bmatrix} B_\mu \\ A^3_\mu \end{bmatrix} \tag{58}$$

So, the Lagrangian expression for $\mathcal{L}_H$ becomes:

$$\mathcal{L}_H = \frac{1}{2}(\partial_\mu\eta)(\partial^\mu\eta) - \frac{1}{2}(-2\mu^2)\eta^2 + \frac{1}{2}\left(\frac{g^2\upsilon^2}{4}\right)W^-_\mu W^{\mu+} + \frac{1}{2}\left(\frac{\upsilon^2(g'^2+g^2)}{4}\right)Z_\mu Z^\mu + ... \tag{59}$$

Due to the fact that $cos\theta_W = \frac{g}{\sqrt{g^2+g'^2}}$ we find that the mass of $W^\pm$ is smaller than Z^0 by a factor of $cos\theta_W$, meaning:

$$\frac{M_W}{M_Z} = cos\theta_W \tag{60}$$

We go back now to the Yukawa term because he is the one that will give mass at leptons and quarks. We consider for example the case of electron(m=e):

$$\mathcal{L}_H = -G_e \left\{ \begin{bmatrix} v_e & e \end{bmatrix}_L \begin{bmatrix} 0 \\ \frac{\upsilon+\eta}{\sqrt{2}} \end{bmatrix} e_R + \overline{e}_R \begin{bmatrix} 0 & \frac{\upsilon+\eta}{\sqrt{2}} \end{bmatrix} \begin{bmatrix} V_e \\ e \end{bmatrix}_L \right\} = \frac{\upsilon+\eta}{\sqrt{2}} \left(\overline{e}_L e_R + \overline{e}_R e_L\right)(-G_e) \tag{61}$$

We know that $\overline{e}e = \overline{e}_L e_R + \overline{e}_R e_L$ so we have:

$$\mathcal{L}_{Yuk,e} = -\frac{G_e \upsilon}{\sqrt{2}} \overline{e}e - \frac{G_e}{\sqrt{2}} \eta \overline{e}e \tag{62}$$

So we obtain the following mass for the electron:

$$m_e \equiv \frac{G_e \upsilon}{\sqrt{2}} \tag{63}$$

We achieved, after the symmetry breaking, to obtain the mass for the electron but not for the neutrino. With analogous calculations, we obtain the masses of the muon and the tau leptons.

Now, we will obtain the relations for the mass of the quarks from the $\mathcal{L}_{Yuk,q}$ term. We have a new doublet this time from the one for the leptons. The Higgs doublet is:

$$\Phi_c = -it_2 \Phi^* = \begin{bmatrix} -\overline{\varphi}^0 \\ \varphi^- \end{bmatrix} \tag{64}$$

After the symmetry breaking it becomes:

$$\Phi_c \longrightarrow \Phi_c' = \frac{1}{\sqrt{2}} \begin{bmatrix} \upsilon + \eta \\ 0 \end{bmatrix} \tag{65}$$

We consifer the case of u,d quarks. The Yukawa term for them is:

$$\begin{aligned} \mathcal{L}_{Yuk,u,d} = -G_d \begin{bmatrix} \overline{v} & \overline{d} \end{bmatrix}_L \begin{bmatrix} 0 \\ \frac{\upsilon+\eta}{\sqrt{2}} \end{bmatrix} d_R - G_u \begin{bmatrix} \overline{v} & \overline{d} \end{bmatrix}_L \begin{bmatrix} \frac{\upsilon+\eta}{\sqrt{2}} \\ 0 \end{bmatrix} u_R + h.c \Leftrightarrow \\ \Leftrightarrow \mathcal{L}_{Yuk,u,d} = -m_d \overline{d}d - m_u \overline{u}u - \frac{m_d}{u} \overline{d}d\eta - \frac{m_u}{u} \overline{u}u\eta \end{aligned} \tag{66}$$

with $m_d \equiv \frac{G_d \upsilon}{\sqrt{2}}$ and $m_u = \frac{G_u \upsilon}{\sqrt{2}}$.

We obtain the same results for the rest quarks(c,s,t,b) with only the coupling constants to differ.

1.2 The Top Quark

As we mentioned before, the top quark is one of the six quarks. It's existence was expected from the 1977 when the bottom quark was discovered in Fermilab, due to the fact that quarks come in spin doublets. It was until 1995 and after many experiments that the top quark was discovered from the CDF and $D\emptyset$ experiments at Tevatron collider. In these experiments, a large amount of $t\bar{t}$ pair production was found.

The top quark is the heaviest, so it decays before the hadronisation. It's mass is one of the most significant properties for the Standard Model, for both theoretical and experimental reasons.It constitutes a major input to the global electroweak fits, used to verify the self- consistency of the SM. Its value is also directly related to the stability of electroweak vacuum, because among all SM particles it is the largest contributor in terms of radiative corrections to the mass and self-coupling of the Higgs boson. From the experimental perspective, it pro- vides an ideal benchmark to determine the calibration and performance of the detector as well as of reconstruction algorithms.

The current most precise measurement of the top quark mass is:

$$m_{top} = 172.04 \pm 0.19(stat + JSF) \pm 0.75(syst)GeV. \tag{67}$$

The top quark decays with electroweak manner to a W boson and one down-type quark(q = d,s,b). The amptitude of the interaction is given by:

$$\Gamma(t \longrightarrow W^+q) = \frac{|V_{tq}|^2 m_t^3}{16\pi u^2}\left(1 - \frac{M_W^2}{m_t^2}\right)^2\left(1 + 2\frac{M_W^2}{m_t^2}\right)\left[1 - \frac{2a_s}{3\pi}\left(\frac{2\pi^2}{3} - \frac{5}{2}\right)\right] \tag{68}$$

Due to the fact that $|V_{tb}| \approx 0.99$ and therefore $BR(t \longrightarrow W^+q) = \frac{|V_{tb}|^2}{\sum_q |V_{tq}|^2} \approx 1$ we conclude that the top quark most of the times it decays to bottom quark.

The W boson decays hadronically:

$$W^+ \longrightarrow \left\{u\bar{d}, c\bar{s}\right\} \tag{69}$$

and leptonically:

$$W^+ \longrightarrow \left\{e^+\nu_e, \mu^+\nu_\mu, \tau^+\nu_\tau\right\} \tag{70}$$

All the quarks have colors, so they have more degrees of freedom and that's why the hadronically decays are more likely than the leptonic ones. In fact, the branching ratio is:

$$\frac{BR(W^+ \longrightarrow \left\{u\bar{d}, c\bar{s}\right\})}{BR(W^+ \longrightarrow \left\{e^+\nu_e, \mu^+\nu_\mu, \tau^+\nu_\tau\right\})} = \frac{6}{3} \tag{71}$$

1.3 Top Quark Production

The top quark is being produced at the LHC through strong and electroweak interactions. The production through strong interactions leads to $t\bar{t}$ pair production. There $t\bar{t}$ pairs are produced by:

- **Gluon Fusion**:

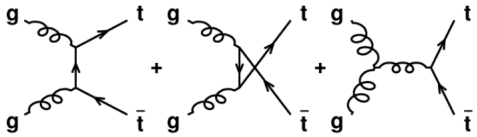

Figure 1.4: *$t\bar{t}$ production from gluon fusion*

- **q$\bar{\text{q}}$ Interactios**:

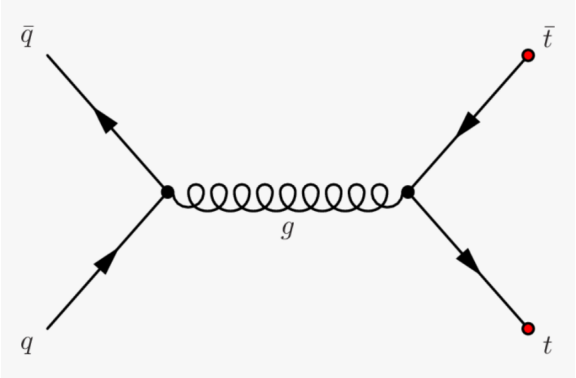

Figure 1.5: *$t\bar{t}$ production from $q\bar{q}$ interactions*

The cross section for the $t\bar{t}$ production that is measured at $\sqrt{s} = 13TeV$ and we will use at the analysis is:

$$\sigma_{t\bar{t}} = 832.8^{+19.8+35.1}_{-29.2-35.1} pb \tag{72}$$

The production through electroweak interactions leads to one top quark at the final state ("single top production"). As we will see later, there are three main modes of single top production. The most dominant one is the t-channel with measured cross section at $\sqrt{13}TeV$:

$$\sigma_{t,t-ch} = 130 \pm 1(stat.) \pm 19(syst). \tag{73}$$

The single top production produces an independent statistical sample for measuring the mass of the top quark. This process occurs at a lower energy scale compared to the production of $t\bar{t}$. The t-channel dictates the color connection only between the top quark and the proton, from which the original b quark comes, and not the whole event as observed in $t\bar{t}$. Therefore, such measurements provide a useful test for large unknown systemic effects resulting from the modeling of non-perturbative QCD processes in Monte Carlo simulations.

Chapter 2

Compact Muon Solenoid(CMS) Detector

2.1 Introduction

The Large Hardron Collider(LHC) is the biggest(27km) and most powerfull particle accelerator that has ever been built. He accelerates protons close to the speed of light, in clockwise and anti-clowckwise directions and collides them at four specific points at it's circumference. In these four points, the energy from the collisions transforms to mass, unleaching particles to all directions.

The Compact Muon Solenoid (CMS) detector, is situated at one of these points. He acts as a giant camera, taking "highlights" from the particle collisions, even 40 millions per second. Even though most particles that are being created are unstable, they decay to more stable ones which are being detected from CMS. Identifying all the stable particles, measuring their momentum and their energies, the detector can reconstruct the "image" of the collision for further study.

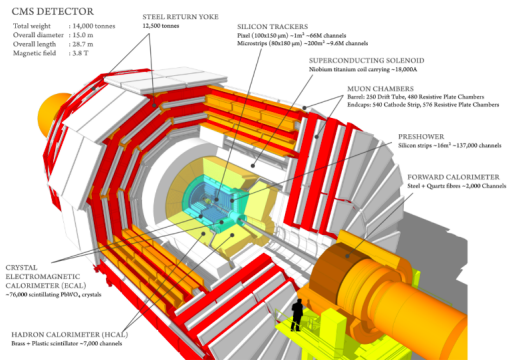

Figure 2.1: *CMS Detector*

The name comes from the fact that although the detector is small(15m height and 20m length - Compact), achieves his goal. Also, he is designed to detect muons(Muon) with great precision and he is comprised with the biggest solenoid superconductive magnet(Solenoid).

His function consists of:

- Bending and Tracking particles
- Energy Measurement
- Muon Detection

2.2 Bending and Tracking of particles

A powerful magnet is needed to bend the charged particles as they come out from the point of the collisions. That bending has two goals:

- It helps the identification of the charge of the particle, as positive and negative particles bend to different directions when the same magnetic field is applied.
- It helps the measurement of the particle's momentum due to the fact that high momentum particles are being bend less than lower ones.

The solenoid magnet is made from cylindrical coil with superconductive fibers. That means that when electric current passes through them, there is no resistance, which leads to creation of magnetic field of magnitude 4Tesla, 100 thousand times more powerful than the Earth's magnetic field.

The momentum of particles is crucial because we gain insight as to what happens during the collisions. One method for momentum measuring is to determine the track that the particle follows while in a magnetic field. The more curved the track is the lesser the particle's momentum is. The CMS Tracker record the tracks of charged particles and determines their position at specific places.

The Tracker can reconstruct the tracks of high energy muons, electrons and hadrons(particles formed by quarks) and the tracks from decays of short-lived particles, like b quarks.

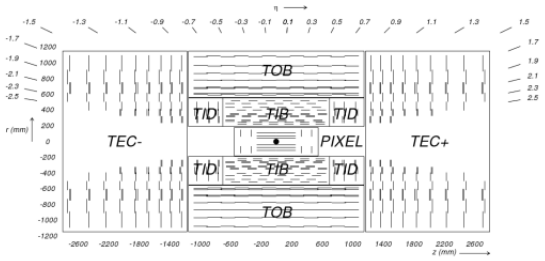

Figure 2.2: *The CMS Tracker*

The detector has 5.2m length and covers region of $r < 1.2m$ and $|\eta| < 2.5$. Due to the high luminocity pf LHC, the detector must have very good resolution and resistance to radiation. Also, it must be possible to achieve this high resolution by having as little material as possible so that the detector does not cause significant losses to the particles passing through. The detector consists of large strip silicon detectors that internally have a small silicon detector with high precision pixels (10μm) which is close to the point of collision. In both cases there are layers parallel to the barrel and the endcaps.

2.3 Energy Measurement

Information about the energies of the particles produced during collisions is very important to understand what really happens during these collisions. That information, is collected by two calorimeters. The Electormagnetic Calorimeter(ECAL) is the inner layer and measures the energy of photons and electrons by stopping them completely. The hadrons, which are made up of quarks and gluons, pass through the ECAl and stop at the outer layer, the Hardron Calorimeter (HCAL).

The individual parts of ECAL are:

- **ECAL Barrel (EB)**: In this part the crystals are slightly turned in order to point to a point of collision. It consists of 61200 cut pyramid-shaped crystals with 23cm length and $2.2 \times 2.2cm^2$ side area, which defines its resolution. The angular width covered by this piece is $|\eta| < 1.48$.

- **ECAL Endcaps (EE)**: In each endcap there are crystals corresponding to the EB part with different dimensions (length 22cm and area $2.86 \times 2.86cm^2$). Their number is 3662 in each endcap and they extend the calorimeter coverage up to $|\eta| < 3$.

- **ECAL Preshower (ES)**: This part is in front of the endcap tracks and covers an area of $1.65 < |h| < 2.6$. It consists of lead absorbers equipped with silicon strip detectors, which have an area accuracy of 1.90 $times61mm^2$. This part

has a small thickness corresponding to $3X_0$ and its role is to be able to separate the process $\pi^0 \longrightarrow \gamma\gamma$, due to the very small angle between the two photons in large η.

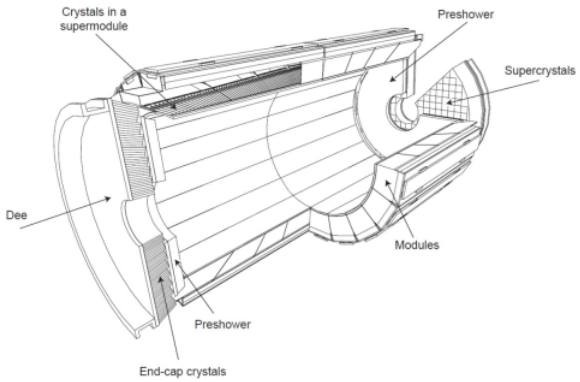

Figure 2.3: *ECAL Calorimeter*

HCAL measures the energy of hadrons reaching the detector and is also used to indirectly measure the presence of non-interacting, uncharged particles, neutrinos. Its main parts are:

- **ECAL Barrel (HB)**
- **ECAL Endcap (HE)**
- **ECAL Outer (HO)**
- **ECAL Forward (HF)**

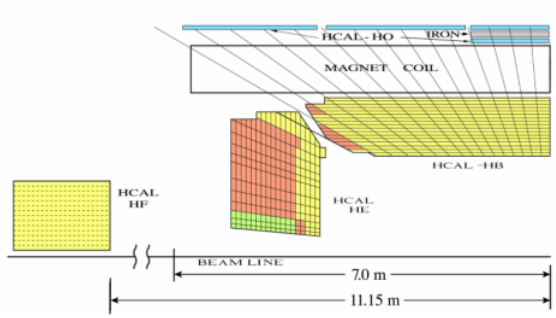

Figure 2.4: *HCAL Calorimeter*

2.4 Muon Detection

The particle detected by the CMS is the muon, which belongs to the same category as the electron, in leptons, only it is 200 times heavier. The muons do not stop by the calorimeters, so a special system for detecting muons had to be built.

The muon system has total coverage of $|\eta| < 2.4$ and consists of a combination of detectors of three different types:

- **Drift Tube (DT) Chambers** in the barel area with coverage $|h| < 2.1$. The DTs system consists of 5 cylinders concentric coaxial with the detector. Each disk has 4 stations of different radius. Each pipe is 4cm in diameter and in the center there is a wire and a mixture of argon and carbon dioxide gases. When a muon passes through the gas, it ionizes the molecules, and the electrons generated are directed to the wire due to an electric field inside the tube. By detecting the point where the electrons fell on the wire and the sliding time, the orbit of the muon is calculated.

- **Cathode Strip Chamber (CSC)** to manage the highest particle rates due to the short response time, and the heterogeneity of the magnetic field in the range $0.9 < |\eta| < 2.4$. They have positively charged wires (anodes) and negatively charged (cathodes) placed vertically. The wire mesh is in a gas mixture. When a muon passes ionizes the gas molecules and the electrons produced are led to the cathodes creating an "avalanche". The signal produced by it, gives information about the trajectory of the passed particle.

- **Resistive Plate Chambers (CSC)** located in both the barrel and the end-cap and cover a range of $|h| < 2.1$. They complement the previous ones, providing information on scandal. They consist of two plates, one positively charged which acts as a cathode and a negatively charged one which has the role of the cathode and in between there is gas. When a muon passes through the gas it causes ionization. Due to the charged plates in the gas area there is an electric field. Thus the electrons produced by ionization are accelerated and create an avalanche. The products of the avalanche are led to the ascent where they are collected, thus giving information about the snow that passed. The electric field is such that the signal comes in much less time than the frequency of collisions.

Chapter 3

Physics of particle collisions at LHC

3.1 Proton-proton collisions

3.1.1 Proton Structure and Parton Scattering

At first, protons were considered to be elementary particles, but in the Standard Model they are prescribed as hadrons, particles composed by quarks. Specifically, they are a bound state of three valence quarks, two up type quarks of charge $\frac{2}{3}e$ and one down type quark of charge $\frac{1}{3}e$.T he rest masses of quarks contribute only about 1% of a proton's mass. The remainder is due to quantum chromodynamics binding energy, which includes the kinetic energy of the quarks and the energy of the gluon fields that bind the quarks together. So, protons contain a large amount of quarks and glouons which are called partons. The parton distribution inside the proton is what we call proton structure.

The distribution of proton's four-momentum to its partons is the main characteristic to proton collisions. For a given parton the probability density function is given in terms of:

$$f = f_i(x, \mu_F^2), \qquad i = g, u, \bar{u}, d, \bar{d} \tag{74}$$

The term μ_F is called factorisation scale and and represents the portion of the hard-scattering of partons that can be measured by pertubative methods from the portion described from PDFs.

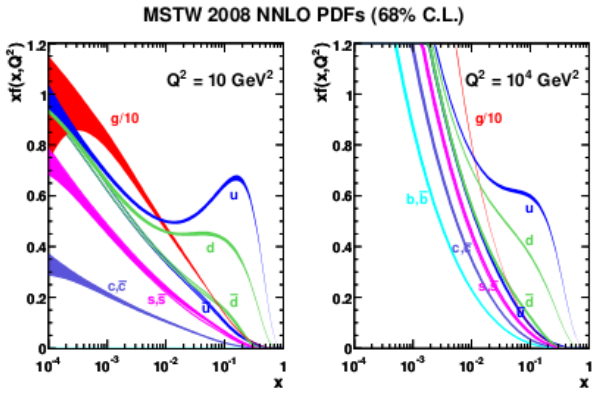

Figure 3.1: *Parton PDFs from MSTW group*

When two protons with four-momentums P_a and P_b collide inelastic, in reality, a parton from one proton collides with another from the other proton. Each parton carries a portion from the four-momentum of the proton:

$$\begin{aligned} p_a &= x_a P_a \\ p_b &= x_b P_b \end{aligned} \tag{75}$$

So the energy as the center of mass, given two partons, is not that of the proton($\sqrt{s} = 13TeV$) but is given in terms of:

$$\hat{s} = x_a x_b \sqrt{s} \tag{76}$$

So, in order to obtain one single top event at the final state, the following statement must be satisfied:

$$\hat{s} > m_{top}^2 \rightarrow x_a x_b > 1.810^{-4} \tag{77}$$

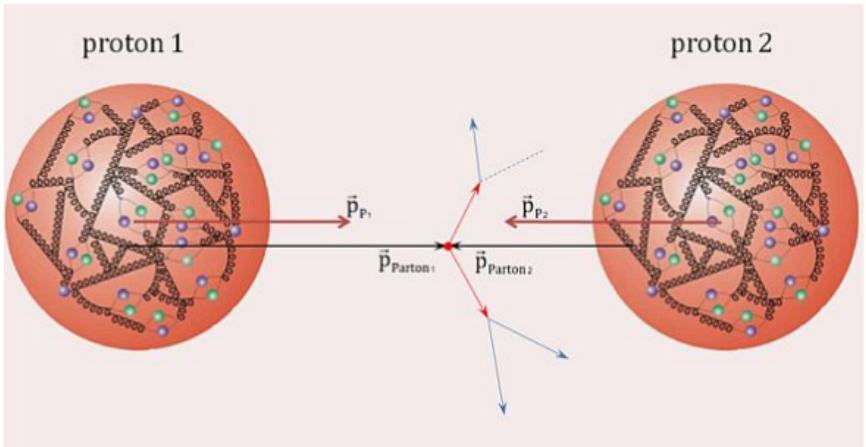

Figure 3.2: *Parton collisions*

3.1.2 Kinematic Variables

In order to describe what happens during these collisions and to further reconstruct properties that we want to measure we have to determine the values of certain kinematic variables.

The proton beams travel move on the z-axis(beam plane) and the collision happens at the xy-plane(transverse plane). So, the system of center of mass and the system of laboratory are identical. As we mentioned, due to the fact that the collision actual happens between the partons, the z-component of the momentum is undefined. This is the reason we use longitudinal Lorentz boost invariant variables.

The first variable that satisfies the aforementioned restriction is the transverse momentum*, which is defined as follows:

$$\begin{aligned} &\vec{p_T} \equiv (p_x, p_y) = (p_T cos\varphi, p_T sin\varphi) \\ &p_T \equiv |p_T|^2 \end{aligned} \tag{78}$$

Some particles are not detected, such as the neutrinos, so their momentum can't be directly measured, it can only be estimated. For that reason we use the variable called "Missing Transverse Momentum" which is defined as:

$$\not{\vec{p}_T} = -\sum_i \vec{p}_{T,i} \tag{79}$$

The physical meaning is that normally we demand the conservation of momentum, which means that the transverse components of momentum in the final products must sum up to zero. Due to the fact that we can't measure the momentum of neutrino, we assume that his momentum is given by this variable.

We define another variable, the rapidity, as:

$$y \equiv \frac{1}{2} log \frac{E + p_z}{E - p_z} \tag{80}$$

Which under longitudinal Lorentz boost changes by a constant, so the Δy quantity remains invariant. The angle of collision(φ) and rapidity are two highly correlated variables. Specifically, for mass-less particles(m=0) we have the pseudorapidity(η):

$$\eta = \frac{1}{2} log cot \frac{\theta}{2} \tag{81}$$

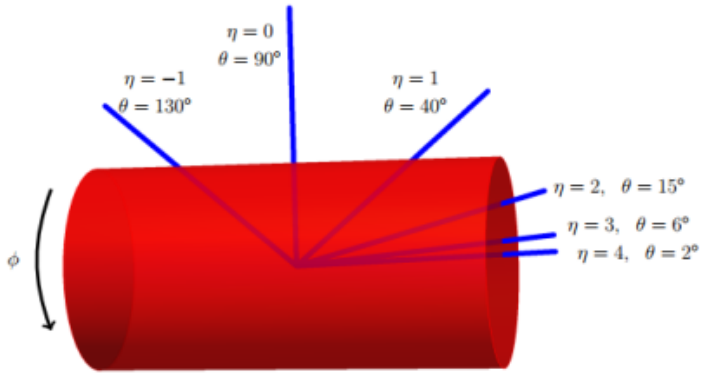

Figure 3.3: *Correlation between η and φ*

The next variable that we are using is the angular distance ΔR. The definition is:

$$\Delta R \equiv \sqrt{(\Delta y)^2 + (\Delta \varphi)^2} \tag{82}$$

We can see the similarities with the angular metric:

$$(d\Omega)^2 = (d\theta)^2 + sin^2\theta(d\varphi)^2 \tag{83}$$

If we write θ in terms of η we get:

$$(d\Omega)^2 = \frac{1}{cosh^2\eta}(d\eta)^2 + (d\varphi)^2 \tag{84}$$

So we choose the definition (15).

The main variable we examine is the invariant mass of a particle who has four-momentum p^μ and decays to other particles. The definitions is:

$$m^2 = \left(\sum_i p_i^\mu\right)^2 \tag{85}$$

We mentioned previously, that some particles can't be detected, for example in the decay $W \longrightarrow l\nu_l$ we can't detect the neutrino. In these case we use the variable, the transverse mass, which is calculated only from the transverse components. The transverse mass is:

$$m_T = \sqrt{(E_{1,T})^2 + (E_{2,T})^2 - (\vec{p}_{1,T})\,2 - (\vec{p}_{2,T})^2} \tag{86}$$

Generally, we have $0 \leq m_T \leq m$. If the particles are parallel to the beam we have $m_T = 0$ and if the particles are in transverse plane we have $m_T = m$.

Another key point we have to address is the classification of jets to "b-tagged" jets and to "non b-tagged" or "light" jets. To begin with, A jet is a narrow cone

of hadrons and other particles produced by the hadronization of a quark or gluon. A b-tagged jet is a jet originates from a b type quark. Hadrons containing bottom quarks have sufficient lifetime that, they travel some distance before decaying. On the other hand, their lifetimes are not so high as those of light quark hadrons, so they decay inside the detector rather than escape.

The last quantity that we will define in this section is the Luminocity and it describes the efficiency of the detector. If we have two beams of protons that are colliding, the one with n_1 protons and the other with n_2 protons, with collision frequency f and standard deviations s_x,s_y respectively, we define luminocity as:

$$L = f\frac{n_1 n_2}{4\pi s_x s_y} \tag{87}$$

This quantity tells us how many particles can we compress in one area of space at a given time. Obviously, this does not mean that all these particles will inevitably collide, but the more particles we compress in this area, the more likely they are to collide.

On the other hand, the cross section σ) for a collision is a measure of probability for the collision to happen. Therefore, if we multiply the luminocity with the cross section, we will get the number of collisions:

$$R = \sigma L \tag{88}$$

3.2 Signal and Background definition

Top quarks are produced from proton-proton(pp) collisions at the Large Hardron Collider. Single top quark events are produced through charged - current interaction via W boson exchange. The leading order(LO) production of single top events is divided to three main modes, the t channel, the tW channel and the s channel. From them, the t-channel is the most dominant. The Feynman diagrams for the three proccesses are:

t-channel

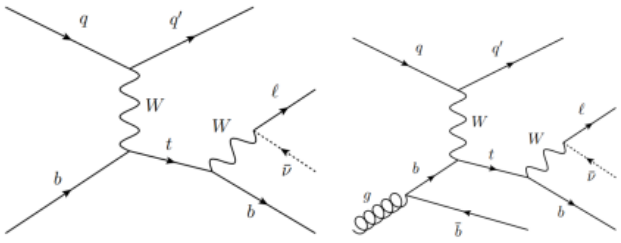

Figure 3.4: *Feynman diagrams of t-channel single top production*

We treat the left Feynman diagram as the signal process. In this mode the final state consists of one light flavored quark, one lepton and one or two b-tagged jets. The one b-tagged case comes from a light b-jet originating from a proton and at the two b-tagged case, the light jet originates from gluon splitting. Another difference is that at the first case, the b-jet from the top decay will be central while at the second case will be forward with low p_T meaning that the extra b-tagged jet will not be able to be reconstructed. So, at the final state, we demand exactly one b-tagged jet, one lepton and the initial light jet.

tW-channel

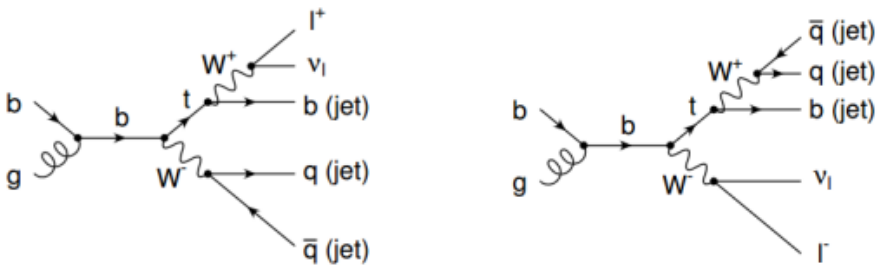

Figure 3.5: *Feynman diagrams of Wt-channel single top production*

In this mode we have another W boson at the final state alongside the top quark. So, if we want exactly one lepton at the final state, the one W boson must decay leptonically and the other hadronically. Also, in this mode we have three jets at the final state, but we demand two as mentioned before.

s-channel

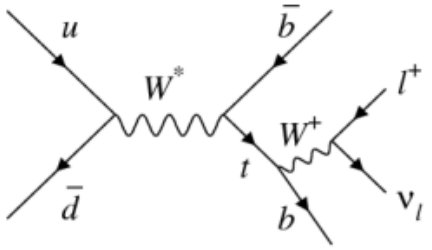

Figure 3.6: *Feynman diagrams of s-channel single top production*

In this channel we have two b-tagged jets in the final state, one coming from top decay. This background has small cross section and the selection of one b-tagged jet can further reduce it.

top anti-top pair production

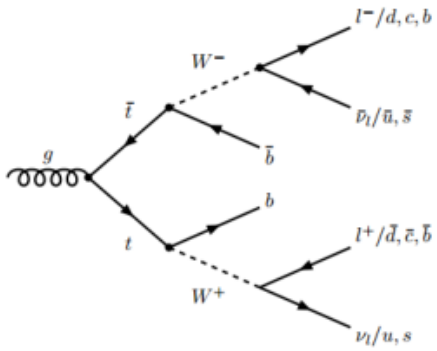

Figure 3.7: *Feynman diagram of $t\bar{t}$ production*

The top anti-top production is the main source of top quark production. The case of interest is the one where the W boson originating from the top quark decays leptonically while the other decays hadronically.This process is the main background process, which as we will see later is being supressed from the one b-tagged requirement.

W+jets

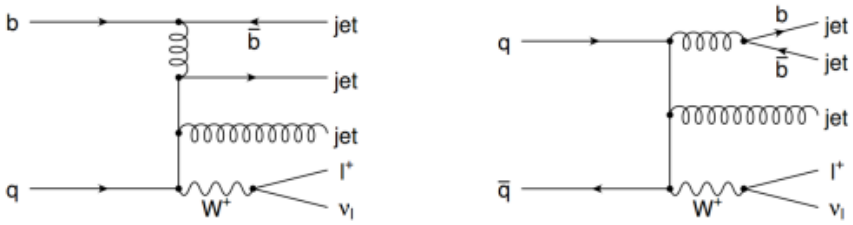

Figure 3.8: *Feynman diagrams of W + jets procedure*

In this process we have W boson production alongside multiple b-tagged jets. The discriminating difference from the singal process is that the b-tagged jet and the lepton do not originate from top decay, so they will not give the correct invariant mass at the reconstruction.

Z+jets(Drell-Yan)

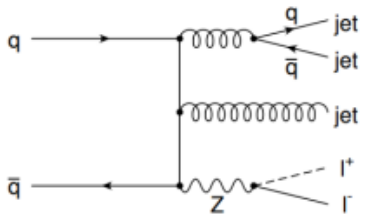

Figure 3.9: *Feynman diagrams of $Z + jets$ procedure*

This one is also called Drell Yan process. It is similar to $W + jets$ but now insteaf of a W boson we have a Z boson. The cross section here is lower so this procedure contribute less than the $W + jets$. Further in the analysis, we treat them as one process.

Diboson

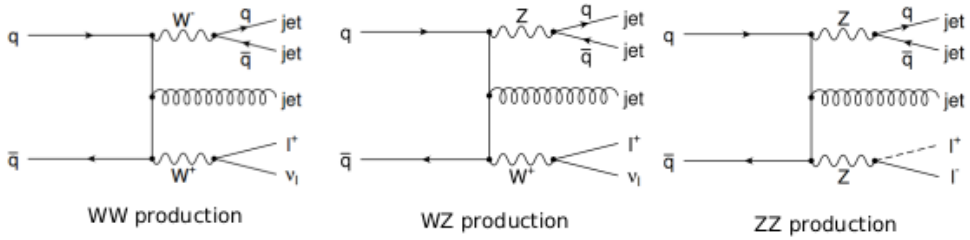

Figure 3.10: *Feynman diagrams of Diboson production*

In this process we have the production of two vector bosons(WW,WZ,ZZ). We care about the situation that one of the bosons decays leptonically while the other decays to a pair of quarks. Again, the cross section is very small so this process is encapsulated in the $W/Z + jets$ processes.

QCD Multijet production

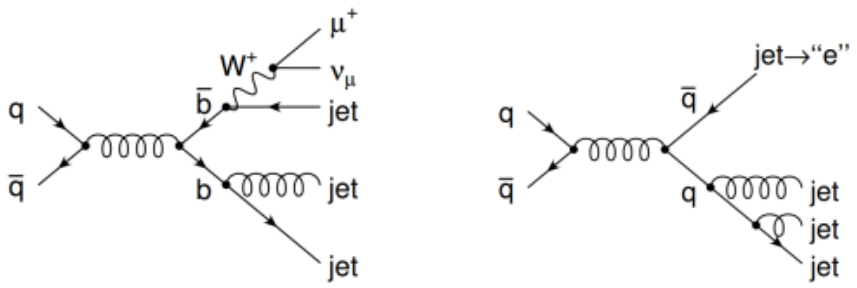

Figure 3.11: *Feynman diagrams of QCD multijet production*

This background process originates from parton 2 $\longrightarrow$ 2 interactions. In some cases, a lepton is produced through decays of heavy flavored quarks or from hadrons. Therefore these events may mimic the final state of the signal. Also, the detector may misidentificate a jet to an electron, which is called "fake" lepton.

So, to sum up the aforementioned, our signal process is the t-channel mode. We divide the background process to three categories. The main one is the top anti-top production($t\bar{t}$), in which we include the other two single top processes, the tW-channel and the s-channel. The second one is the $W + jets$ process in which the $Z + jets$ and $Diboson$ processes are included. The last one, is the QCD multijet process.

Chapter 4

Analysis

4.1 MC samples and Data

As we mentioned, the t-channel mode of the single top region the signal process of this analysis. Our first goal is to achieve as pure signal sample as possible. We achieve that by surpressing the background processes using some techniques as we will see further on.

Our first step is to determine the distributions of variables that the detector measures, for both signal and background, in order to compare them with data and extract our measurement. We begin our analysis working on Monte Carlo samples, by building models to describe the shape of each process.

Each sample contains some statistical fluctuations which are correlated to the number of generated events. The more generated events we have, the less are the fluctuations. The goal is to have as minimum as possible fluctuations or far less amount of them as to the one we have on actual data. For that reason, the number of generated events is bigger in MC samples than in data. For a given phase space, a particular process may be abundant but, in the region of interest it may be suppressed. That provides a problem in which even if we have a large amount of generated events, very few of them will be useful in the particular region of the phase space that we consider. For example for the DY process the differential cross-section falls rapidly with the energy. To solve problems like these, one splits the phase space into subsets with respect to some variable, and generates events separately on each subset. All the Monte Carlo samples that we used in the analysis are shown in Table 4.1.

MC Samples - Single Top(ST)	Cross Section(pb)
t-channel top	136.02
t-channel anti-top	80.95
tW top	35.6
tW anti-top	35.6
s-channel	10.32
MC Samples - Top-Anti-top	Cross Section(pb)
$t\bar{t}$	832
MC Samples - W+jets(LO)	Cross Section(pb)
$H_T \in [70, 100]GeV$	1353
$H_T \in [100, 200]GeV$	1346
$H_T \in [200, 400]GeV$	359.7
$H_T \in [400, 600]GeV$	48.91
$H_T \in [600, 800]GeV$	12.05
$H_T \in [800, 1200]GeV$	5.501
$H_T \in [1200, 2500]GeV$	1.329
$H_T \in [2500, Inf]GeV$	0.03216
MC Samples - W+jets(NLO)	Cross Section(pb)
0 Jets	49670
1 Jet	8264
2 Jets	2628
MC Samples - Drell-Yan(DY)	Cross Section(pb)
$H_T \in [70, 100]GeV$	169.9
$H_T \in [100, 200]GeV$	147.4
$H_T \in [200, 400]GeV$	40.99
$H_T \in [400, 600]GeV$	5.678
$H_T \in [600, 800]GeV$	1.367
$H_T \in [800, 1200]GeV$	0.6304
$H_T \in [1200, 2500]GeV$	0.1514
$H_T \in [2500, Inf]GeV$	0.003565
MC Samples - Diboson	Cross Section(pb)
WW	115.00
WZ	47.13
ZZ	16.523

Table 4.1: *MC Samples*

4.1.1 Event Selection

At this point, we treat each sample as a separate dataset. As we said, our signal final state consists of an isolated lepton, a neutrino and two jets, one of them must be b-tagged. For the lepton, we consider a muon(anti-muon) study. We have to implement those rules on each dataset. These restrictions are called "cuts". More precisely, all the cuts that we used as baseline are:

- Exactly two jets with the one being b-tagged
- Exactly one lepton, either muon or anti-muon
- No isolated and veto leptons
- $p_{T,lepton} > 30$ Gev with $|\eta| < 2.4$
- $p_{T,jets} > 30$ Gev with $|\eta| < 2.4$ for the b-tagged and $|\eta| < 4.7$ for the other

Also, the leptons are required to fire the HL triggers of tight isolation, which for the muons are:

- HLT_IsoMu27_v
- HLT_IsoTkMu24_v

These are the basic cuts that we must have in order to have the required final state. In the next sections, we will implement four extra cuts in order to suppress the background processes.

4.1.2 Data Driven QCD Multijet Background

In Table 4.1, there are no Monte Carlo samples for the QCD background. The main reason for that, is the fact that although the QCD process has a very large cross section($\approx$ mb), in the region that we are looking her contribution is minimal. With the addition of the various cuts, the final events we get from QCD MC samples are minimal, so the modeling could not happen satisfactorily. The tiny selection efficiency leads immediately to some important problems for a simulation. So, the modeling and the normalization of QCD occurs from an approach on data.

So, we defined our signal region as follows:

- 1 Lepton
- 0 Non Isolated Leptons
- Triggers for isolated leptons fired

We go now to the non isolation region, which is orthogonal to previous:

- 0 Leptons
- 1 Non Isolated Lepton
- Triggers for non isolated leptons fired

We assume that the non Isolation region has high purity in QCD events and that the shape of QCD in this region is the same in the Isolation region. The reason for the later is that both these events have the same nature.

Now we have to estimate the yield of QCD, by measuring the total events from data(N_{data}) and the ones from all the MC processes(N_{MC}) and attributing their difference in the variable we want to estimate. More preciselly we have:

$$\begin{aligned} N_{qcd} &= N_{data} - N_{MC} \\ N_{MC} &= N_{signal} + N_{t\bar{t}} + ... \end{aligned} \tag{89}$$

4.1.3 Top Quark Reconstruction

In this section we have to calculate the four-vector of top's quark momentum. We know that in each vertex of a Feynmann diagram, the four-momentum is conserved. So, for the tWb vertex we have:

$$p_{top} = p_W + p_b \tag{90}$$

Where p_b is the four-momentum of the b-tagged jet, which from the jet reconstruction can be calculated appropriately. Now, at Wlv vertex we have:

$$p_W = p_l + p_v \tag{91}$$

Again, the p_l component can be calculated because the detector can measure all the variables needed for the lepton reconstruction. The problem lies in the calculation of the neutrino's four-momentum. As we said before, the neutrino is not detected, so we assume his tranverse components in momentum are equal to $p_{T,miss}$ variable. Even with this assumption, the p_z component can not be calculated.

The way we treat this situation of a missing degree of freedom is by requiring the W boson to be "on-shell" $\longrightarrow p_W^2 = M_W^2$. So, the equation (91) becomes:

$$\begin{aligned} p_W^2 = (p_l + p_v)^2 = M_W^2 \Leftrightarrow \\ \Leftrightarrow M_W^2 = \left(E_l + \sqrt{\not{p}_T^2 + p_{z,v}^2}\right)^2 - \left(\vec{p}_{T,l} + \vec{\not{p}}_T\right)^2 - (p_{z,l} + p_{z,v})^2 \\ M_W = 80.4 Gev \end{aligned} \tag{92}$$

This equation is quadratic in $p_{z,v}$ and solving it the expression for $p_{z,v}$ can obtained as:

$$\begin{aligned} p_{z,v} = \frac{\Lambda p_{z,l}}{p_{T,l}^2} \pm \frac{1}{p_{T,l}^2}\sqrt{\Lambda^2 p_{z,l}^2 - p_{T,l}^2\left(E_l^2 \not{p}_T^2 - \Lambda^2\right)} \\ \Lambda = \frac{M_W^2}{2} + \vec{p}_{T,l} \cdot \vec{\not{p}}_T \end{aligned} \tag{93}$$

As we see, two possible cases arise from the solution:

- If the discriminant is positive, there are two possible solutions for $p_{z,v}$. This occurs in 65% of all cases. From them, we choose the one with the lowest absolute value and the reason for that is that in the 63.4% of the selected events with real solutions, the smallest $|p_{z,v}|$ solution is closer to the true neutrino p_z than the other solution.
- If the discriminant is negative, we have complex solutions for $p_{z,v}$, which are not physically accepted. This occurs in 35% of all cases, due to finite $\not{p}_T$ resolution. The solution is that the imaginary is eliminated by setting $M_{T,W} = M_W$ which leads to null discriminant. This new condition gives two curves on transverse plane. Each one is a candidate for the $\vec{p}_{T,v}$. The solution corresponding to the minimal distance between $\vec{p}_{T,v}$ and $\vec{\not{p}}_T$ is chosen.

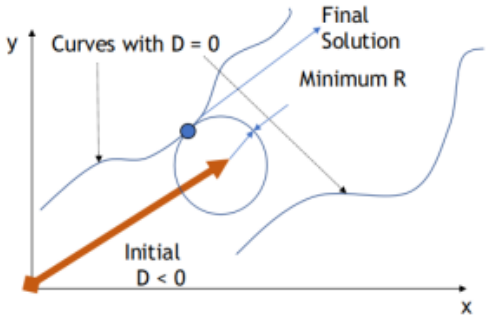

Figure 4.1: *The CMS algorithm for negative discriminant solutions*

To prove that the algorithm works, we first look at the distribution of the transverse component of the W mass before the reconstruction. The distribution, for example we present a signal/$t\bar{t}$ comparison, is:

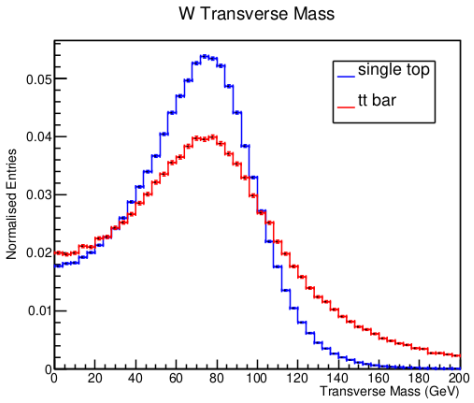

Figure 4.2: *Transverse W mass before reconstruction*

Now, after the reconstruction, for the positive case of the discriminant, we expect no events after the 80.4 GeV restriction we imposed. For the negative one, we expect all the events to yield the value of 80.4 GeV.

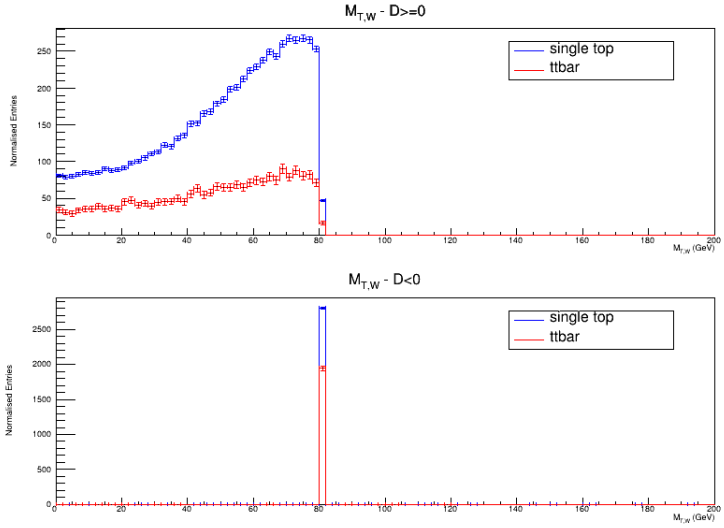

Figure 4.3: *Transverse W mass after reconstruction*

4.2 Maximum Likelihood Fit

At this stage of the analysis, we have reconstructed a variable, the m_{lvb} from the MC simulations, that will act as our estimator for the true mass of the top quark(m_{top}^{true}). We will use this variable to perform a Maximum Likelihood[1] fit(ML Fit).

Now, we have to find an appropriate model for each process which will act as a probability distribution. When we find each model, we will combine them to one total model and perform a combined fit on our samples. These shapes must be discriminating between the signal process and the backgrounds. Although it is an obvious approach, we want it for the purpose of the Likelihood to be as "healthy" as possible. Also, we want the ML fit to be well behaved, meaning it should be robust to statistical fluctuations and give an unbiased estimation for the value and the error. We perform that by creating multiple pseudodata and performing the fit on them. This procedure is called Toy Monte Carlo Validation.

Before we begin our search for model candidates for each process, we have to perform a normalization on the events we have. We have to find the expected yield of each sample(N_{exp}. We do that by taking the integral of the distributions, the number of events that passed our selection criteria and rescaling using the cross section and luminocity of the detector. So, we obtain:

$$N_{exp} = \sum_i \sigma_i L_{int} \frac{N_{i,pass}}{N_{i,gen}} \tag{94}$$

This expression tells us that the fraction of events in the phase space of interest, estimated from MC samples, is multiplied with the total expected yield $\sigma i L_{int}$, to

[1]This procedure is analyzed in Appendix A

give the expected yield in that region.

4.2.1 Cut Based Selection

We mentioned before that our goal is a good separation between the signal and the various backgrounds, we want high purity in our signal sample. Also, we have an estimator from the reconstruction. Now, if we define some variables, that have a strong correlation to our estimator and can discriminate the signal from the background, we will achieve high signal purity.

The first variable is the $|\eta|$ of the non b-tagged jet. Due to the fact that the q quark is forward in the signal region, this variable can discriminate the signal from all the other background processes

The second variable is the angle between the lepton and the non b-tagged jet at the rest frame of top quark. Again, we use this variable to supress all the background processes because the top quark is highly polarised.

The third variable is the angular distance between the lepton and the b-tagged jet. This variable is use to supress the $W + jets$ process.

In order to achieve the purity that we want we have to put some extra cuts on these variables. We find the optimal combination of these cut values by working as:

- We pick one of the variables as our pivot variable. We plot the distribution of the variable and we see which area it can discriminate the signal from the background processes.

- In this area, we pick one starting value and we calculate the ratio of signal over background by calculating the integral of each process.

- Then, we pick a step and we perform deviations with this step on the initial value and recalculate the signal over background ratio.

- We compare the two ratios and we keep the greater one, then we take the second value for the cut as our initial and we make another deviation.

- Once we find the optimal cut for this variable, we apply the cut and we continue with the same algorithm to the next variable

This "naive" cut optimisation procedure is shown in the next figures:

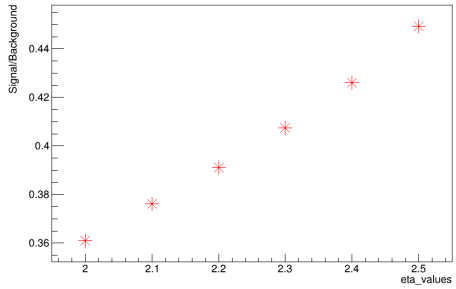

(a) $|\eta|$ *selection*

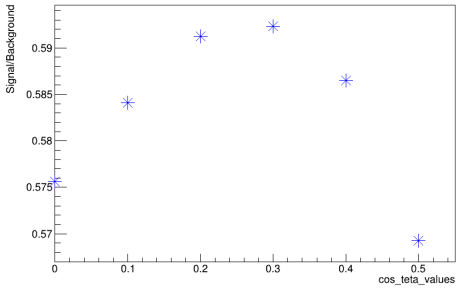

(b) $cos\theta^*$ *selection*

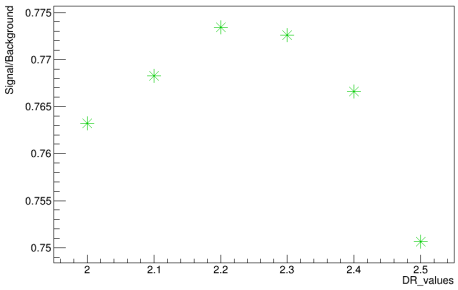

(c) *DR selection*

Figure 4.4: *Cut Selection*

Below, we have the distributions of these variables, before applying the cuts and after. Also, we present a stack histogram of the estimator m_{lvb} before and after the cut procedure to observe if we achieve a sufficient signal purity.

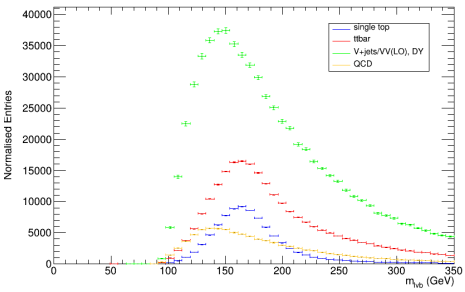

(a) *Before cuts*

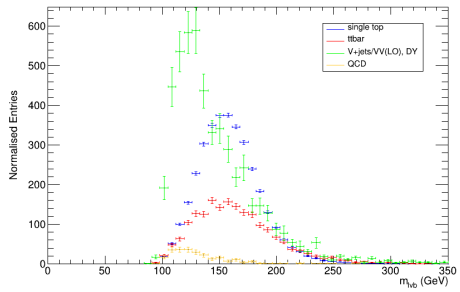

(b) *After cuts*

Figure 4.5: *Estimator* m_{lvb}

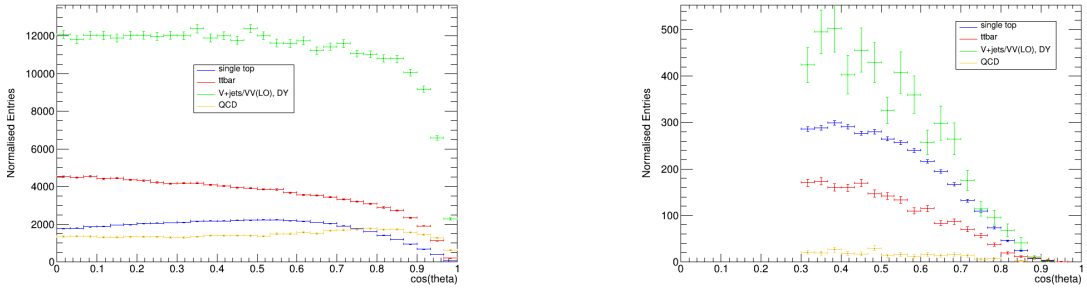

(a) *Before cuts* **(b)** *After cuts*

Figure 4.6: *Variable cosθ**

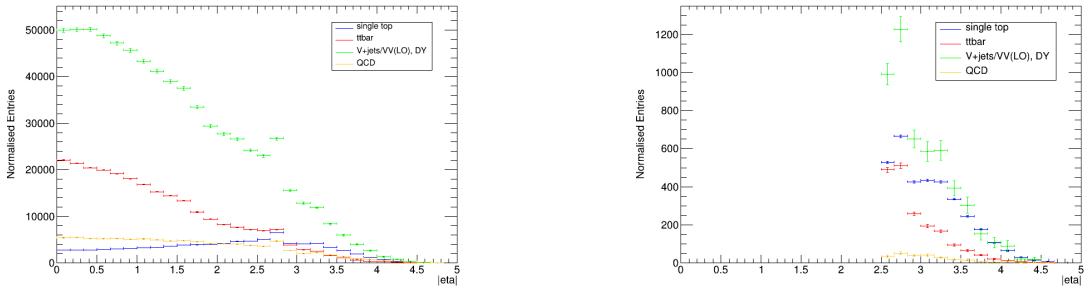

(a) *Before cuts* **(b)** *After cuts*

Figure 4.7: *Variable* η_{ljet}

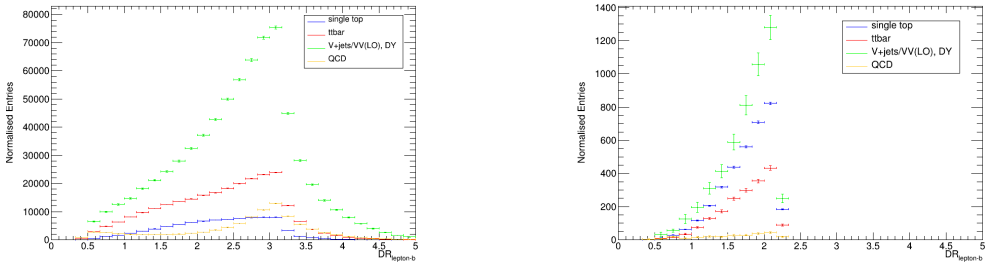

(a) *Before cuts* **(b)** *After cuts*

Figure 4.8: *Variable* $DR_{lepton-bjet}$

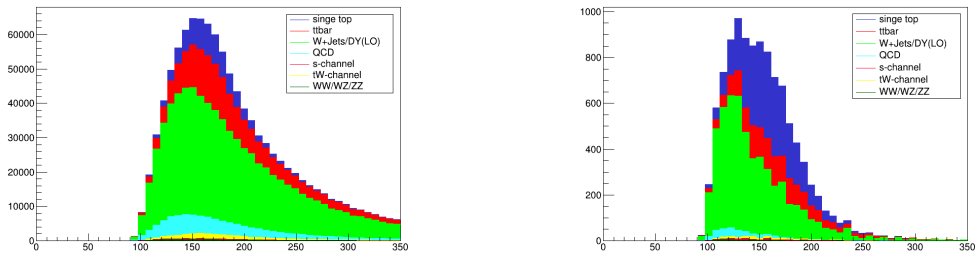

(a) *Before cuts* **(b)** *After cuts*

Figure 4.9: *Stacked histogram of estimator*

In order to supress the QCD background, we implement a cut on a fourth variable, the transverse mass of the W boson. The main reason that we pick this variable comes from the fact that the QCD process contains no W bosons. This cut also optimize the supression of the $Z + jets$ background but this process is already a subdominant background so we do not expect large changes.

4.2.2 Model Selection for Signal and Background

In the analysis, we had multiple mass samples from which we built the individual models for each procedure. The mass sample $172.5Gev$ is called nominal and it is the one that contains more events and in general has a better statistical description. For each process, we fill present the figure for the nominal mass sample. The rest figures from all the other mass samples are apposed in Appendix B.

Parametric description of the t-channel single top signal

The signal template for the single top process is chosen to be a sum of a lognormal core and a Crystall Ball function to describe the tail as presentes in the following:

$$F_{t-ch} = f_{sig} Lognormal(\mu_{log}, \sigma_{log}) + (1 - f_{sig}) CrystallBall(\mu_{log}, \sigma_{CB}, a_{CB}, n_{CB}) \quad (95)$$

where the parameter f_{sig} controls the relative contribution of Lognormal and the Crystall Ball function in F_{t-ch}. The parameter is n_{CB} is kept fixed at 2.65633 due to instability if kept non fixed. Also, the n_{CB} is highly correlated with the parameter a_{CB} so if kept non fixed it contributes to higher errors. The template is:

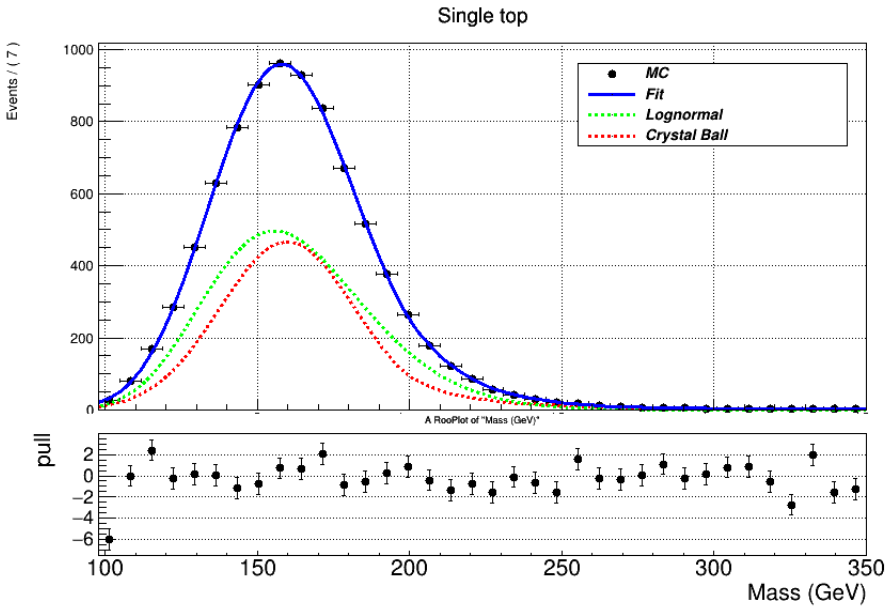

Figure 4.10: *Best fit shape of the signal template*

Parametric description of top backgrounds

The top background template, $F_{t\bar{t}}$, consists of $t\bar{t}$,tW and s-channel signel top contribution. The latter two processes account for only 6.3% of the final sample in the muon final state and are absorbed with $t\bar{t}$ due to their individual interference effects. The top background template is modeled with a sum of a Gauss core and a Novosibirsk function.

$$F_{t\bar{t}} = f_{t\bar{t}} Gauss(\mu_g, \sigma_g) + (1 - f_{t\bar{t}}) Novosibirsk(\mu_g, \sigma_{novo}, \tau) \tag{96}$$

where τ describes the skewness of the distribution. The template is:

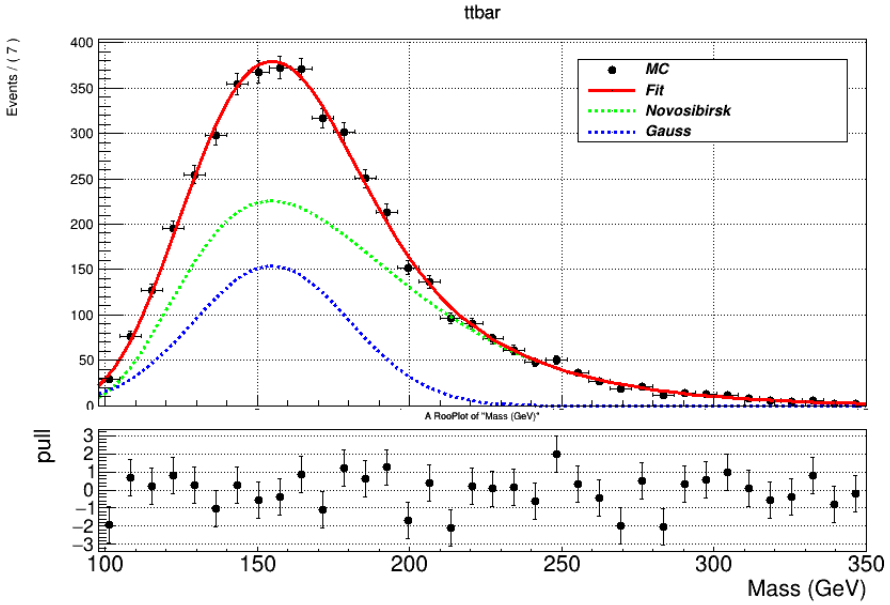

Figure 4.11: *Best fit shape of the $t\bar{t}$ template*

Parametric description of the EWK backgrounds

The electroweak template, F_{EWK} contains contributions from W + jets, Z + jets and diboson processes. This template does not depend on the top quark mass. We use the Novosibirsk function:

$$F_{EWK} = Novosibirsk(\mu_{EWK}, \sigma_{EWK}, \tau) \tag{97}$$

again, τ parameter describes the skewness. The model seems to describe reasonably well given the level of fluctuation seen in the MC distribution which occurs due to mismodelling of W/Z + heavy flavor background in the simulated events.

The MC data we use for the modeling of the EWK background are taken from Leading Order(LO) processes. This is done due to lack in statistics from NLO MC samples in the final phase space.

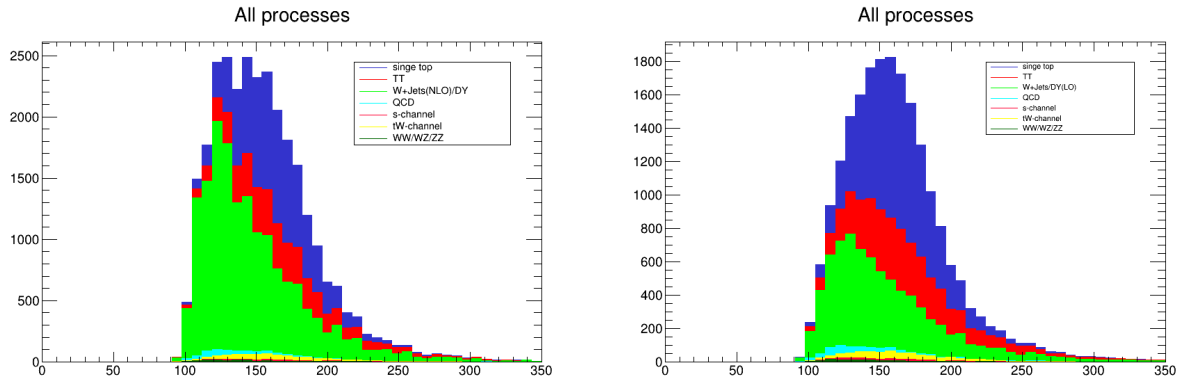

(a) *W+jets NLO* **(b)** *W+jets LO*

Figure 4.12: *Comparison of NLO - LO shapes*

Although the shape is taken from LO MC samples, the expected number of events will be calculated from NLO samples, for its is more precise. We do that by taking as scale for the normalisation the ratio NLO/LO of events. In our analysis is found to be $k = 2.38746$.

The template for the EWK background is:

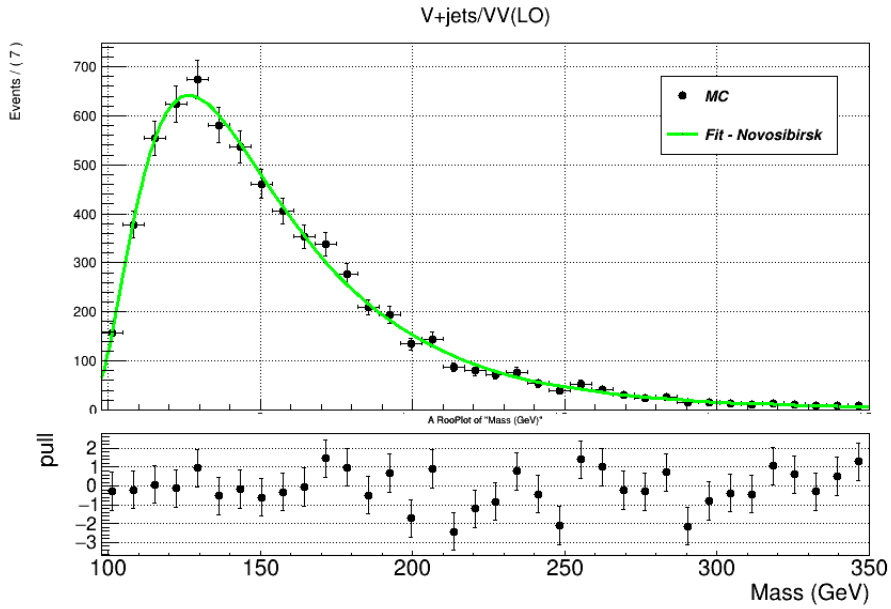

Figure 4.13: *Best fit shape of the EWK template*

Parametric description of the QCD background

The parametric template, F_{QCD} is taken from the Non Isolation region and the normalisation factor from the diferrence $N_{data} - N_{MC} = N_{QCD}$. Again, as for the

EWK backgrounds, the model does not depend on the top quark mass, so we use again a Novosibirsk function:

$$F_{QCD} = Novosibirsk(\mu_{QCD}, \sigma_{QCD}, \tau) \tag{98}$$

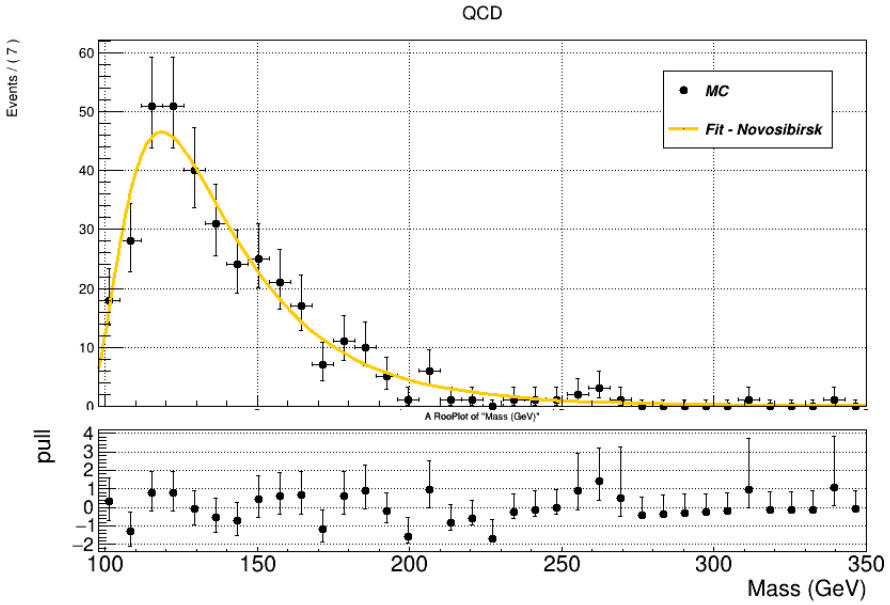

Figure 4.14: *Best fit shape of the QCD template*

4.2.3 Linearity Check

As mentioned in the previous section, we built our model upon various mass samples, meaning that each fit on each mass sample gives a set of estimations for each of the parameters of the template. In general, we want the values from each sample to be linear dependent.

The way we do the linearity check is:

- From each mass sample we take the estimated values for each parameter and then we plot them
- We perform a linear fit, $y = a * x + b$
- We adjust the estimated parameter with the values a,b

For the single top, the values are summurised in the next Table:

Parameters of ST template	Values
f	0.488932 ± 0.0401887
mean	$a = 0.816073 \pm 0.0274714$ $b = 19.629 \pm 4.75114$
a_{CB}	-1.60079 ± 0.0408104
n_{CB}	2.65633 ± 0.332116
σ_{log}	1.17996 ± 0.00286679
σ_{CB}	$a = 0.357127 \pm 0.0573926$ $b = -39.4975 \pm 10.0163$

Table 4.2: *Values for single top template*

For the $t\bar{t}$ background, the values are:

Parameters of $t\bar{t}$ template	Values
f	0.317617 ± 0.0265126
mean	$a = 0.874198 \pm 0.112202$ $b = 2.2452 \pm 19.391$
σ_g	27.1201 ± 0.768371
σ_{novo}	33.6679 ± 0.455814
τ	-0.425494 ± 0.0142935

Table 4.3: *Values for $t\bar{t}$ template*

Due to the fact that in EWK and QCD background there is no mass, we only work on one mass sample, so we do not have linearity checks for these processes. Their parameters are kept fixed to the central values. The linearity plots for single top and $t\bar{t}$ processes are show below:

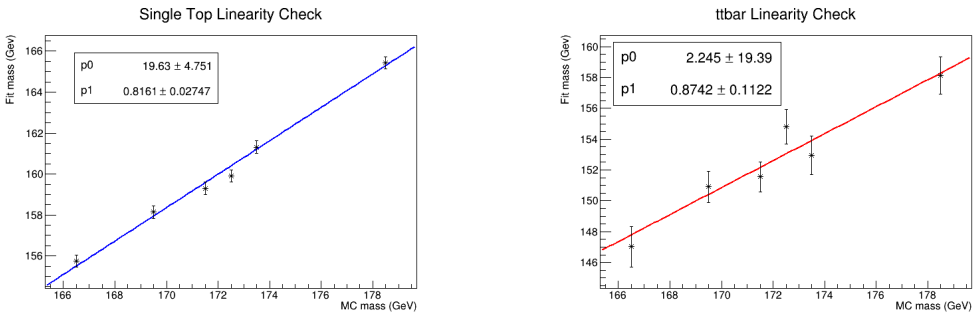

(a) *Single Top* **(b)** $t\bar{t}$

Figure 4.15: *Linearity checks*

4.2.4 Combined Fit

After finding the suitable template for each process, we are in position to extract the template for the combined fit of all procedures. This template can be written as:

$$F_{total} = r_{sig}F_{t-ch} + r_{t\bar{t}}F_{t\bar{t}} + r_{EWK}F_{EWK} + r_{QCD}F_{QCD} \tag{99}$$

where r_i factors express the contribution of each process. We remind that, before we perform the combined fit, we have to normalise the QCD contribution with the scale factor $N_{QCD} = N_{data} - N_{MC}$ due to the fact that we extracted the template from data but we use it in the MC study.

We start at initializing the r_i factors at 1, supposing there is equal contribution of each process. Then, in all r_i factors we apply Gaussian constraints. The mean values of the constraints are the nominal estimations from MCN_i^{nom}, and the standard deviations are 5% $N_{t\bar{t}}$ for the $t\bar{t}$, and 20% for the signal and the EWK background. These values are arbitary, but they are bigger than the known precision so the results will be reliable. The percentage for the $t\bar{t}$ is smaller, because its cross section is of higher theoretical precision.

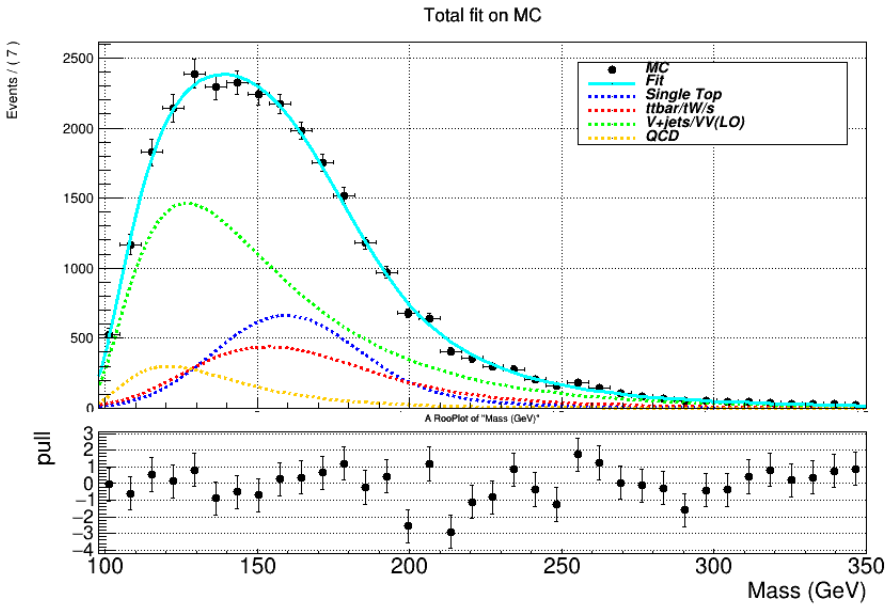

Figure 4.16: *Combined fit on nominal mass sample*

The first check to see if the fit procedure is performed well enough is to check if the shapes of the estimated m_{top}^{MC} and the r_i factors are parabolic with no point of incontinuity and no "bumps" in the shape.

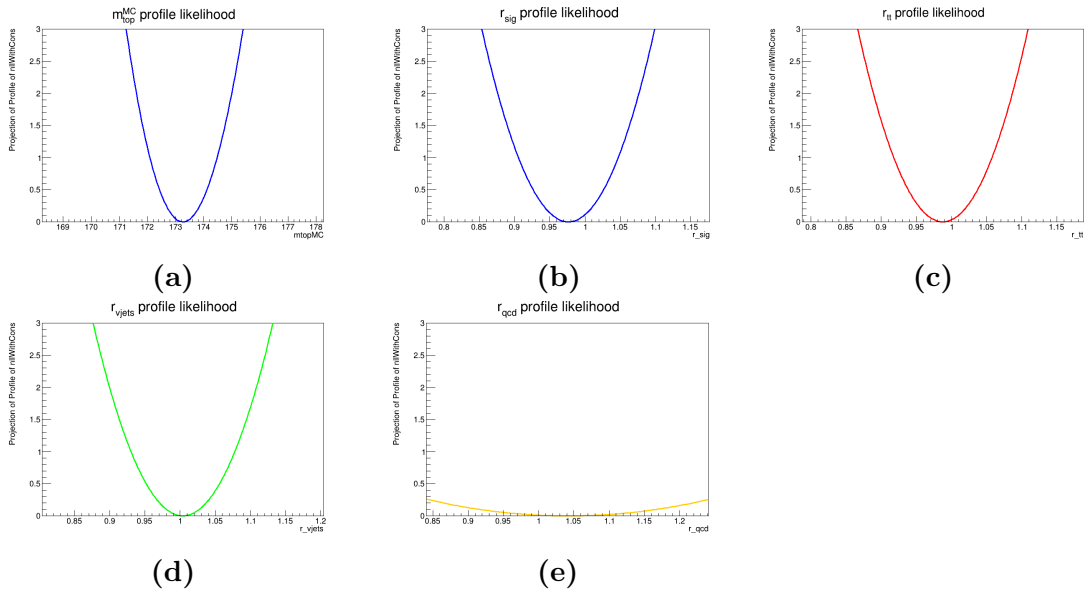

(a) **(b)** **(c)**

(d) **(e)**

Figure 4.17: *Profile Likelihoods - Nominal mass sample*

We observe the continuous parabolic shape, so the fit is "healthy".

One thing we can check also is the correlation that the r_i factors have with the estimated m_{top}^{MC} parameter. For that purpose, we use the contour ellipsoids which are two dimensional sections of the Likelihood. The information we get from these is from the deviation of their ellipsoid axes, the smaller it is, the smaller the correlation is.

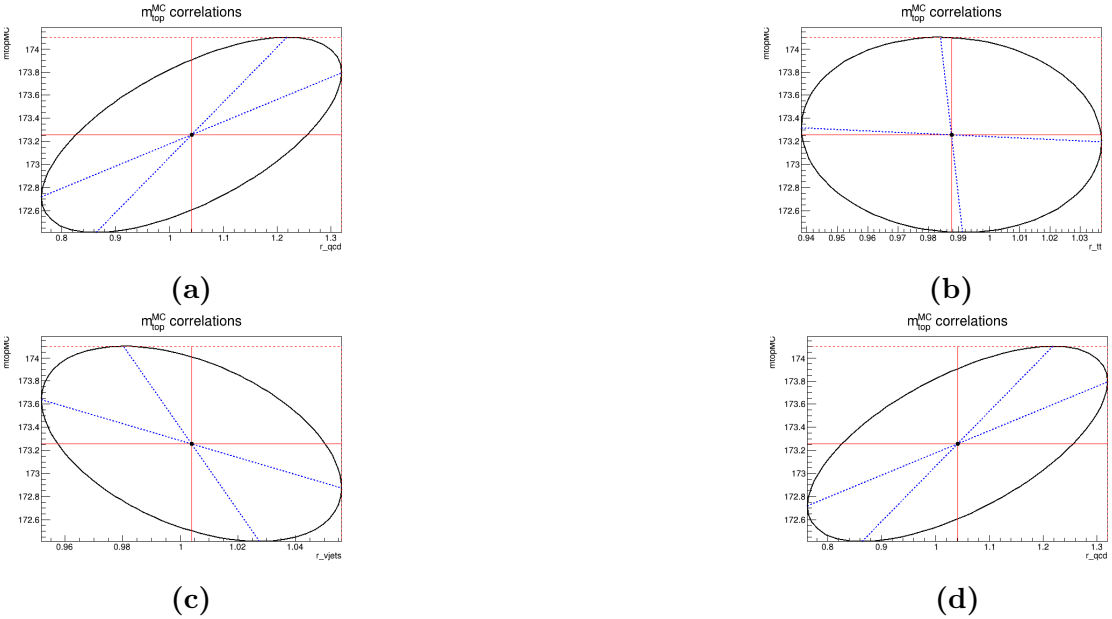

(a) **(b)**

(c) **(d)**

Figure 4.18: *Ellipsoid correlations with* m_{top}^{MC}

4.2.5 MC Toys Validation and fit on Data

In this stage of the analysis, we have to check if the fit procedure contains any bias. The method we use is called MC Toys Validation. With this method we check some properties of the ML fit by generating pseudodata from the model and applying the fit procedure on them. More specifically we perform the following steps:

- We pick a mass i.e 172.5GeV and we initialize the factors r_i at 1
- We generate $N_i^{nom} \approx$ Poisson $(N_i^{expected})$ events for each background and signal that follow the corresponding template
- Then we add all the events to make the pseudo-dataset
- We perform the ML fit on the pseudo-dataset
- We perform all the above multiple times

Now, we can extract some variables whose histograms can show us if we have some bias in our model. The main variables are:

- Error δN_{fit} or σ_{fit}
- Pulls for N i.e $g = \frac{N_{fit} - N_{in}}{\sigma_{fit}}$

If the pull distributions are standard Gaussian, with mean value $< pull >= 0$, which means unbiased estimation of yield and with $\sigma_{pull} = 1$, which means unbiased yield error estimation, then the estimator is unbiased. Of course, we expect these values to be close to 0 and 1 respectively and not exactly 0 and 1 but compatible within error. Also, the higher number of toys we use, the closer these values are to 0 and 1 and the lower the errors are.

We present the Toys Validation for the m_{top}^{MC} parameter, the estimator for the reconstructed mass. We used $N_{toys} = 1000$.

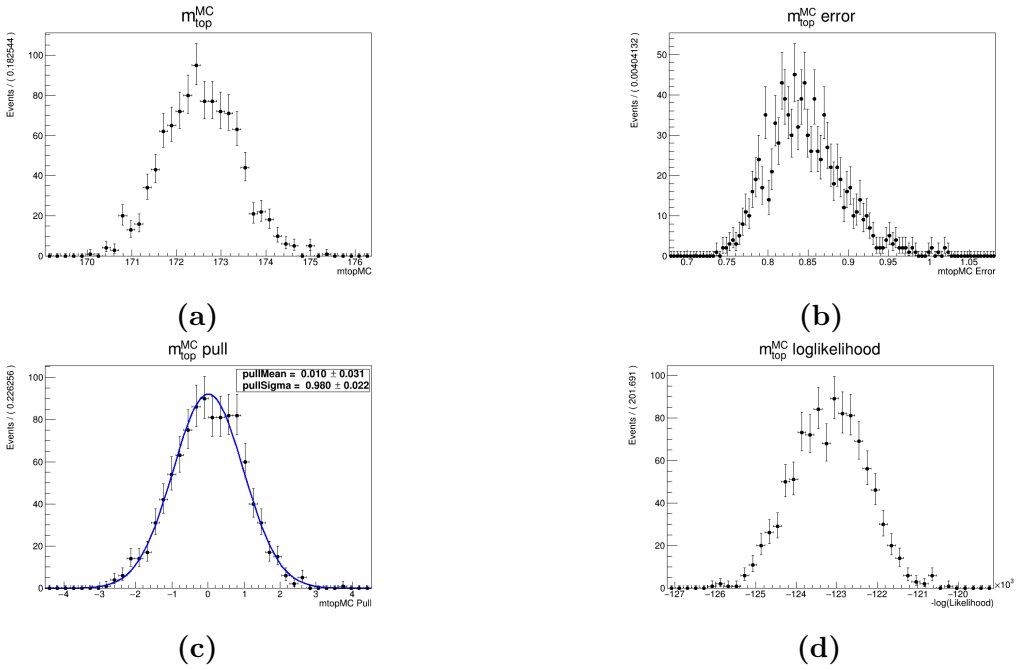

Figure 4.19: *Toys Validation on m_{top}^{MC} - Nominal mass sample*

We observe that the model is both healthy and unbiased, so now we can apply it to the real data. The data that are being used in this analysis, are recorded with the CMS detector in 2016 year. The combined fit on data yields:

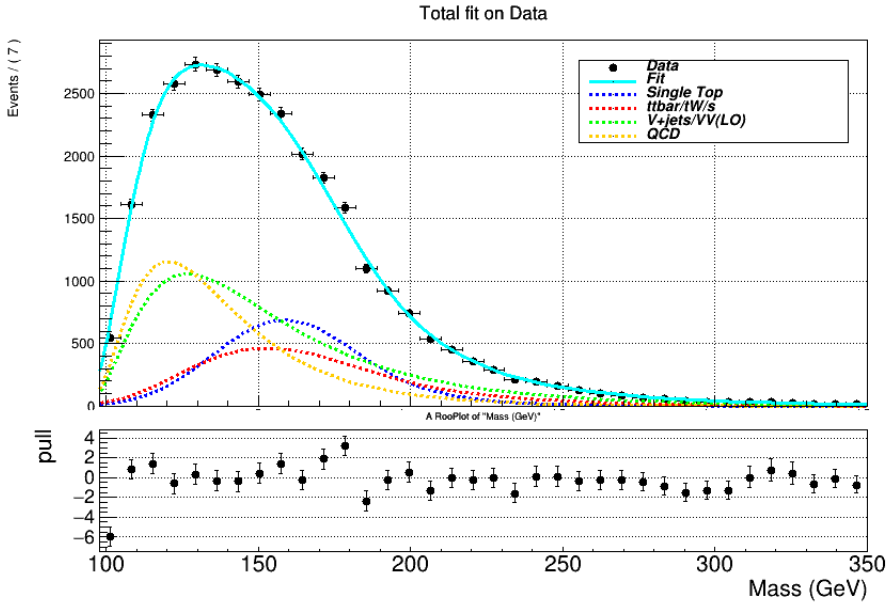

Figure 4.20: *Combined Fit on Data*

Once again we have to check if the fit is well behaved through the expected continuous parabolic shape of the estimated m_{fit} and the contribution factors r_i.

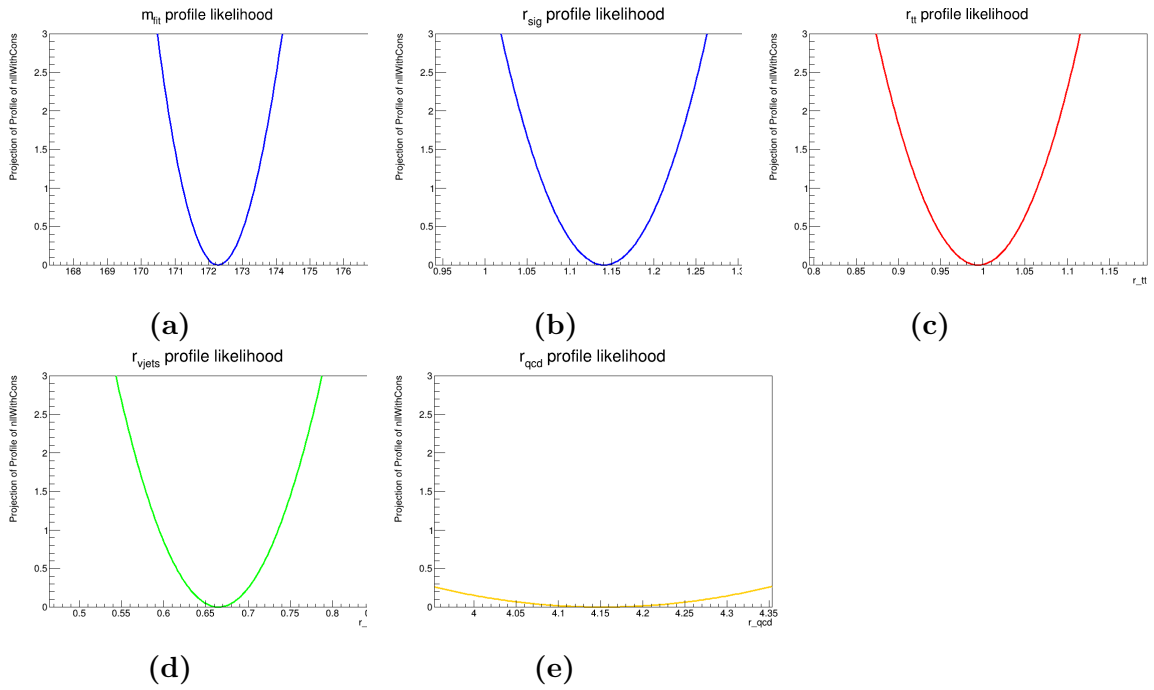

Figure 4.21: *Profile Likelihoods - Data*

4.2.6 Error Propagation

By performing the fit on data we extracted an estimation for the mass parameter. This estimation is called m_{fit}. Now, we need to extract the value for the real mass of top quark(m_{true}). We assume a linear dependency between these two parameters:

$$m_{fit} = a * m_{true} + b \tag{100}$$

The coefficients a, b can be taken from a linear fit on the MC samples m_{fit}^{MC} parameter. This method is called calibration.

Along with the estimation of m_{fit} from data we get also an estimation for its error(σ_{mfit}). Due to the fact that the coefficients a, b have their own error, it is a false assumption to say that the error of m_{true} is equal to the error of m_{fit}. So, the error must be obtained through error propagation.

Let's say we have a function $y = f(P_1, P_2, ..., P_N)$ then the generic formula for error propagation that encapsulates the correlation factors ρ_{ij} is:

$$(\sigma_y)^2 = \sum_{i=1}^{N} \sum_{j=1}^{N} \frac{\partial y}{\partial P_i} \frac{\partial y}{\partial P_j} \rho_{ij} \sigma_{P_i} \sigma_{P_j} \tag{101}$$

where $\rho_{ii} = 1$.

In our case, all three parameters have correlation with the m_{true} but we assume that the m_{fit} parameter is not correlated with calibration a,b parameters. So, the covariance matrix has the following form:

$$Cov = \begin{bmatrix} (\sigma_a)^2 & -1 * \sigma_a\sigma_b & 0 \\ -1 * \sigma_a\sigma_b & (\sigma_b)^2 & 0 \\ 0 & 0 & (\sigma_{m_{fit}})^2 \end{bmatrix} \tag{102}$$

If we solve with respect to m_{true} we have:

$$m_{true} = \frac{m_{fit} - b}{a} \tag{103}$$

The differentials with respect to a, b, m_{fit} accordingly are shown in the next matrix:

$$\begin{bmatrix} \frac{-m_{fit}+b}{a^2} & -\frac{1}{a} & \frac{1}{a} \end{bmatrix} \tag{104}$$

Performing the linearity check on the MC sample we obtain the following:

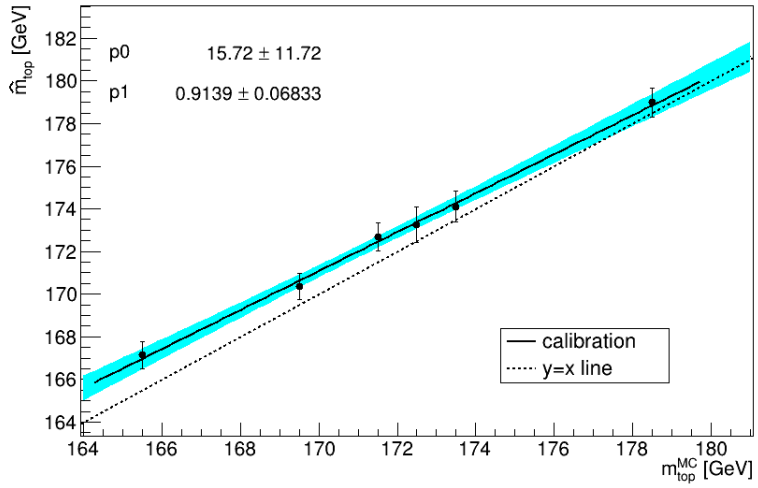

Figure 4.22: *Calibration method*

4.3 CPT Invariance

Many of the profound ideas in nature manifest themselves as symmetries. A symmetry in a physical experiment suggests that something is conserved, or remains constant, during the experiment. So conservation laws and symmetries are strongly linked.

Three of the symmetries which usually, but not always, hold are those of charge conjugation (C), parity (P), and time reversal (T):

- Charge conjugation(C): reversing the electric charge and all the internal quantum numbers, meaning:
$$C|p>=|\overline{p}> \tag{105}$$
The conservation under C yields:
$$C|p>=\pm|p>=|\overline{p}> \tag{106}$$

- Parity (P): space inversion; reversal of the space coordinates, but not the time. The weak interactions are not invariant under parity transformation, i.e the antimuon emitted in pion decay
$$\pi^+ \longrightarrow \mu^+ + \nu_\mu \tag{107}$$
always come out left handed. The weak interactions are also not invariant under C. The charge conjugation of the above interactions would yield:
$$\pi^- \longrightarrow \mu^- + \overline{\nu}_\mu \tag{108}$$
with a left-handed muon, whereas in fact the muon always comes out right-handed. If we combine the two operations, the left-handed antimuon turns into a right handed muon, which is what we observe in nature.

- Time reversal (T): replacing t by -t. This reverses time derivatives like momentum and angular momentum.

In our analysis, we constructed a model demanding a single lepton in the final state with muon flavor, regardless of muon charge. So the model describes a muon in the final state, either positive or negative. One way to check the CPT invariance is to apply the current model on data containing only positive muons in the final state and on data containing only negative muons. If we obtain analogous results, within statistical error, the CPT invariance applies.

Fit on positive muons

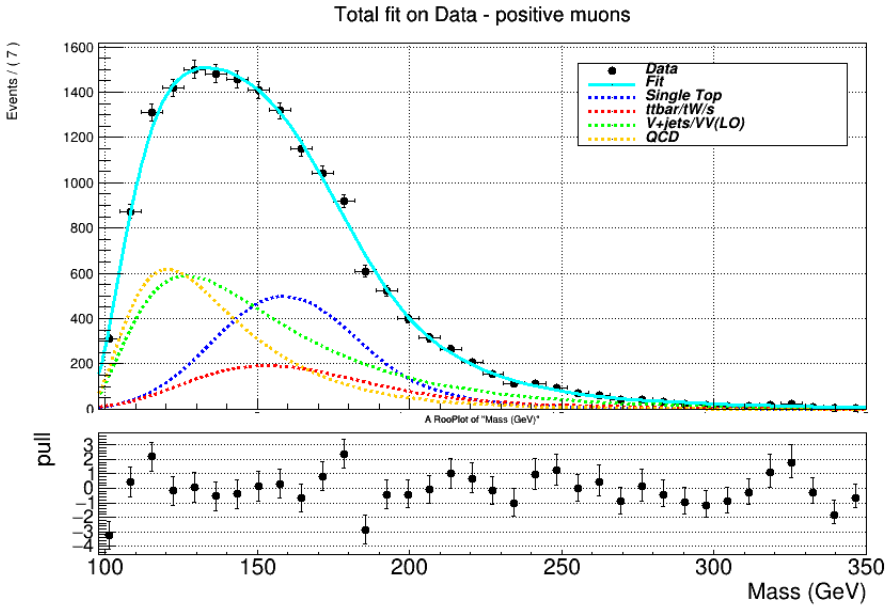

Figure 4.23: *Fit on data - positive muons*

Fit on negative muons

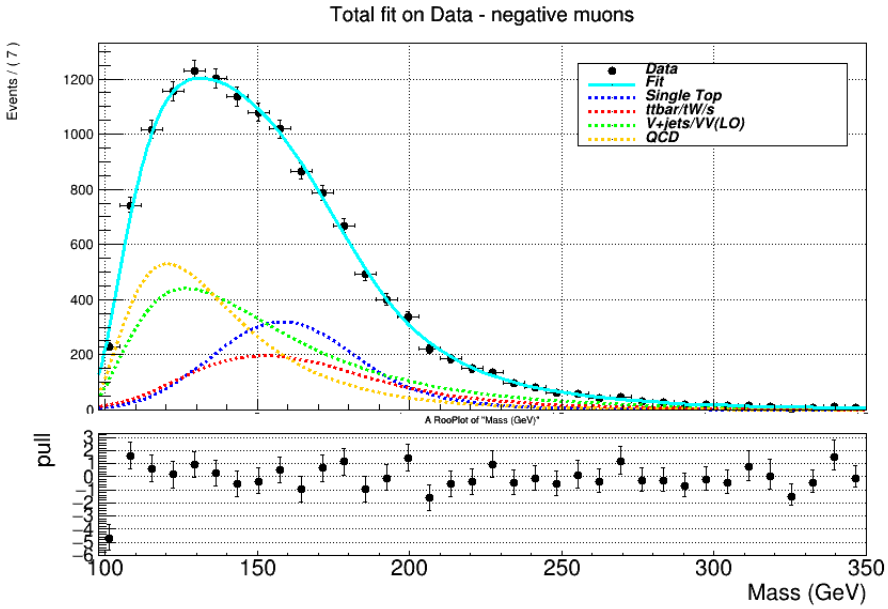

Figure 4.24: *Fit on data - negative muons*

For the extraction of the mass value and its error in each case we work as before but we apply the calibration of the total model. The reason we can do that, is that we estimate a parameter which, theoretically, does not depend upon charge conjugation.

Chapter 5

Results and Conclusions

The mass of the top quark measured using t-channel single top events, obtained from the postfit m_{fit} distribution followed by calibration and error propagation for the error value, inclusive of the charge of the muon in the final state, is given by:

$$m_t = 171.31 \pm 0.85(stat.)GeV \tag{109}$$

The masses of the top quark and anti-top quark are determined separately by requiring positively and negatively charged muons in the final state, respectively:

$$\begin{aligned} m_t &= 171.66 \pm 1.08(stat.)GeV \\ m_{\bar{t}} &= 170.77 \pm 1.29(stat.)GeV \end{aligned} \tag{110}$$

The mass ratio of the top antiquark to the top quark is estimated to be:

$$R_{m_t} = \frac{m_t}{m_{\bar{t}}} = 0.995 \pm 0.009(stat.) \tag{111}$$

and the mass difference between top quark and antiquark is obtained to be:

$$\Delta_{m_t} = m_t - m_{\bar{t}} = 0.89 \pm 1.56(stat.)GeV \tag{112}$$

The estimated value of R_{m_t} and Δ_{m_t} is in agreement with unity and zero respectively, within the uncertainties and indicate no violation of CPT symmetry.

In this thesis the mass of the top quark of the single top t-channel process was measured. The result is compatible with the standard model prediction as well as with a measurement from a recent analysis. No systematic uncertainties were included in the result. The statistics would be significantly improved if the electron dataset was used for the estimation. In this analysis, tools of maximum likelihood fitting were used and the importance of validating the characteristics of the fit through Toy MC Validation was shown, since it provides a framework that the choice of the way to extract the parameter of interest is unbiased and quantitatively checked to be well behaved.

Appendix A

Maximum Likelihood Fit

A.1 Definition

The maximum likelihood (ML) technique, refers to the problem of estimating the values of the parameters of a model $\theta_j, j = 1, ..., m$ given a dataset of N measurements $x1, ..., x_N$. This is called fit procedure. In general, each measurement is a vector with n components, so the fit is n-dimensional. A function which uses the probability density of observing x for a given set of parameters f (x; ϑ), is called Likelihood function. For N independent measurements of the same experiment is defined as:

$$L(\{x_i\}\,;\theta) = \prod_{i=1}^{N} f(x_i^1, ..., x_i^n; \theta_1, ..., \theta_m) \tag{113}$$

By maximizing the following quantity, we can determine the estimator of Maximum Likelihood($\hat{\theta}$):

$$\left.\frac{\partial L(x;\theta)}{\partial \theta_i}\right|_{\theta=\hat{\theta}} = 0 \ \forall \ \theta_i \tag{114}$$

or equivalently minimizing the $-logL(x;\theta)$.

An estimation ϑ is dependent of the given dataset, and therefore has statistical fluctuations, so is accompanied by an error.

In order to calculate the error,for large number of measurements, the likelihood function is approximated as a Gaussian, or equivalently the $-logL$ as parabolic. In this case the covariance matrix C is defined as the inverse of the Hessian matrix, which is the matrix of second derivatives:

$$C_{ij} = \left[-\frac{\partial logL(\{x_i\}, \theta_1, ..., \theta_m)}{\theta_i \theta_j}\right]^{-1}_{\theta_{i,j}=\hat{\theta}_{i,j}} \tag{115}$$

This method yields always symmetric errors for the estimations $\hat{\theta} \pm \sigma_i$, where $\sigma_i = \sqrt{C_{ii}}$. Also the correlation coefficients of the different parameters are found by

the non diagonal elements of C , namely $\rho_{ij} = \sqrt{C_{ij}}/\sigma_i\sigma_j$.

In general, the shape of Likelihood is not Gaussian. Then, a way to estimate the uncertainties, which is numerically equivalent for the Gaussian case, is to use the contour defined by values ϑ' such that:

$$-logL(\theta') = -logL_{max} + \frac{1}{2} \tag{116}$$

where $L_{max} \equiv L(\{x_i\}, \hat{\theta})$ and is called 1-sigma contour. The projection of this curve on a parameter θ_i defines the error interval of the estimation $[\theta_i - \Delta\theta_-.\theta_i + \Delta\theta+]$ which is in general asymmetric. This definition is exact, and in the case that the error of Gaussian approximation is not consistent with the $\Delta\theta_\pm$, the approximation is invalid.

A.2 Extended Likelihood

In high energy physics, usually the fit has as parameters the yield of signal events (s) which follow a probability distribution function $f_s(x;\theta_s)$, and the yield of the background events (b) which follow $f_b(x;\theta_b)$[1]. The $\theta_{s,b}$ are other parameters defining the shapes of the distributions. Then the total events number N is depending on s, b since $N = s + b$, and follows a Poisson distribution with mean $s + b$

$$N \approx Poisson(N;, s+b) = \frac{(s+b)^N}{N!} e^{-(s+b)} \tag{117}$$

Thus, the Likelihood is written as:

$$L(\{x_i\}, s, b, \theta_s, \theta_b) = \frac{(s+b)^N e^{-(s+b)}}{N!} \prod_{i=1}^{N} [df_s(x_i;\theta_s + bf_b(x_i;\theta_b)] \tag{118}$$

This type of likelihood functions where the number of data N depends on parameters of distribution is called "Extended Likelihood function".

A.3 Binned Maximum Likelihood Fit

In the previous sections, each event enters separately into the likelihood and thus the method is called "Unbinned" ML fit. This is the statistically optimal procedure, but its CPU consuption increases linearly with number of events N . For this reason, in high energy physics the most popular implementation is the "Binned" ML, where the events are grouped in bins of the observables x. The counted event numbers in the bins are used in the likelihood function. When the theoretical template cannot

[1] Although there could be more than one backgrounds we consider one background without any loss of generality

be a continuous PDF, but it comes from a binned histogram of generated events with Monte Carlo, then Binned ML fit is the only to perform a fit.

We consider one fitted variable x[2] which is partioned into N bins. If n is the total number of independent events and n_i the number of events in bin i, then each bin is a Poissonian experiment with observed number of events n_i. In case of a continuous PDF $f(x;\theta)$, in order to find the expected number m_i of events in each bin, we integrate the corresponding PDF and multiply by n. Thus, we obtain:

$$\mu_i = \mu_i(\theta) \equiv \int_{bini} f(x_i;\theta_1,...,\theta_m)dx \tag{119}$$

Therefore each bin has a distribution Poisson$(n_i; m_i(\theta))$.

The Likelihood function is:

$$L = \prod_{i=1}^{N} Poisson(n_i; m_i(\theta)) = \prod_{i=1}^{N} \frac{\mu_i^{n_i}(\theta)}{n_i!} e^{-\mu_i(\theta)} \tag{120}$$

In case where the number of events per bin is big enough, the Poisson distributions can be approximated by Gaussian with mean value μ_i and sigma $\sqrt{\mu_i}$. Then, taking the $-2logL$ and dropping the terms which do not contain fit parameters, we obtain the χ^2 minimization method:

$$\sum_{i=1}^{N} = \frac{(n_i - \mu_i(\theta))^2}{\mu_i(\theta)} \tag{121}$$

A.4 Simultaneous fitting

In several analyses, the dataset can be separated into regions, regarding their content in signal or background events. The region which has most of signal events is called "signal region" (SR), while a region which is dominant by some background processes, or even better only one of them, are called "control regions" (CR). Let's assume for simplicity there are two regions, a signal and a control. The dataset in the signal(control) region will be denoted as $x_{sr}(y_{cr})$ where x, y can be the same or different variables. Then if θ_c are common parameters in the two regions, while $\theta_{sr(cr)}$ refer only to one of them, the Likelihood function can be written as:

$$L(\{x_{sr}\}\{y_{sr}\};\theta_c,\theta_{sr}.\theta_{cr}) = L_{sr}(\{x_{sr}\};\theta_c,\theta_{sr})L_{cr}(\{y_{cr}\};\theta_c,\theta_{cr}) \tag{122}$$

where the $L_{sr(cr)}$ are the corresponding regions likelihoods. Therefore, for the common parameters, more events will be used and a more precise estimation will be extracted. Such a fit where two or more datasets are fitted with common parameters is called "simultaneous". Simultaneous fitting is a method that allows exploiting better the available data, and is therefore popular in High Energy Physics analyses.

[2]The same holds for multidimentional fits

Appendix B

Rest of mass samples figures

In the main analysis, we apposed the model templates, the Likelihood scans, the MC Toys Validation plots and the combined fit on MC only for the nominal mass sample(172.5Gev). Below, we will show all the equivalent plots for each mass sample that we worked on in order to show the consistency of the model on each sample.

B.1 Single Top Modeling

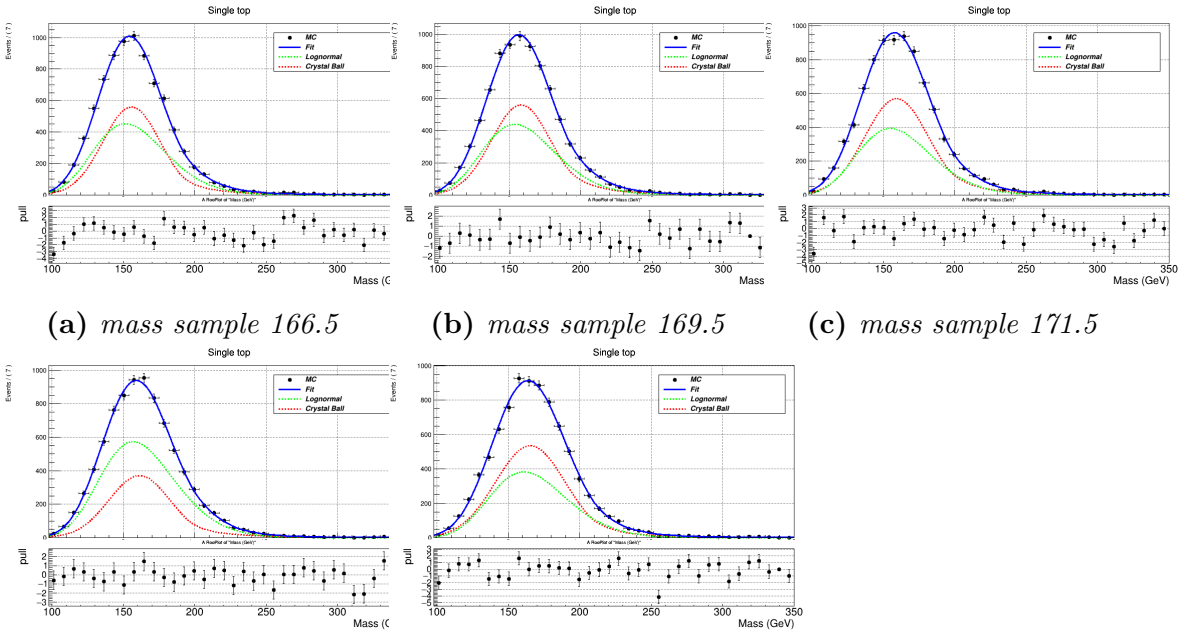

(a) *mass sample 166.5* **(b)** *mass sample 169.5* **(c)** *mass sample 171.5*

(d) *mass sample 173.5* **(e)** *mass sample 178.5*

Figure B.1: *Mass samples in signal region*

B.2 Modeling of $t\bar{t}$

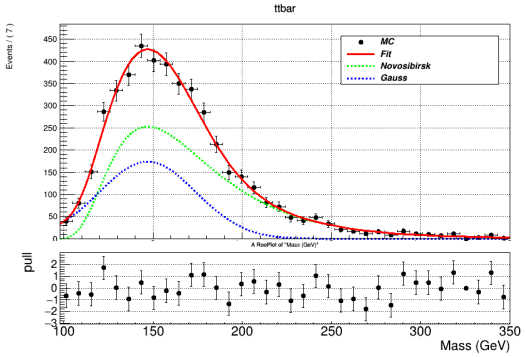

(a) *mass sample 166.5*

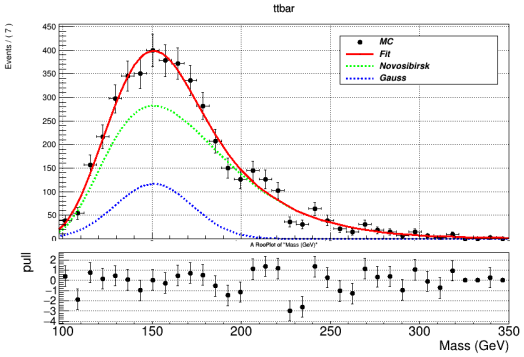

(b) *mass sample 169.5*

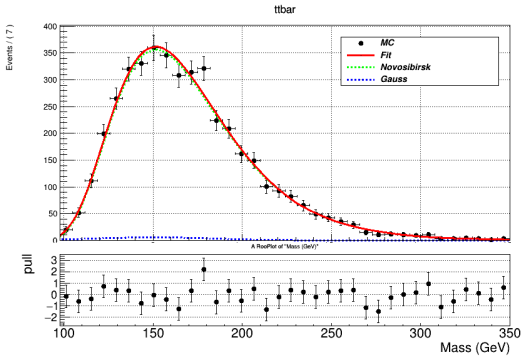

(c) *mass sample 171.5*

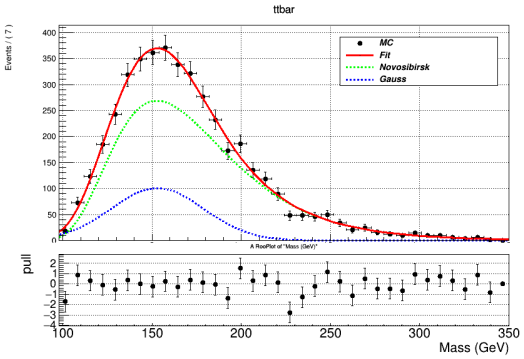

(d) *mass sample 173.5*

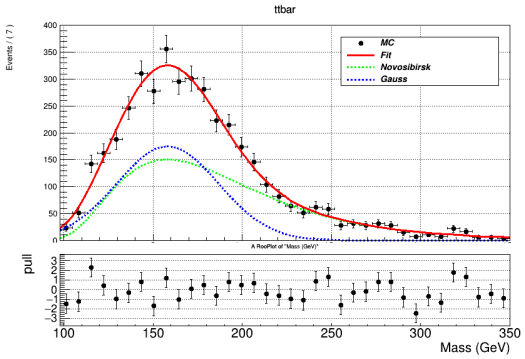

(e) *mass sample 178.5*

Figure B.2: *Mass samples in $t\bar{t}$ region*

B.3 Profile Likelihoods in 1D

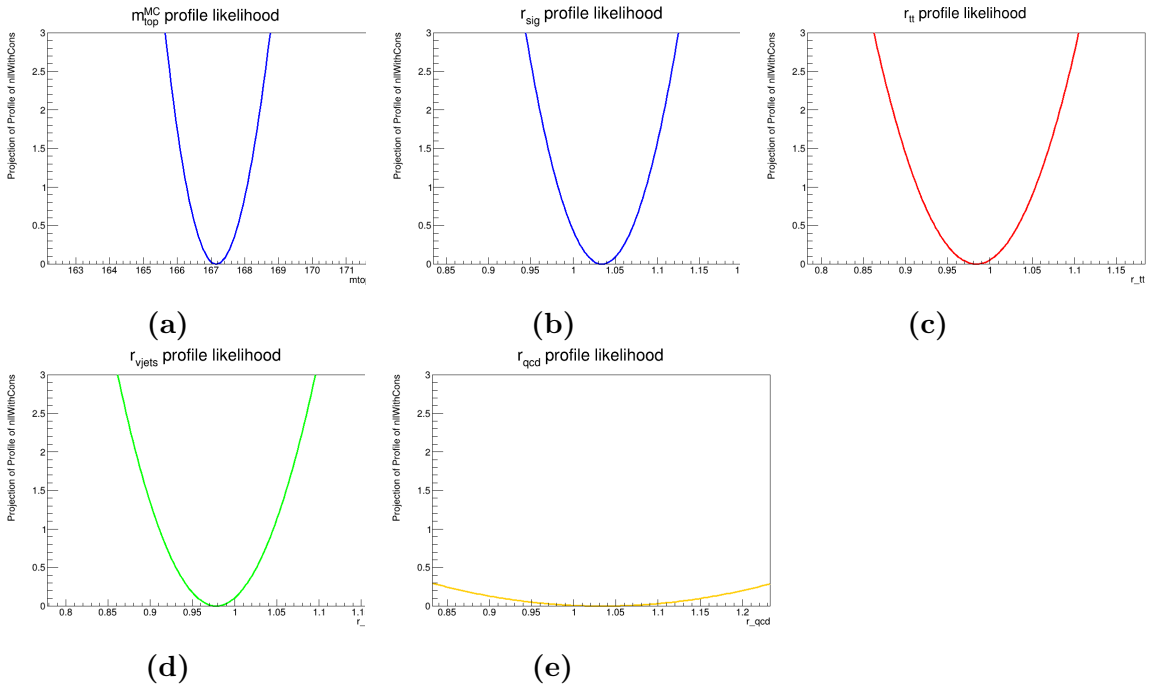

Figure B.3: *Mass sample 166.5*

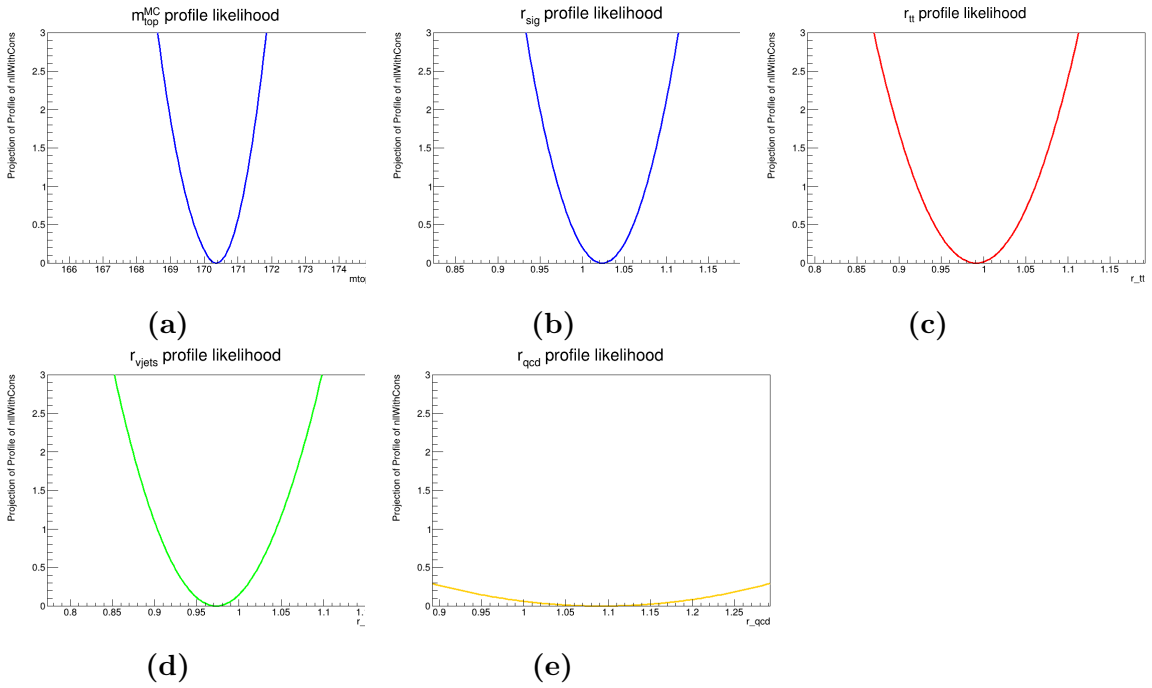

Figure B.4: *Mass sample 169.5*

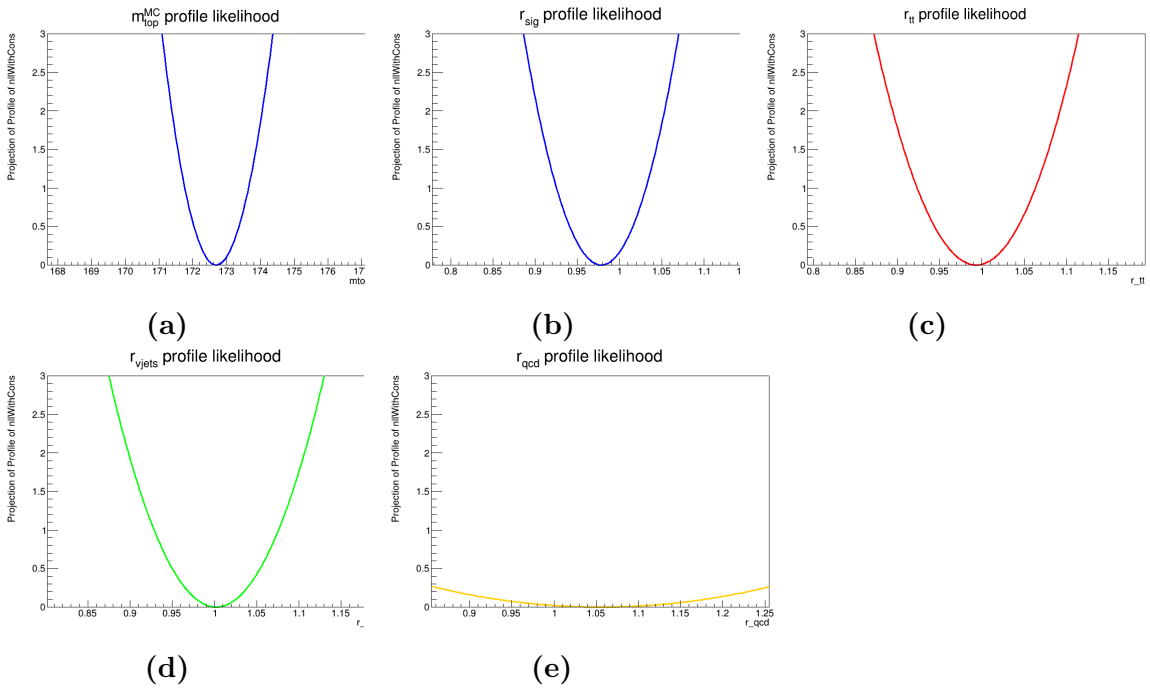

(a) (b) (c)

(d) (e)

Figure B.5: *Mass sample 171.5*

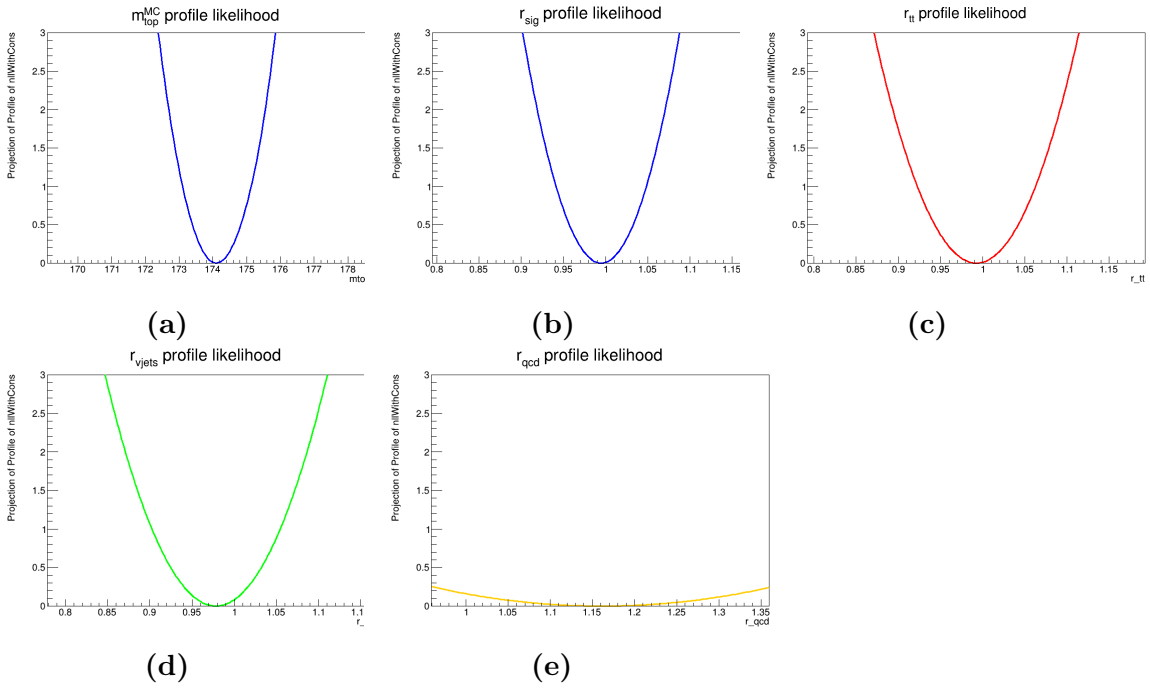

(a) (b) (c)

(d) (e)

Figure B.6: *Mass sample 173.5*

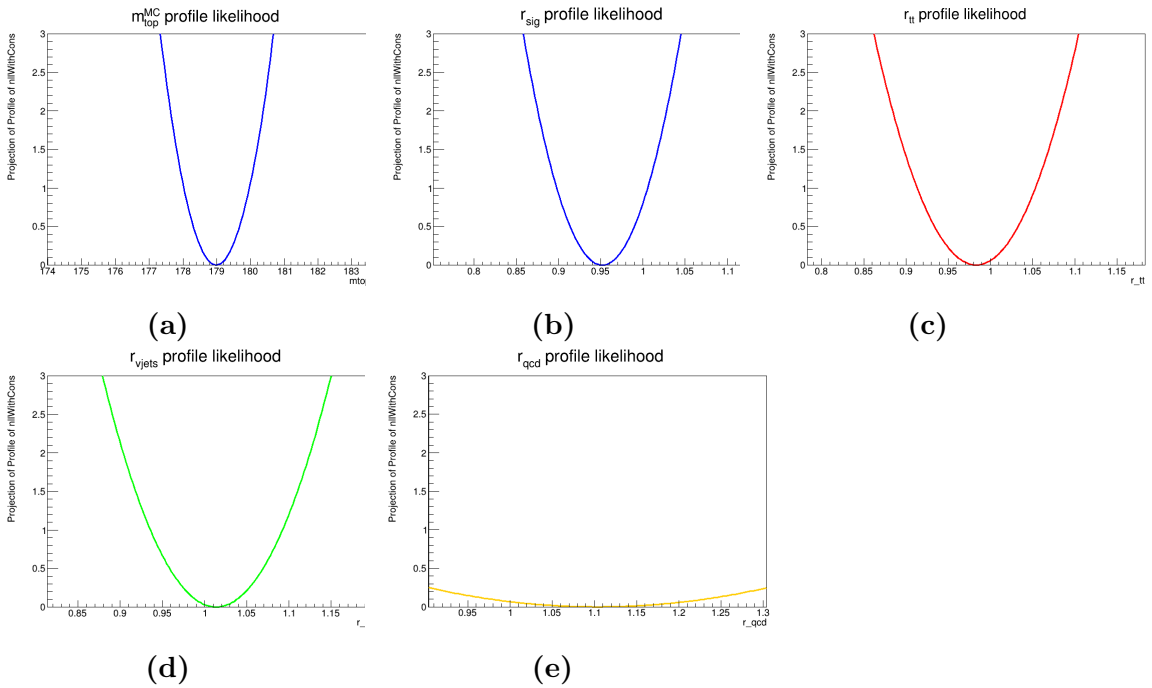

Figure B.7: *Mass sample 178.5*

B.4 Likelihood contours in 2D

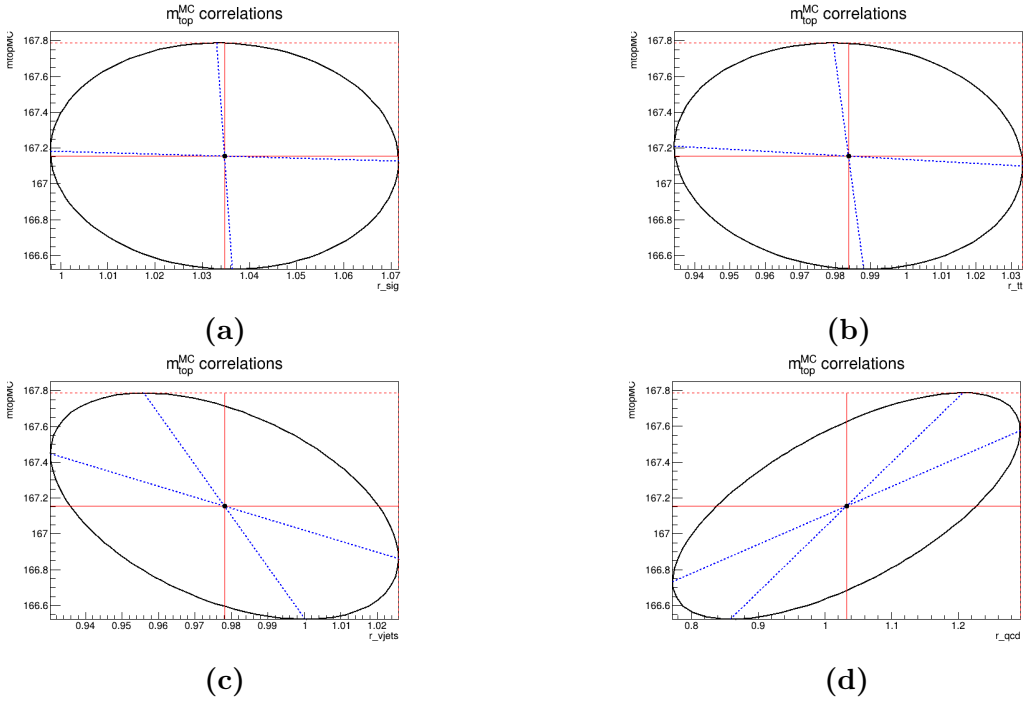

Figure B.8: *Mass sample 166.5*

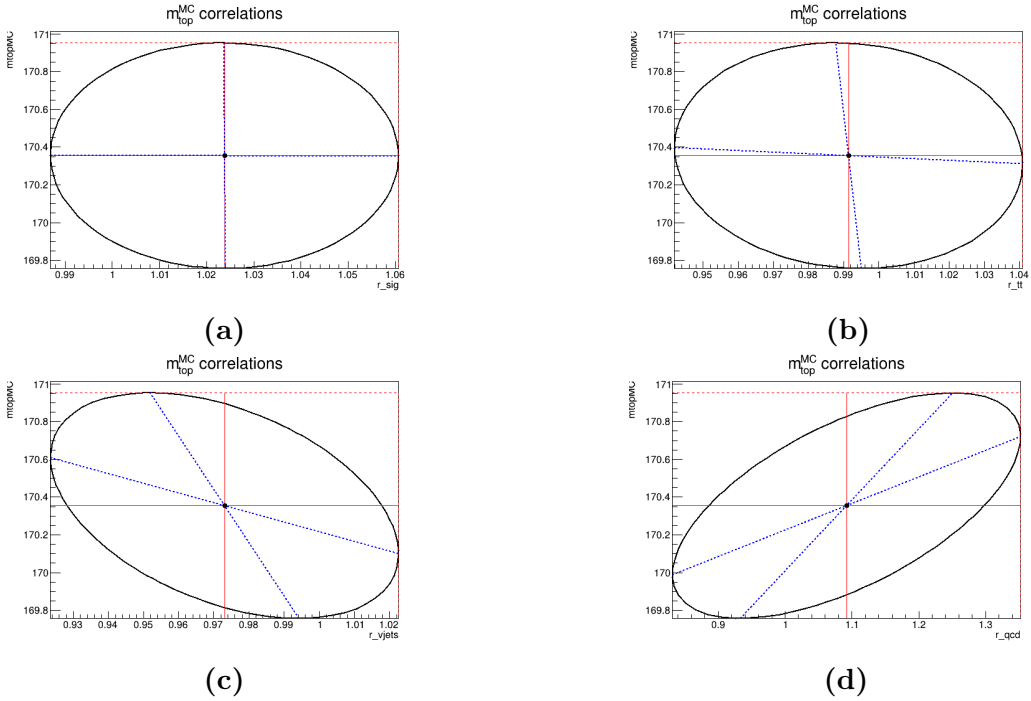

Figure B.9: *Mass sample 169.5*

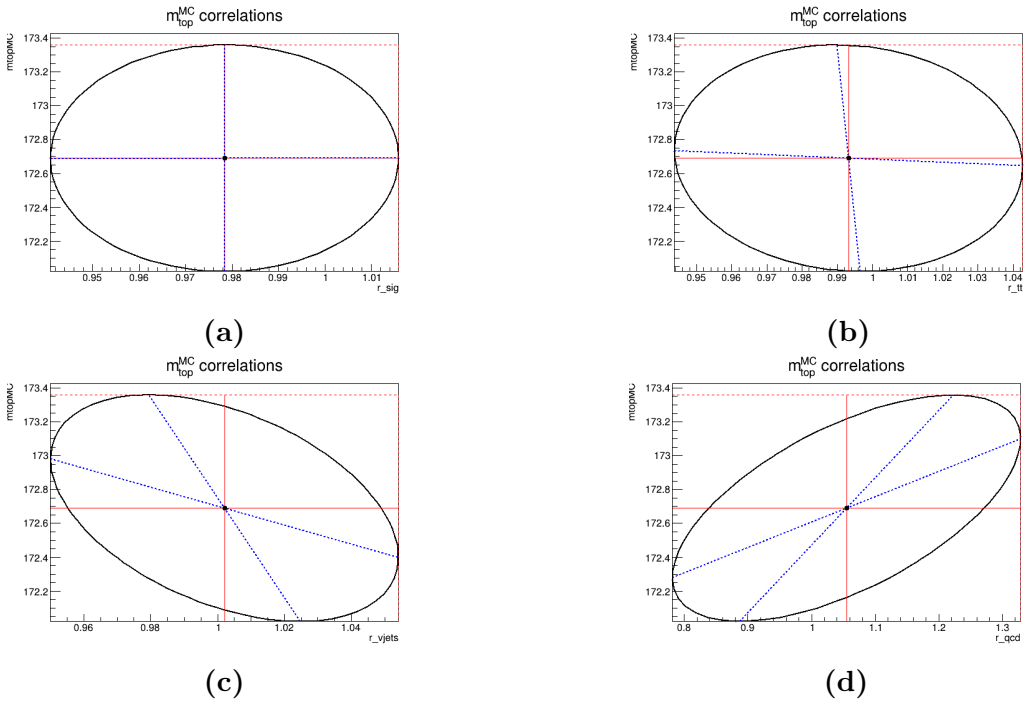

Figure B.10: *Mass sample 171.5*

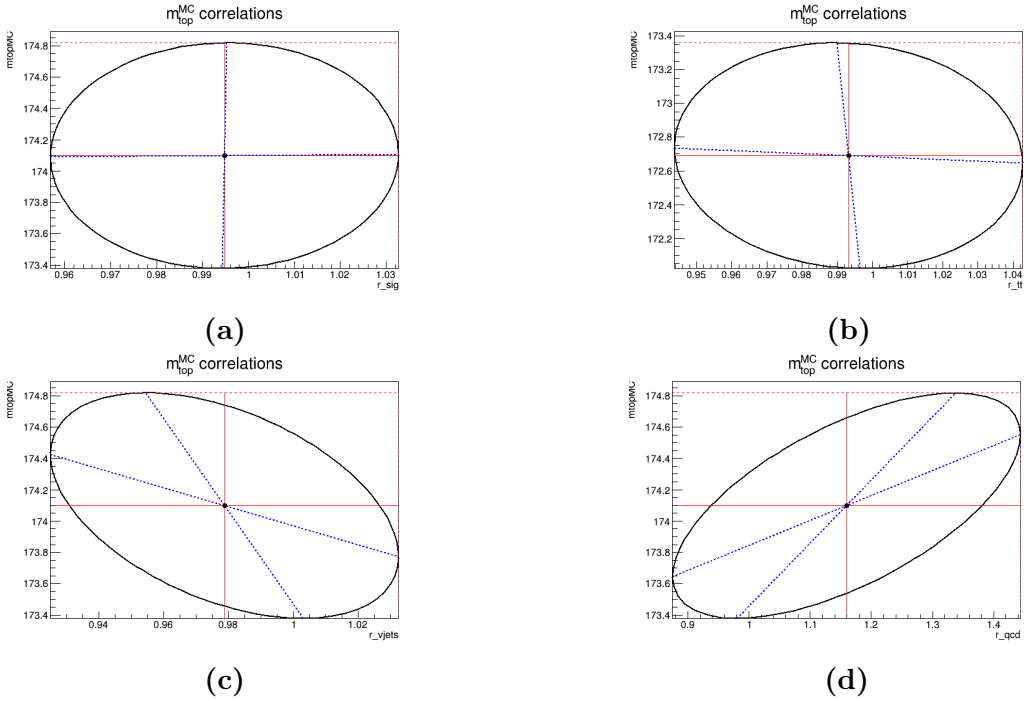

Figure B.11: *Mass sample 173.5*

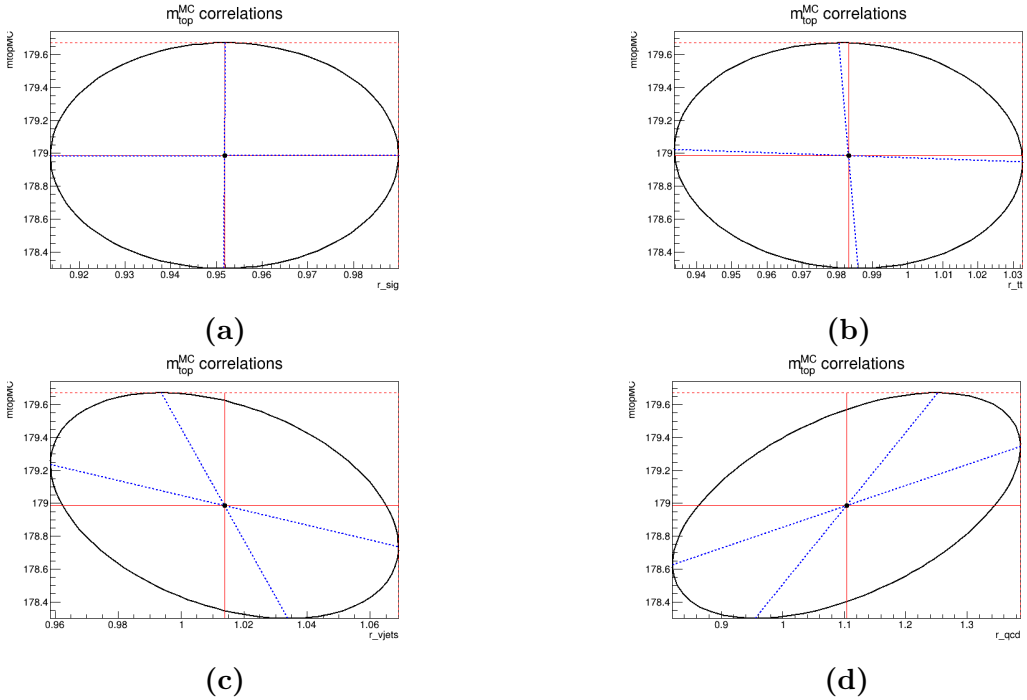

Figure B.12: *Mass sample 178.5*

B.5 MC Toys Validation

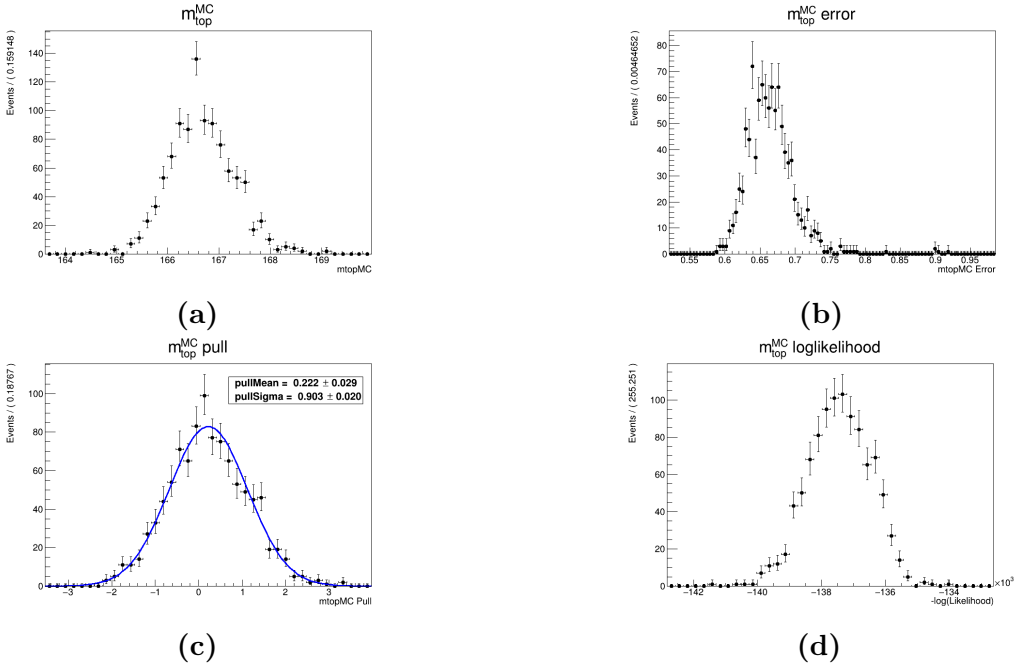

Figure B.13: *Mass sample 166.5*

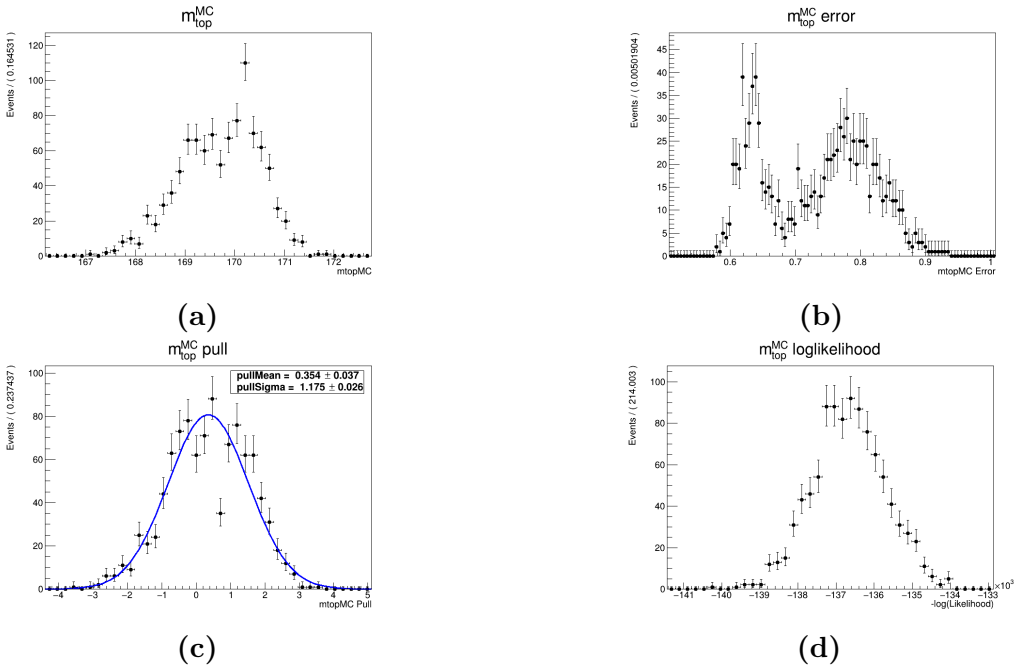

Figure B.14: *Mass sample 169.5*

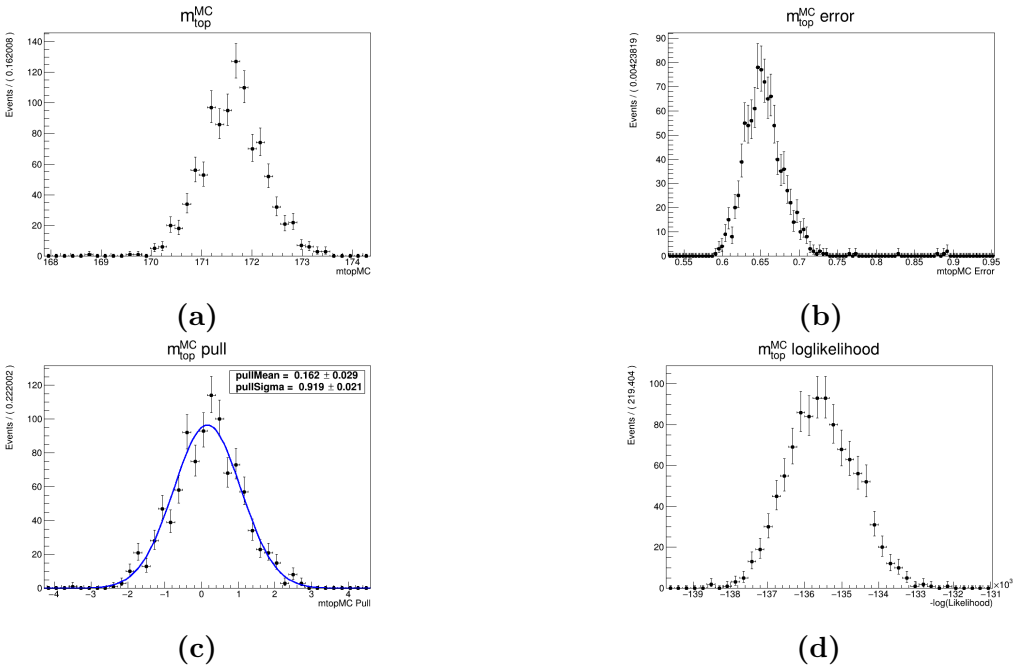

Figure B.15: *Mass sample 171.5*

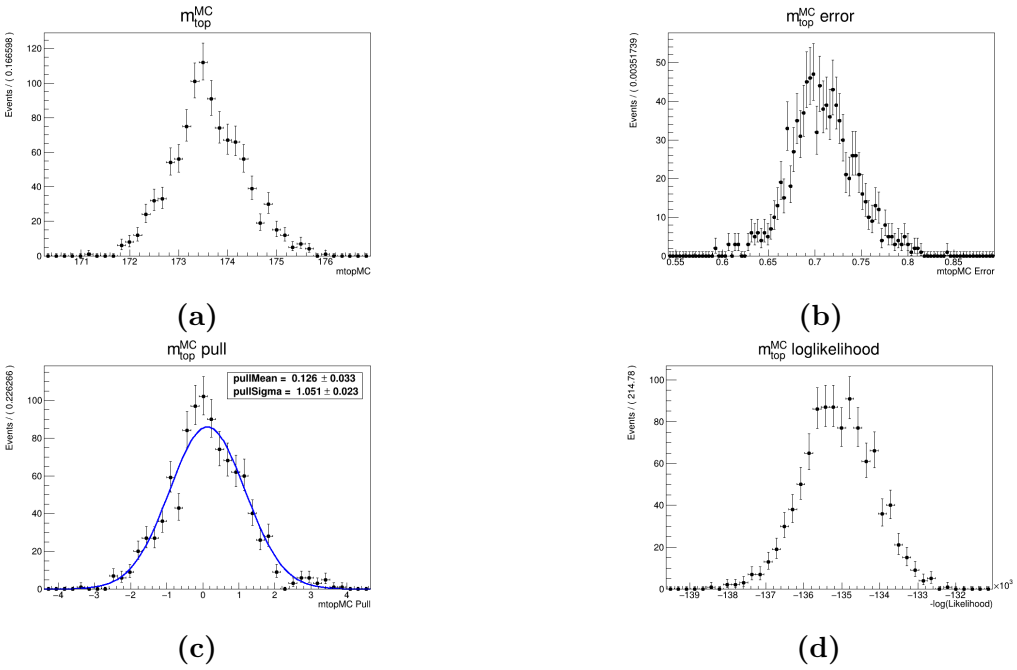

Figure B.16: *Mass sample 173.5*

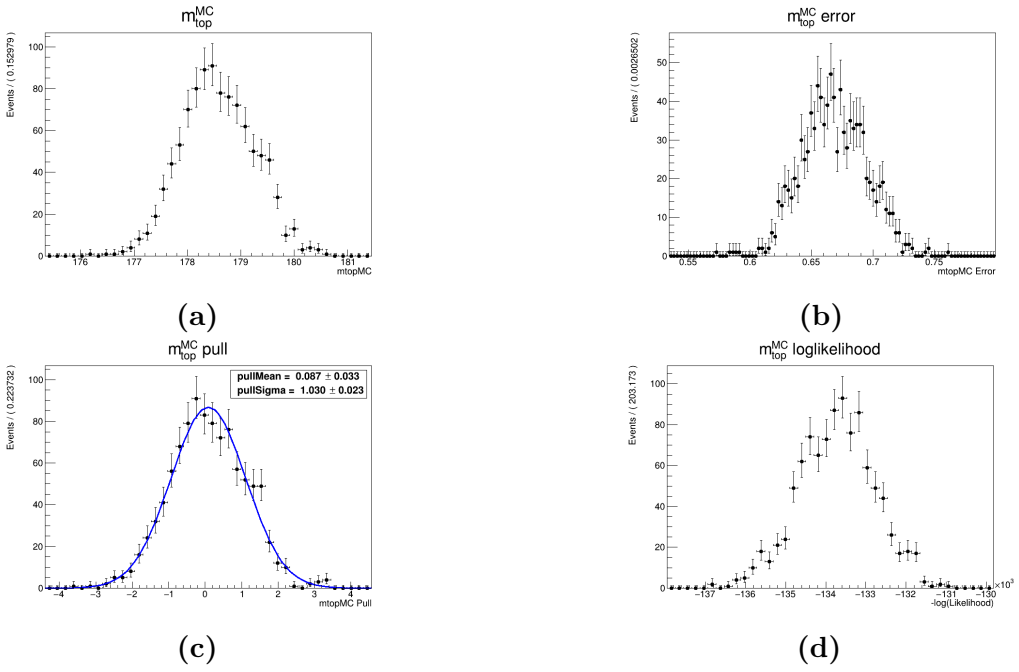

Figure B.17: *Mass sample 178.5*

B.6 Combined fit on MC

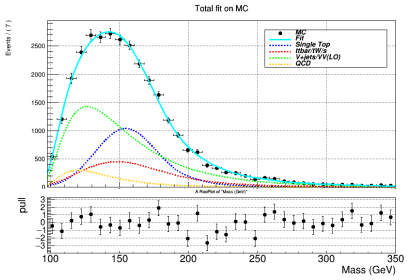

(a) *Mass sample 166.5*

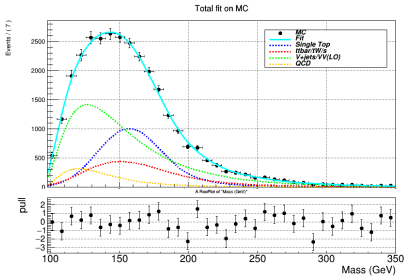

(b) *Mass sample 169.5*

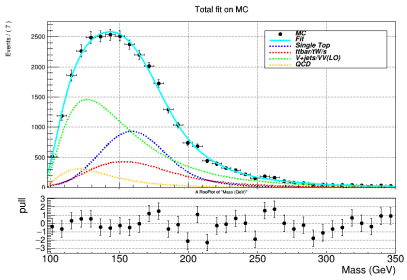

(c) *Mass sample 171.5*

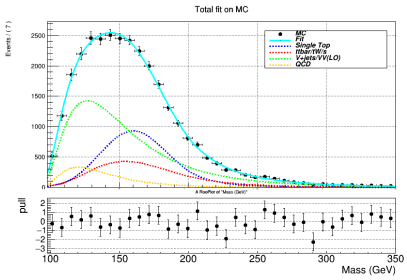

(d) *Mass sample 173.5*

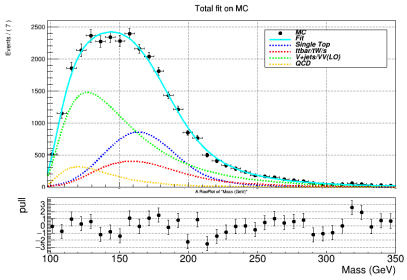

(e) *Mass sample 178.5*

Figure B.18: *Combined fit on MC*

List of Figures

List of Tables

Bibliography

[1] David Griffiths, *Introduction to Elementary Particles*, Wiley

[2] Alan Martin, Francis Halzen, *Quarks and Leptons: An Introductory Course in Modern Particle Physics*, Wiley

[3] B.R Martin, G.Shaw, *Particle Physics*, Wiley

[4] Donald H. Perkins, *Introduction to High Energy Physics*, Wiley

[5] Ilya Narsky, Frank C. Porter, *Density Estimation and Supervised Learning*, Wiley

[6] Olaf Behnke, Kevin Kroeninger, Gregory Schott, and Thomas Schoerner-Sadenius, *Data Analysis in High Energy Physics "A Practical Guide to Statistical Methods"*, Wiley

[7] Konstantinos Koutroumpas, Sergios Theodoridis, *Pattern Recognition*, Accademic Press

[8] Matthew D. Schwartz, *Collider Physics*, TASI

[8] Matthew D. Schwartz, *Quantum Field Theory and the Standard Model*, Cambridge University Press 2014.

[9] A.D. Martin, W.J. Stirling, R.S. Thorne, G. Watt, Parton distributions for the LHC, arXiv:0901.0002v3 [hep-ph] 7 Jul 2009

[10] Ulrich Husemann, Top-Quark Physics: Status and Prospects. arXiv:1704.01356v2

[11] CMS Collaboration, Measurement of the top quark mass using events with a single reconstructed top quark in pp collisions at $\sqrt{s} = 13$TeV. arXiv:2108.10407 [hep-ex]

[12] ATLAS Collaboration, "Measurement of the top quark mass in the $\bar{t}t \longrightarrow$ lepton+jets channel from $\sqrt{s} = 8$ TeV ATLAS data and combination with previous results", Eur. Phys. J. C 79 (2019) 290, doi:10.1140/epjc/s10052-019-6757-9, arXiv:1810.01772.

[13] CMS Collaboration, "Measurement of the top quark mass using proton-proton data at $\sqrt{s} = 7$ and 8 TeV", Phys. Rev. D 93 (2016) 072004, doi:10.1103/PhysRevD.93.072004, arXiv:1509.04044.

[14] CMS Collaboration, "Measurement of the top quark mass with lepton+jets final states using pp collisions at $\sqrt{s} = 13$ TeV", Eur. Phys. J. C 78 (2018) 891, doi:10.1140/epjc/s10052-018-6332-9, arXiv:1805.01428.

[15] CMS Collaboration, "Measurement of the top quark mass in the all-jets final state at $\sqrt{s} = 13$ TeV and combination with the lepton+jets channel", Eur. Phys. J. C 79 (2019) 313, doi:10.1140/epjc/s10052-019-6788-2, arXiv:1812.10534.

[16] CMS Collaboration, CMS Physics

[17] CMS Collaboration, Detector Drawings, CDS

[18] CMS Collaboration,The CMS Experiment at the CERN LHC